AFRL-VA-WP-TR-2002-3002

STRUCTURAL TECHNOLOGY AND ANALYSIS PROGRAM (STAP)

Delivery Order 0017: Active Vibration Suppression Technology Buffet Load Alleviation (BLA) Program

Jay K. Burnham

The Boeing Company
P.O. Box 516
St. Louis, MO 63166-0516

JUNE 2001

FINAL REPORT FOR THE PERIOD 24 MAY 1999 – 30 AUGUST 2000

AIR VEHICLES DIRECTORATE
AIR FORCE MATERIEL COMMAND
AIR FORCE RESEARCH LABORATORY
WRIGHT-PATTERSON AIR FORCE BASE, OH 45433-7542

REPORT DOCUMENTATION PAGE

Form Approved OMB No. 0704-0188

1. REPORT DATE (DD-MM-YYYY)	2. REPORT TYPE	3. DATES COVERED (FROM - TO)
01-06-2001	Final	24-05-1999 to 30-08-2000

4. TITLE AND SUBTITLE
Structural Technology and Analysis Program (STAP) elivery Order 0017: Active Vibration Suppression Technology Buffet Load Alleviation (BLA) Program
Unclassified

5a. CONTRACT NUMBER
F33615-95-D-3216
5b. GRANT NUMBER
5c. PROGRAM ELEMENT NUMBER

6. AUTHOR(S)
Burnham, Jay K. ;

5d. PROJECT NUMBER
5e. TASK NUMBER
5f. WORK UNIT NUMBER

7. PERFORMING ORGANIZATION NAME AND ADDRESS
The Boeing Company
P.O. Box 516
St. Louis, MO63166-0516

8. PERFORMING ORGANIZATION REPORT NUMBER

9. SPONSORING/MONITORING AGENCY NAME AND ADDRESS
Air Vehicles Directorate
Air Force Research Laboratory
Air Force Materiel Command
Wright-Patterson AFB, OH45433-7542

10. SPONSOR/MONITOR'S ACRONYM(S)
11. SPONSOR/MONITOR'S REPORT NUMBER(S)

12. DISTRIBUTION/AVAILABILITY STATEMENT
APUBLIC RELEASE
,

13. SUPPLEMENTARY NOTES

14. ABSTRACT
See report

15. SUBJECT TERMS

16. SECURITY CLASSIFICATION OF:			17. LIMITATION OF ABSTRACT	18. NUMBER OF PAGES	19. NAME OF RESPONSIBLE PERSON
a. REPORT	b. ABSTRACT	c. THIS PAGE	Same as Report (SAR)	93	EM108, (blank) lfenster@dtic.mil
Unclassified	Unclassified	Unclassified			19b. TELEPHONE NUMBER International Area Code Area Code Telephone Number 703767-9007 DSN 427-9007

NOTICE

USING GOVERNMENT DRAWINGS, SPECIFICATIONS, OR OTHER DATA INCLUDED IN THIS DOCUMENT FOR ANY PURPOSE OTHER THAN GOVERNMENT PROCUREMENT DOES NOT IN ANY WAY OBLIGATE THE US GOVERNMENT. THE FACT THAT THE GOVERNMENT FORMULATED OR SUPPLIED THE DRAWINGS, SPECIFICATIONS, OR OTHER DATA DOES NOT LICENSE THE HOLDER OR ANY OTHER PERSON OR CORPORATION; OR CONVEY ANY RIGHTS OR PERMISSION TO MANUFACTURE, USE, OR SELL ANY PATENTED INVENTION THAT MAY RELATE TO THEM.

THIS REPORT IS RELEASABLE TO THE NATIONAL TECHNICAL INFORMATION SERVICE (NTIS). AT NTIS, IT WILL BE AVAILABLE TO THE GENERAL PUBLIC, INCLUDING FOREIGN NATIONS.

THIS TECHNICAL REPORT HAS BEEN REVIEWED AND IS APPROVED FOR PUBLICATION.

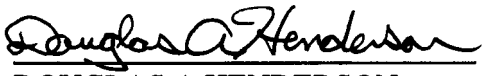

DOUGLAS A. HENDERSON
Aerospace Engineer
Structural Dynamics Branch

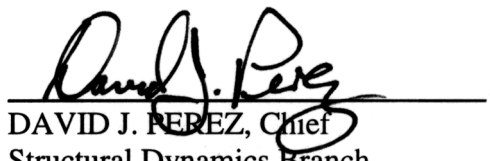

DAVID J. PEREZ, Chief
Structural Dynamics Branch
Structures Division

JEFFREY S. TURCOTT, Lt. Col., USAF
Deputy Chief, Structures Division
Air Vehicles Directorate

Do not return copies of this report unless contractual obligations or notice on a specific document require its return.

REPORT DOCUMENTATION PAGE

Form Approved
OMB No. 0704-0188

1. REPORT DATE *(DD-MM-YY)*	2. REPORT TYPE	3. DATES COVERED *(From - To)*
June 2001	Final	05/24/1999 – 08/30/2000

4. TITLE AND SUBTITLE

Structural Technology and Analysis Program (STAP)

Delivery Order 0017: Active Vibration Suppression Technology Buffet Load Alleviation (BLA) Program

5a. CONTRACT NUMBER F33615-95-D-3216

5b. GRANT NUMBER N/A

5c. PROGRAM ELEMENT NUMBER 62201F

6. AUTHOR(S)

Jay K. Burnham

5d. PROJECT NUMBER 2401

5e. TASK NUMBER ST

5f. WORK UNIT NUMBER AP

7. PERFORMING ORGANIZATION NAME(S) AND ADDRESS(ES)

The Boeing Company
P.O. Box 516
St. Louis, MO 63166-0516

8. PERFORMING ORGANIZATION REPORT NUMBER

BOE BLEND-FINAL

9. SPONSORING/MONITORING AGENCY NAME(S) AND ADDRESS(ES)

Air Vehicles Directorate
Air Force Research Laboratory
Air Force Materiel Command
Wright-Patterson Air Force Base, OH 45433-7542

10. SPONSORING/MONITORING AGENCY ACRONYM(S)

AFRL/VASS

11. SPONSORING/MONITORING AGENCY REPORT NUMBER(S)

AFRL-VA-WP-TR-2002-3002

12. DISTRIBUTION/AVAILABILITY STATEMENT

Approved for public release: distribution is unlimited.

13. SUPPLEMENTARY NOTES

14. ABSTRACT

This report was developed under the STAP Delivery Order Contract F33615-95-D-3216 DO 0017.

This final report documents the development of an experimental buffet load alleviation (BLA) system that utilizes distributed piezoelectric actuators in conjunction with a closed-loop rudder control system to reduce the structural dynamic response of fighter aircraft vertical tails to buffet loads. The BLA system was defined analytically with a detailed finite element model of the tail structure and piezoelectric actuators. Oscillatory aerodynamics were included along with a buffet forcing function to complete the aeroservoelastic model of the tail with rudder control surface. Two single-input single-output (SISO) controllers were designed, one for the active rudder and one for the active piezoelectric actuators. The results from the analytical open- and closed-loop simulation were used to predict the system performance.

15. SUBJECT TERMS

SBIR Report, Vibration Suppression, Buffet Loads, Piezoelectric, Active Fiber Composite, Damping, Active Vibration Control, Unsteady Aerodynamics, Piezoelectric Actuator, Vibratory Rudder Actuation

16. SECURITY CLASSIFICATION OF:			17. LIMITATION OF ABSTRACT:	18. NUMBER OF PAGES	19a. NAME OF RESPONSIBLE PERSON (Monitor)
a. REPORT	b. ABSTRACT	c. THIS PAGE			Douglas A. Henderson
Unclassified	Unclassified	Unclassified	SAR	96	19b. TELEPHONE NUMBER *(Include Area Code)* (937) 255-5200 x407

TABLE OF CONTENTS

LIST OF FIGURES

LIST OF FIGURES (Continued)

LIST OF FIGURES (Continued)

LIST OF TABLES

1.0 INTRODUCTION

This report documents the results from the research and analysis performed by the Boeing Company from May 1999 through August 2000 under contract F33615-95-D-3216 with the USAF Research Laboratory, Wright-Patterson AFB. The contract required the development of an analytical model to simulate an active BLA control system for a fighter aircraft and specified the use of smart actuators, existing control surfaces, advanced amplifiers, and conventional control logic. To take advantage of previous research and development in BLA, the F/A-18A-D aircraft vertical tails were selected for the BLA system development in this report. Although the BLA system developed in this report is specific to the F/A-18 vertical tails, this technology could be adapted to other military and commercial platforms.

1.1 BUFFET BACKGROUND

The capability of modern fighter aircraft to sustain flight at high angles of attack and/or moderate angles of sideslip often results in immersion of part of the aircraft in unsteady, separated, vortical flow emanating from the aircraft's forebody or wings (Figure 1) The flow from these surfaces becomes turbulent and separated when the aircraft is flying at these conditions. This flow contains significant levels of energy over a frequency bandwidth coincident with low-order structural vibration modes of wings, fins, and control surfaces. The induced unsteady pressures that are applied to these lifting surfaces due to the turbulent flow are commonly referred to as buffet. The interaction of the buffet and the structure produces a structural-mode response known as buffeting. Prolonged exposure to the buffet loads has resulted in fatigue of structures on several aircraft. Damage to aircraft due to buffeting has led to redesigns of aircraft structure and increased support costs for the U.S. Air Force, U.S. Navy and the armed forces of other

countries. Time spent inspecting, repairing, and replacing structure impacts the mission availability of the aircraft.

Figure 1. High-Performance Aircraft (F/A-18) at High Angle of Attack (AOA)

For the F/A-18A-D aircraft, unsteady buffet loads from high angle of attack flight impinge on the vertical tails as shown in Figures 1 and 2. These buffet loads contribute toward the fatigue of the vertical tail structure along with the steady aircraft maneuver loads. Strains causing buffet fatigue damage result mainly from the vertical tail vibrating in its first two vibration modes: mode 1, tail 1st bending at ≈15 Hz, and mode 2, tail tail tip torsion at ≈45 Hz [1,2]. Fatigue damage is a function of vibration amplitude and time duration spent at the flight conditions. Plots that illustrate the sensitivity of the buffet fatigue damage to the flight conditions are shown in Figures 3 and 4. The range of dynamic pressure for fatigue damage of modes 1 and 2 is in Figure 3 and similarly, the range of angle of attack for fatigue damage is in Figure 4. The results from these figures are summarized in Table 1 which lists the critical flight conditions for buffet fatigue damage in Levesque [1].

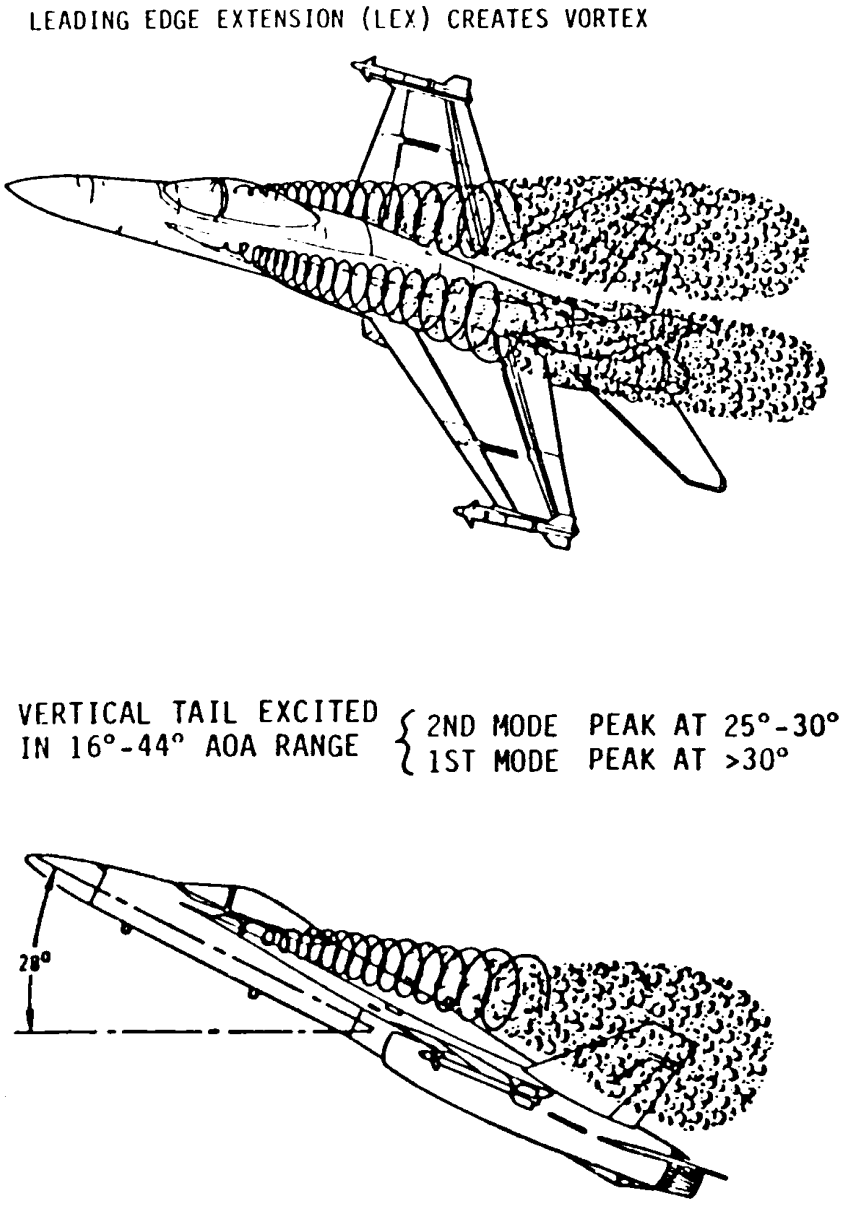

Figure 2. Buffet Excitation of F/A-18 Vertical Tails without LEX Fence

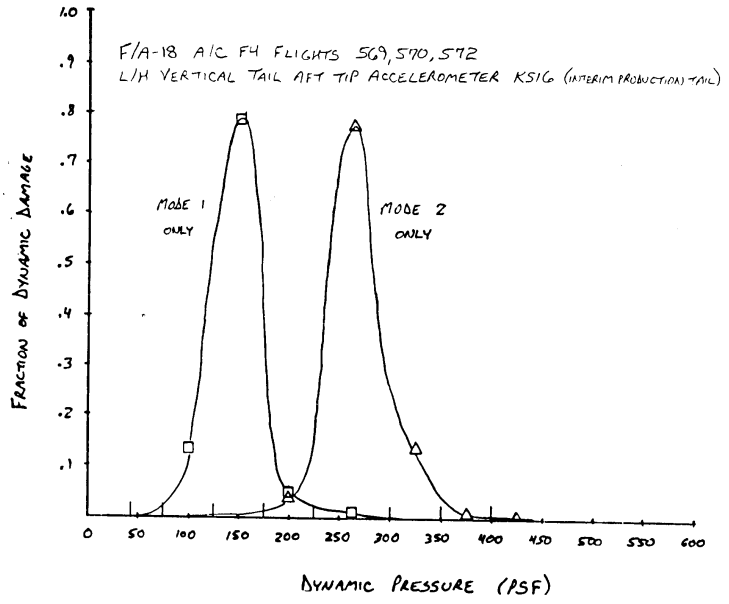

Figure 3. F/A-18 Vertical Tail Buffet Fatigue Damage versus Dynamic Pressure [1]

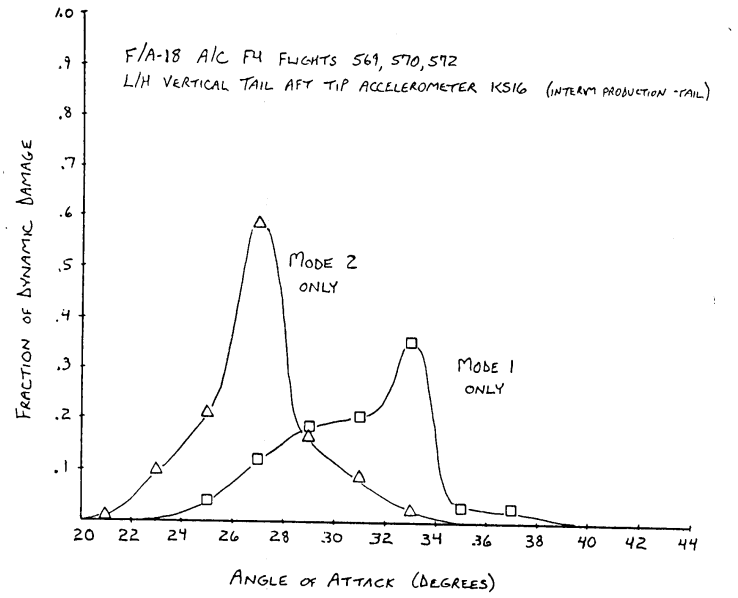

Figure 4. F/A-18 Vertical Tail Buffet Fatigue Damage versus AOA [2]

Table 1. Flight Conditions for F/A-18 Vertical Tail Maximum Buffet Fatigue

Mode	Frequency	Dynamic Pressure Range	AOA Range
1	15 Hz	100 to 200 psf	32 to 34 degrees
2	45 Hz	250 to 350 psf	26 to 28 degrees

The fraction of dynamic damage in Figures 3 and 4 represents the percentage of modal fatigue damage for the aircraft lifetime. For example, a 0.8 fraction of dynamic damage represents 80% of the modal fatigue damage for an aircraft lifetime. For the mode 1 response, over 90% of the buffet fatigue damage occurs in the 75 to 225 psf dynamic pressure range and approximately 75% of the damage occurs within the narrow angle-of-attack range spanning 28°-34°. Similarly for the mode 2 response, over 90% of the damage occurs in the 175-350 psf dynamic pressure range, and approximately 80% of the damage occurs in the angle of attack range of 24°-30°.

1.2 BLA BACKGROUND

Several methods have been investigated previously in an effort to reduce the buffet response and increase the fatigue life of vertical tails on military aircraft. One approach to solving this issue was to add passive damping material to the tails while they are being manufactured Liguore, et al. [3]. Another approach increased the bending stiffness of the tails Ferman, et al. [4]. The F/A-18A-D aircraft have additional structure added to the vertical tails in conjunction with a fence on the wing leading edge extension (LEX) that disperses the vortex prior to impinging on the vertical tail [1,2]. The additional structure in combination with the LEX fence produces a vertical tail that exceeds the fatigue requirements of the U.S. Navy (6,000-hour lifetime). More recently, the F/A-18E/F aircraft has removed the LEX fence and changed the shape of the LEX to relocate the LEX vortices, which reduces the buffet excitation on the vertical tail. These

techniques have been successful at reducing the buffet response of the vertical tails but have increased the cost and gross weight of the vehicle in varying degrees.

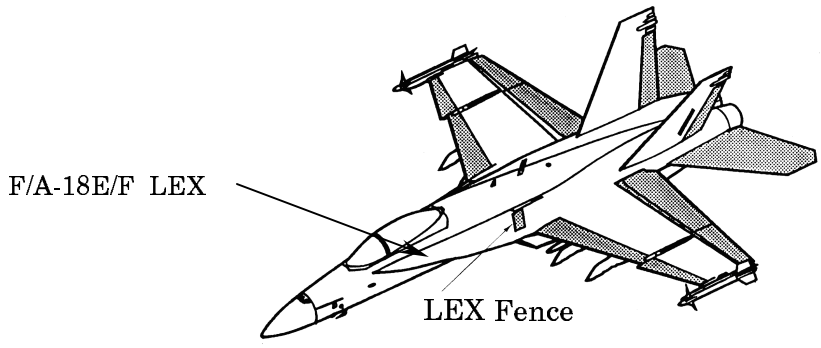

Figure 5. Redesigned LEX on F/A-18E/F for Vertical Tail Buffet Reduction

Another method to reduce the buffet response incorporated an active control system that deflects the rudder in response to measured motion at the tip of the tail [5,6]. This method increases the fatigue life at most angles of attack through control of mode 1 (F/A-18 vertical tail first bending) at 15 Hz. This method is limited to controlling the response of the structural modes within the rudder actuation bandwidth (< 20 Hz on F/A-18A-D aircraft), and therefore, it is not as effective for reducing the fatigue damage from mode 2 at 45 Hz (vertical tail tip torsion).

Investigations and tests of active control of the vertical tail vibration response using smart materials (piezoelectric actuators) distributed over the vertical tail structure has proven to be successful at reducing the overall buffet response [7,8]. The results from a full-scale test on the F/A-18 vertical tail with a piezoelectric actuator-based active control system are documented in Spangler [8]. The testing was completed during 1997 and 1998 at the International Follow-On Structural Test Program (IFOSTP) facility in Melbourne, Australia. The results from the test indicated that the piezoelectric actuators attached to the skin were more effective at reducing the

response of mode 2 (tip torsion at 45 Hz) than mode 1 (first bending at 15 Hz) as shown by the fatigue life improvement comparison in Figure 6 [8].

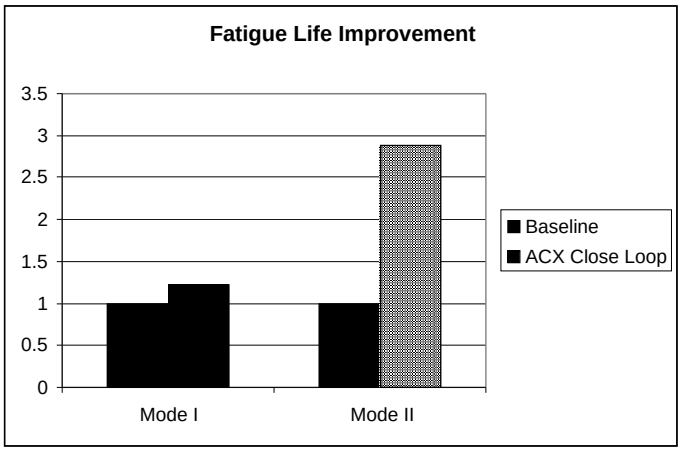

Figure 6. F/A-18 Vertical Tail Fatigue Life Improvement with Active Piezoelectric System [8]

1.3 REPORT ORGANIZATION

This report is organized into nine sections as listed in the Table of Contents. In general, the report is in chronological order with the completion of the BLA system definition and analyses performed. First, an overview of the BLA system design and functional requirements is in Section 2.0, followed by documentation of the finite element model of the vertical tail and piezoelectric actuators, Section 3.0. The analytical aerodynamics used in the system analysis are defined in Section 4.0. This includes the oscillatory aerodynamics and buffet aerodynamic forcing function. The candidate piezoelectric actuators were compared for BLA system performance and cost. The results of these analyses and the recommended actuators are in Section 5.0. The aeroservoelastic model is documented in Section 8.0. The development of the single-input, single-output (SISO) controller for both the rudder and piezoelectric actuators is in Section 7.0. The results from the analytical simulations of the open and closed BLA system are in Section 8.0, along with the results from the fatigue analysis.

1.4 ACKNOWLEDGEMENTS

This work on the Active Vibration Suppression Technology – BLA Program was performed for the U.S. Air Force Research Laboratory (AFRL), under the STAP contract number F33615-95-D-3216 for the period of 26 May 1999 through 31 August 2000. The Boeing Co. would like to thank Mr. Douglas Henderson, contract technical monitor from AFRL, for his professional oversight of this program and for providing technical assistance and program coordination. Mr. Henderson was responsible for assembling The Technical Cooperation Program (TTCP) representatives for the midterm program review. This international team made up of partners from Canada, Australia, and the United States completed a technical program review and developed plans for future BLA research and testing.

The Boeing Co. would also like to acknowledge the work and assistance from Dr. Robert Moses of NASA LaRC on developing the control laws for the active rudder and piezoelectric actuators. Dr. Moses was a valuable asset on this program because of his expertise and experience in BLA programs.

2.0 BLA SYSTEM DESIGN

2.1 SYSTEM DEVELOPMENT

The development of the BLA system for the F/A-18 vertical tail began with research into existing BLA systems to establish a benchmark for system design. Extensive research and testing has been completed in the past 10 years on the development of an active BLA system for vertical tails of fighter aircraft, as described previously in Section 1.2. The results from this research identified two systems that have been effective at actively reducing the buffet response of a

vertical tail. The first system employs the rudder control surface to actively control the vertical tail dynamic response [5,6] and the second system utilizes piezoelectric actuators attached to the skin [7,8]. National Aeronautics and Space Administration (NASA) Langley Research Center (LaRC) developed the combination of these two systems under the SIDEKIC program [9].

The blended system of the rudder and piezoelectric actuator technologies documented in Moses [9] was selected as the basis for the design of the F/A-18 vertical BLA system in this piezoelectric actuators are used to control mode 2 (tip torsion mode near 45 Hz) utilizes the report Figure 7. The application of this combined system in which the rudder actuator is used to

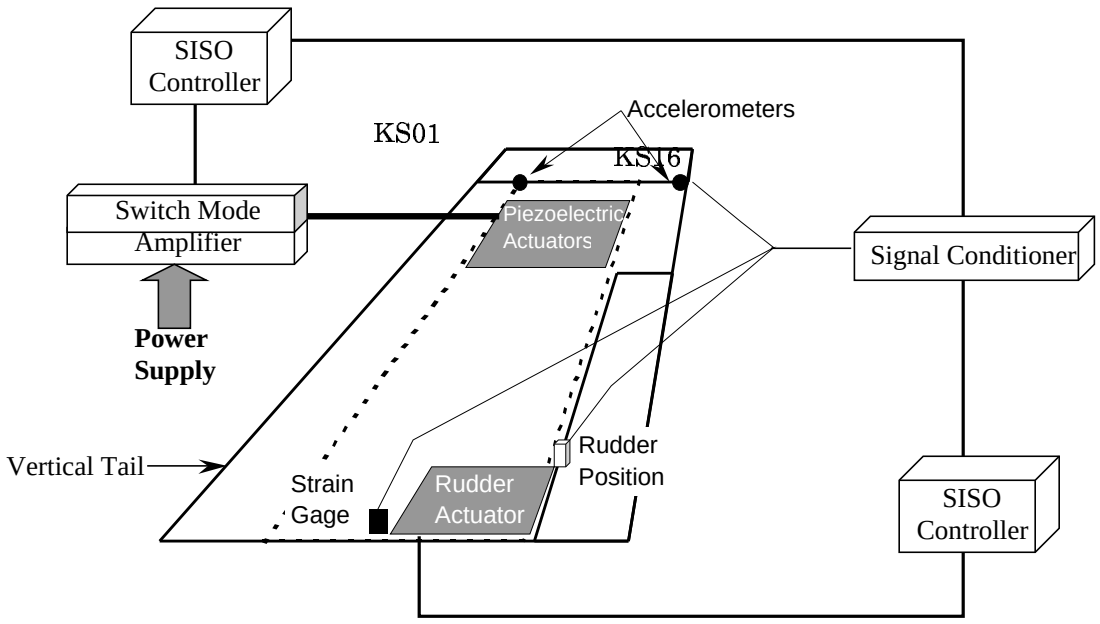

Figure 7. Major Components of BLA System

control the response of the tail mode 1 (first bending near 15 Hz) and the most effective features of each system. The rudder actuator BLA system wind tunnel test [6] was shown to be more effective at reducing the buffet response of mode 1 (30 percent reduction) than mode 2 (12

percent reduction). Additionally, the current F/A-18A-D aircraft rudder actuation bandwidth upper limit is 20 Hz, and therefore, this system would not be economical to extend the control beyond mode 1 (15 Hz). The results from a full-scale ground test of a piezoelectric actuation system [8] proved this system to be effective at reducing the buffet response of mode 2 and only marginally effective for mode 1. The major problem with using the piezoelectric actuators (attached to the tail skin) for controlling mode 1 arises from the strain energy distribution for this mode and the stiffness of the tail structure near the root. From the finite element model (FEM) results in Section3.0, 40 percent of the modal strain energy for mode 1 is in the root springs of the model that represents the aircraft aft fuselage compliance and 50 percent of the modal strain energy is in the tail skins. Of this 50 percent in the tail skins, the majority is located near the root of the tail. The piezoelectric actuators are ineffective near the tail root because of the large structural stiffness in this region (skins greater than 0.2 inch thick supported by the tail attachment root rib). In contrast to this, the piezoelectric actuators are very effective for mode 2 because this mode has 60 percent of the modal strain energy in the tail skins, and this strain energy is concentrated in the upper third of the vertical tail where the skin thickness is closer to a tenth of an inch (0.07 to 0.15 inch).

The major components of the active BLA system are shown in Figure 7. The blended actuator system includes a separate single-input, single-output (SISO) controller for each system. The existing aircraft rudder actuator and servo system is combined with a SISO controller, sensors, and signal conditioner to complete the active rudder system. The piezoelectric actuator system is similar except that the switch mode amplifier, which is connected to the aircraft power supply, drives the piezoelectric actuators. Both systems utilize the response of the two accelerometers and strain gage, shown in Figure 7. The rudder actuation system includes the RVDT to provide rudder position feedback.

2.2 FUNCTIONAL REQUIREMENTS

The functional requirements of the BLA as they apply to both a ground test and a flight test aircraft were listed in Section 2 of Spangler [8]. The requirements for the system integration onto the F/A-18 aircraft are listed in Table 2. The system requirements identify the frequency range, fatigue critical vibration modes, system mass, power requirements and cost.

The BLA system objective is to reduce the buffet response of the F/A-18 vertical tail and extend the operational life of the structure. The current U.S. Navy F/A-18 aircraft service life is 6,000 hours, and the vertical tails are critical, with a life of about 7,500 hours. The next critical component is the wing, with an estimated life of 10,000 hours. A life extension of the vertical tails beyond 10,000 hours would then make the wing critical. To align this work with an initiative on the F/A-18 for a 12,000-hour service life, the target fatigue life extension for the vertical tail is 4,500 hours (12,000 – 7,500). The fatigue critical location on the vertical tail is on the aft root spar, at the tail to aft fuselage attachment. Fatigue analyses at this location have indicated that 41 percent of the fatigue damage is from aircraft maneuver loads and 59 percent is from buffet loads (26 percent mode 1 and 33 percent mode 2). A 25 percent reduction in the buffet loads would exceed the 4,500-hour lifetime extension and exceed the 12,000-hour service life target. The analytical BLA system performance goal was doubled from 25 percent to 50 percent reduction in buffet response to account for differences in the analytical model when compared to test results [9]. The analytical representation of the rudder aeroservoelastic (ASE) model tends to overpredict the rudder effectiveness. The analytical model can be improved with correlation to measured flight test data. The use of free-strain parameters for the piezoelectric

actuators leads toward overpredicting the performance, along with unaccounted for losses due to stacking the actuators and the general nonlinear behavior of the actuators.

Table 2. BLA System Requirements for F/A-18 Aircraft

BLA System	F/A-18 Aircraft Requirement
Frequency Bandwidth	1 – 100 Hz
Critical Vibration Modes: Mode 1 (1st Bending) Mode 2 (Tip Torsion)	 15 – 20 Hz 32 – 52 Hz
Performance Requirement	50percent reduction in RMS response
Mass Added to Tail	< 25 lb. per tail
Total BLA System Mass	< 60 lb. per tail
Operating Temperature	Max Range of -106 °F to +248 °F
Barometric Pressure	3 – 30 in. Hg
Humidity	100percent condensing
Envelope	Actuators not to interfere with spars or internal equipment. Electronics in gun bay or external fuel tank
Power	Able to run on aircraft power supply, Drawing < 25percent of single generator capacity (108-118 VAC at 400 Hz, 3 phase – F/A-18 generator) (28 VDC aircraft power supply)
Cost	<25percent of tail redesign cost to develop system <25percent of tail replacement cost to produce/integrate system
Max. Piezoelectric Voltage	± 1500 Volts (range for two switch mode amplifiers)
System Life	Aircraft life with proper maintenance and component replacement
Maintenance Interval	Aircraft maintenance intervals
Flight Qualification	Flight qualification required

2.3 ANALYTICAL MODELING

In this section, the various mathematical models used in the development of the BLA system are described. The modal equations for aeroelastic response were used to develop a state space representation of the system, similar to previous documented research [5-8]. The total degrees of freedom of the structural dynamic equations of motion for a flexible structure are greatly reduced by transforming the equations from physical coordinates, xyz, to modal coordinates, q. Several controllers were designed and analytical simulations were completed to evaluate the BLA system. The modeling tools used at Boeing in the F/A-18 Structural Dynamics group were utilized to complete this task, namely NASTRAN for structural modeling, N5KM (doublet lattice) for aerodynamic modeling, FAMUSS (Flexible Aircraft Modeling Using State Space) for aeroservoelastic modeling, MATLAB® and SIMULINK for controller design and system simulation.

The F/A-18 vertical tail structure was modeled in NASTRAN, as described in Section 3.1. The results from the normal modes analysis compare well with the measured results, as described in Section 3.1. The normal modes analysis in NASTRAN produces vibratory frequencies, ω, and mode shapes, φ.

The unsteady aerodynamic forces of the vertical tail were represented using a linear doublet lattice computer code, N5KM, as described in Section 4.1. The unsteady aerodynamic forces on the tail result from the tail vibratory motion and are not to be confused with the buffet aerodynamic force on the tail described in Section 4.2. The unsteady aerodynamic forces on the tail are transformed from physical coordinates, xyz, to modal coordinates, q. The NASTRAN vibratory mode shapes, φ, were combined with the unsteady aerodynamic influence coefficient

(AICs) to generate generalized aerodynamic forces at a series of reduced frequencies (k=ωb/V; where ω=oscillatory frequency, b=semi-chord, and V=velocity). These generalized aerodynamic forces were combined with the generalized mass, M, and generalized stiffness, K. Modal damping is expressed as structural damping, g, and is part of the complex stiffness term. The initial equation of motion for the flexible tail in modal coordinates, q(t), is in Equation 1.

$$M\ddot{q}(t) + K(1 + jg)q(t) = \frac{1}{2}\rho V^2 Q(k)q(t) \quad . \qquad 1$$

Equation 1 is solved to assess the aeroelastic stability of the flexible tail. The results from the flutter analysis compared well with the Boeing F/A-18 Project analysis and are in Section 4.1.

The buffet aerodynamic force on the vertical tail was modeled with a similar approach as used in Spangler [8] and is described in Section 4.2. The buffet force is modeled as a Gaussian white noise process with shaping filters and is applied to the vertical tail model at the same location as the IFOSTP shaker attachment [8]. The shaping filters were scaled to match measured response from flight test data as described in Section 4.2 for the six flight conditions analyzed. The unit buffet force, $F_{buf}(t)$, was added to the right hand side of Equation 1 to obtain Equation 2.

$$M\ddot{q}(t) + K(1 + jg)q(t) - \frac{1}{2}\rho V^2 Q(k)q(t) = F_{buf}(t) \quad . \qquad 2$$

The modal force from the piezoelectric actuators was determined from the analytical actuation of the piezoelectric elements on the vertical tail model (Section 3.2). The model was loaded with a delta temperature across the piezoelectric elements that produced a specified strain in these elements (Section 3.2). The resulting grid point forces in the model were multiplied by the

corresponding vibration modeshape for each degree of freedom to determine the piezoelectric modal force, F_{piezo}. The piezoelectric actuator force was added to the right-hand side of Equation 2.

$$M\ddot{q}(t) + K(1+jg)q(t) - \frac{1}{2}\rho V^2 Q(k)q(t) = F_{buf}(t) + F_{piezo}(t) \quad . \qquad 3$$

The aeroservoelastic model for rudder control is described in Section 6. Because the vertical tail structural modes are excited by the rudder control surface deflections, the equations of motion were rewritten to account for the aircraft control surface deflections. The control surface inertia effects, $[M_c]$, and aerodynamic effects, $Q_c(k)$ are included in Equation 4 on the right-hand side with the system input U(t). The buffet modal force and the piezoelectric actuator modal force were separated into a magnitude, F, and a commanded system input, U(t):

$$M\ddot{q}(t) + K(1+jg)q(t) - \frac{1}{2}\rho V^2 Q(k)q(t) = -M_c\ddot{U}(t) + \frac{1}{2}\rho V^2 Q_c(k)U(t) + F_{buf}U(t) + F_{piezo}U(t) \quad . \qquad 4$$

The transfer function frequency response of Equation 4 was computed from the Laplace transform as given by Equation 5. This is the technique used in FAMUSS [12].

$$\left[Ms^2 + K(1+jg) - \frac{1}{2}\rho V^2 Q(k) \right] q(s) = \left[-M_C s^2 + \frac{1}{2}\rho V^2 Q_C(k) + F_{buf} + F_{piezo} \right] u(s) \quad . \qquad 5$$

Equation 5 can be rewritten as a transfer function, output/input. The output is the modal coordinates q and the input is u. This produces the modal transfer function response of the modal coordinates for a rudder input, buffet force input, and piezoelectric actuator input, where $s=j\omega$ and $k=\omega b/V$, as follows:

$$H_q(s) = \frac{q(s)}{u(s)} \quad . \tag{6}$$

$$H_q(s) = \left[Ms^2 + K(1+ jg) - \frac{1}{2}\rho V^2 Q(k) \right]^{-1} \bullet \left[- M_C s^2 + \frac{1}{2}\rho V^2 Q_C(k) + F_{buf} + F_{piezo} \right]. \tag{7}$$

The modal transfer function is transformed to the physical coordinate system using the vibratory mode shapes, ϕ. Equation 8 gives the transfer function in the physical coordinates.

$$H(s) = \frac{y(s)}{u(s)} = \frac{\phi_C q(s)}{u(s)} = \phi_C H_q(s) \, . \tag{8}$$

Equation 7 was solved in FAMUSS [12], over the frequency range of interest, 0.5 to 100 Hz. The transfer function is calculated over a series of frequencies, ω, or Laplace variables, $s=j\omega$. This process involves interpolating the tabulated unsteady aerodynamic terms of Q(k) and Q_c(k), which are a function of $k=\omega b/V$, over the frequency range of interest, ω. A separate transfer function is calculated for each input-output pair.

The next step in FAMUSS was to create an equivalent state space model that could be used in the subsequent time domain transient analysis, SIMULINK. The state space equations are written as follows:

$$\begin{aligned} \dot{x}(t) &= A\, x(t) + B\, u(t) \\ y(t) &= C\, x(t) + D\, u(t) \end{aligned} \quad . \tag{9}$$

Again, FAMUSS was used to develop an equivalent state space model, Equation 9, which matched the original transfer function response, Equation 8. The transfer function frequency

response for a Multi-Input, Multi-Output (MIMO) state space model is shown in matrix form in Equation 10.

$$\hat{H}(s) = C\left[sI - A\right]^{-1}B + D\,. \qquad 10$$

FAMUSS [12] uses a nonlinear optimization technique to determine the individual terms of the state matrices A, B, C, and D that best fits the transfer function response at each tabulated frequency, ω. The resulting aeroservoelastic (ASE) state space model from FAMUSS had three inputs: 1) rudder rotation, 2) buffet force, and 3) piezoelectric actuator force. The six flight conditions for analysis are defined in Section 4.2.

The Math Works Inc. software MATLAB® was used to perform a time history simulation of the vertical tail buffet response. The state space model was incorporated into the MATLAB SIMULINK toolbox. The results from the open-loop system analysis are in Section 8.1. The design of the rudder controller and piezoelectric actuator controller is described in Section 7.0. The results from the closed-loop system simulations are in Section 8.2.

3.0 STRUCTURE MODEL

3.1 VERTICAL TAIL STRUCTURE MODEL

The F/A-18 vertical tail structure was modeled with a modified NASTRAN FEM that Boeing received from AFRL. The original detailed plate/shell model was used in the BLA system analysis from [8]. The model was verified to be similar to the existing detailed model used by

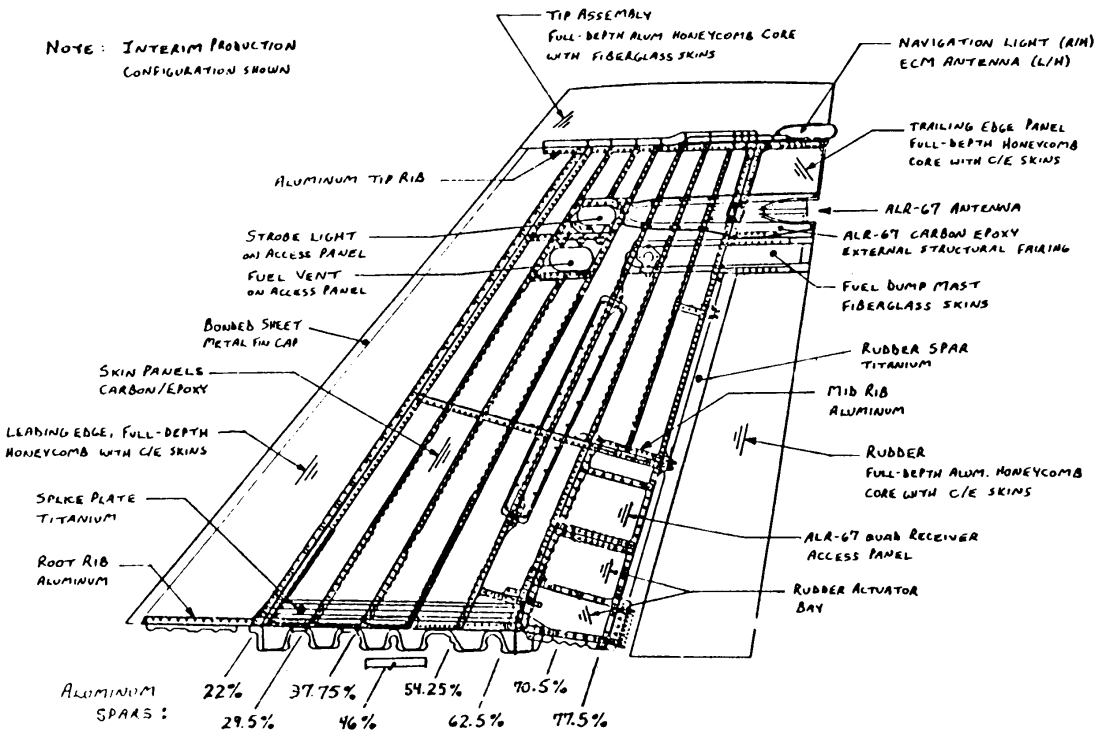

Figure 8. F/A-18 Vertical Tail Structural Arrangement

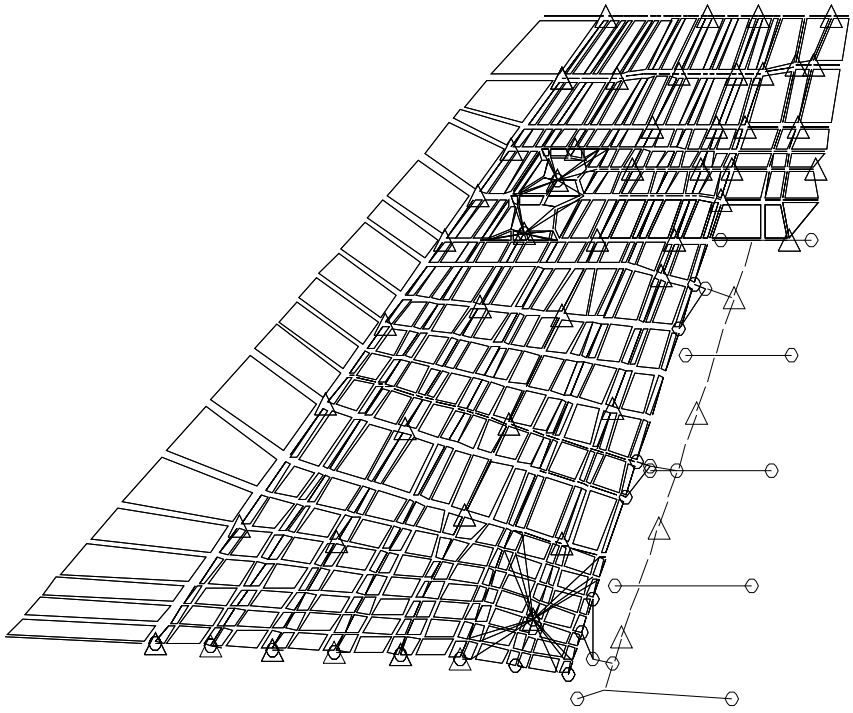

Figure 9. F/A-18 Vertical Tail Finite Element Model

the Boeing F/A-18 project structural dynamics team. The model was updated to include the grids needed for the oscillatory aerodynamic model defined in the next section of this report.

The F/A-18 vertical tail structural arrangement is shown in Figure 8 and a similar view of the FEM is in Figure 9. The detailed model includes the skin elements, spars and ribs. The locations of lumped mass in the model are identified by triangles in Figure 9. The total weight of the model was 284 pounds. The model is cantilevered with attachment springs along the root to represent the compliance of the aft fuselage. The rudder is modeled along the rudder elastic axis with bar elements and attached to the vertical tail with a rotational spring, which represents the rudder actuator.

The results from the normal modes analysis of the model are listed in Table 3 along with the measured frequencies from a ground vibration test of an F/A-18 aircraft in September 1984. The analytical-to-measured percent difference in frequency is less than 3 percent for the buffet critical modes 1 and 2.

Table 3. Comparison of Analytical Model and Measured Modal Frequencies

V. Tail Mode	Description	Analytical Model Frequency - Hz	Measured Frequency - Hz	Percent Difference percent
1	1st Bending	15.3	15.3	0.0percent
2	Tip Torsion	44.7	46.0	-2.8percent
3	Rudder Rotation	49.6	49.6	0.0percent
4	2^{nd} Bending	64.4	73.8	-12.7percent
5	Tip 2^{nd} Torsion	92.9	84.2	-10.3percent

The modeshapes of the first four modes of the analytical model are displayed in Figures 10 through 13. Two views are displayed for each mode, a trimetric view and front view. The

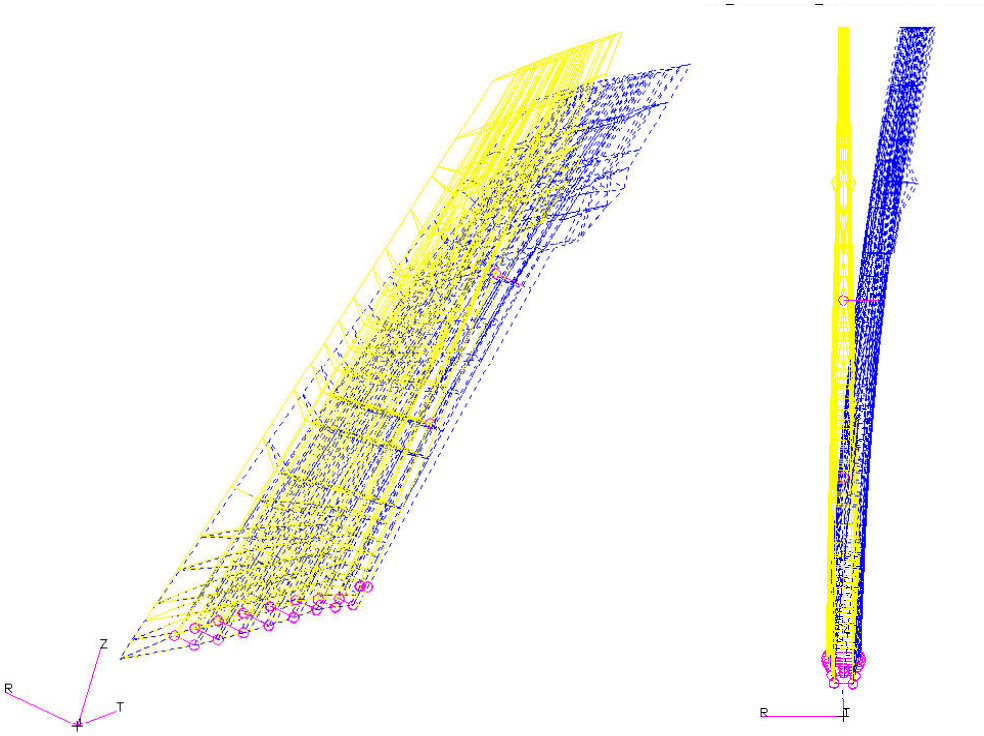

Figure 10. Baseline Analytical Modeshape: Mode 1, 15.3 Hz, 1st Bending

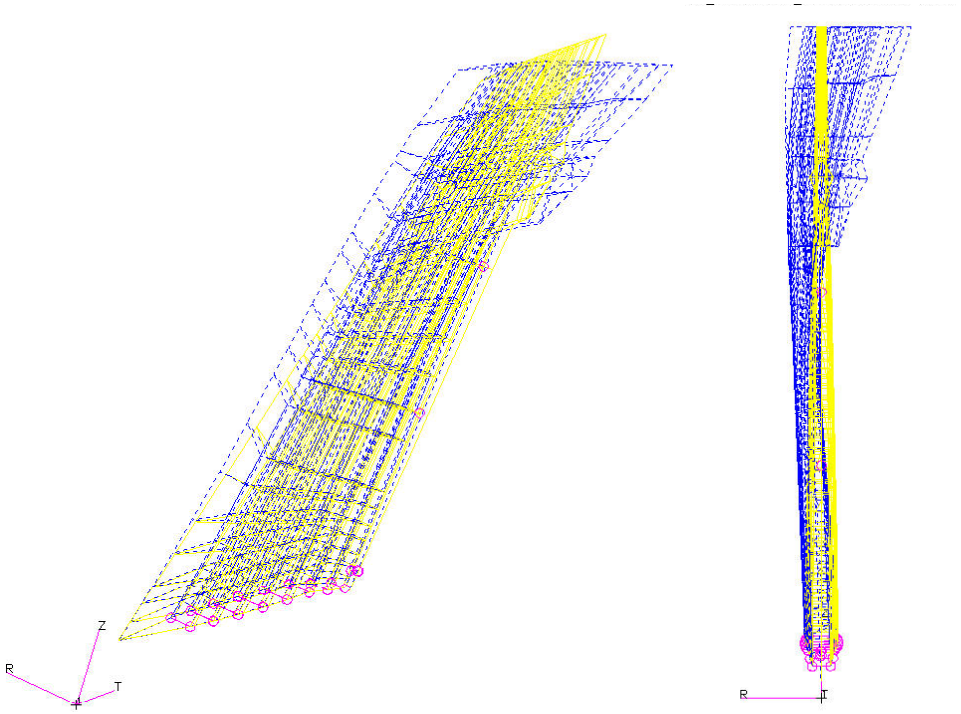

Figure 11. Baseline Analytical Modeshape: Mode 2, 44.7 Hz, Tip Torsion

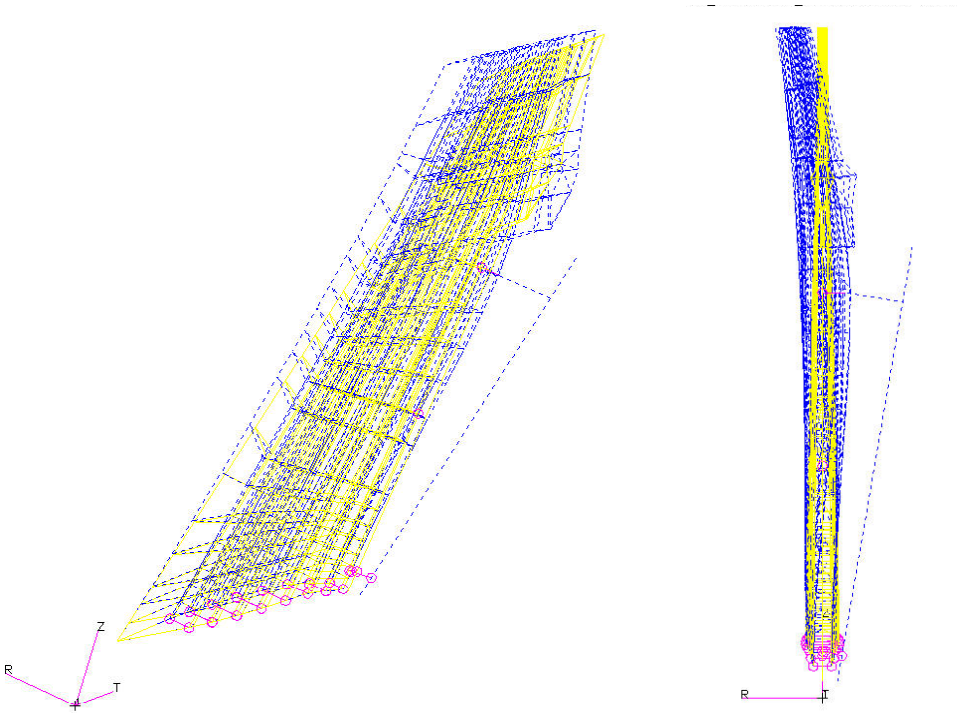

Figure 12. Baseline Analytical Modeshape: Mode 3, 49.6 Hz, Rudder Rotation

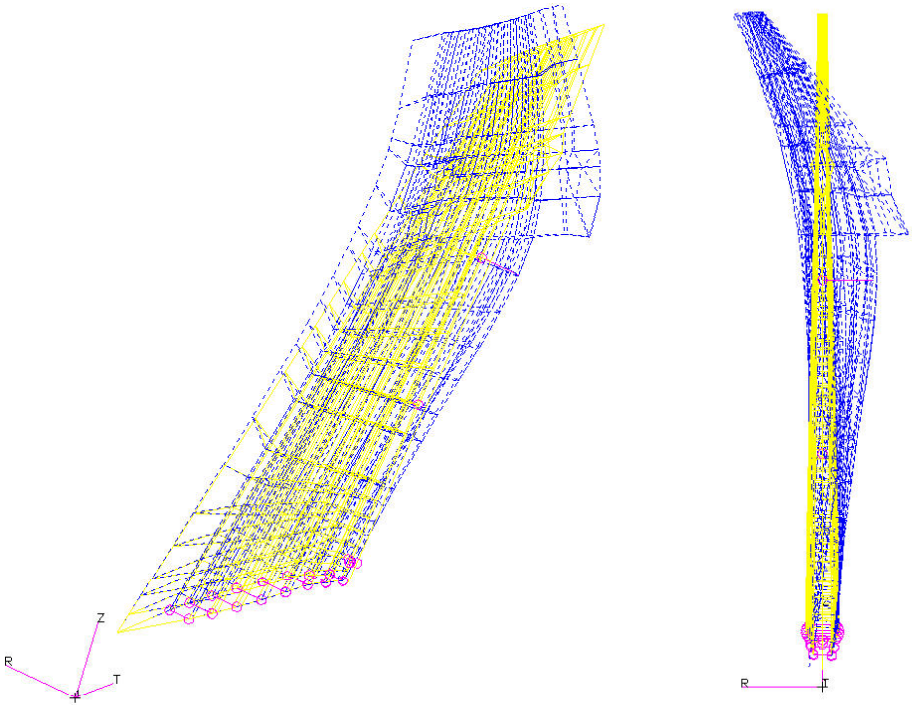

Figure 13. Baseline Analytical Modeshape: Mode 4, 64.4 Hz, 2nd Bending

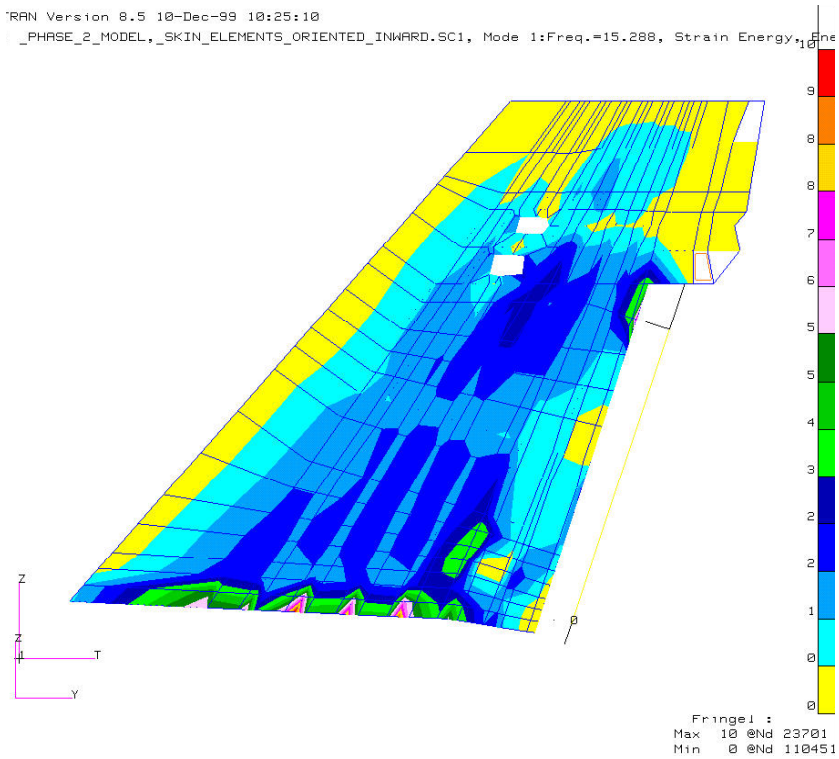

Figure 14. Baseline Modal Strain Energy Density: Mode 1, 15.3 Hz, 1st Bending

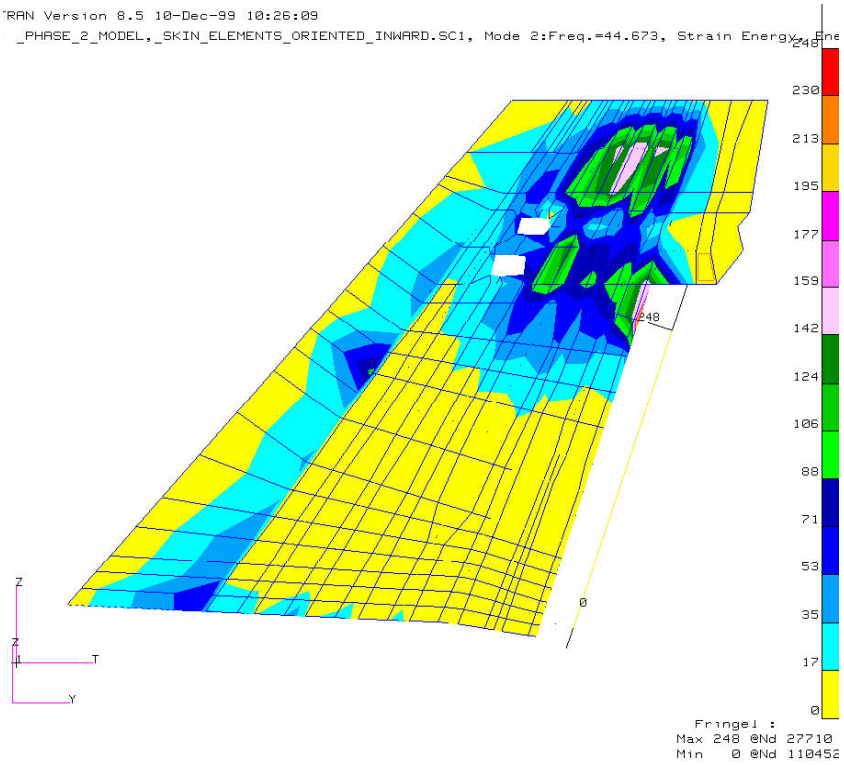

Figure 15. Baseline Modal Strain Energy Density: Mode 2, 44.7 Hz, Tip Torsion

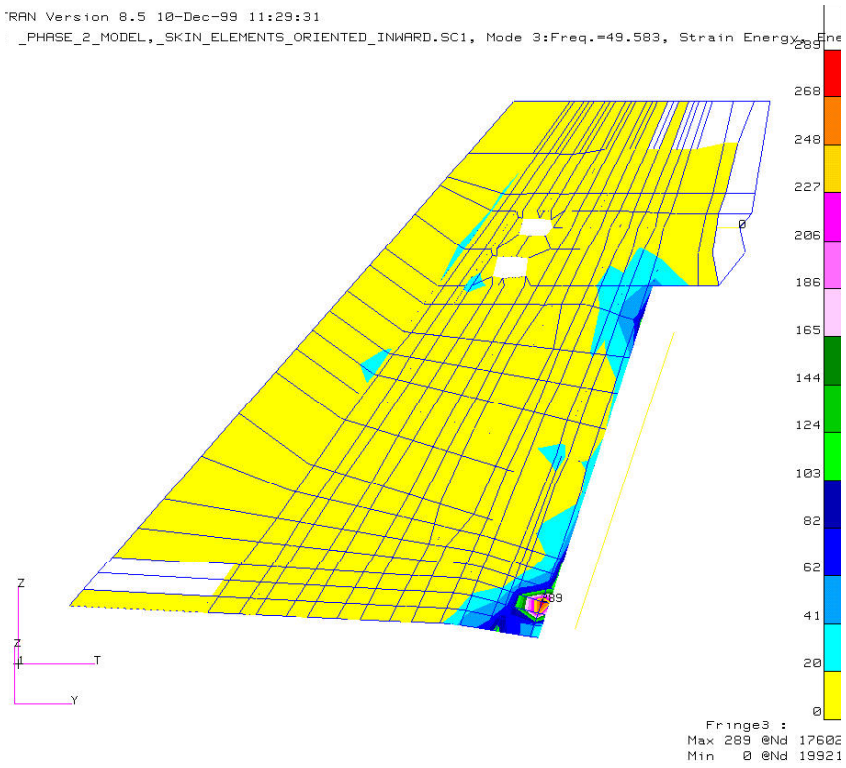

Figure 16. Baseline Modal Strain Energy Density: Mode 3, 49.6 Hz, Rudder Rot.

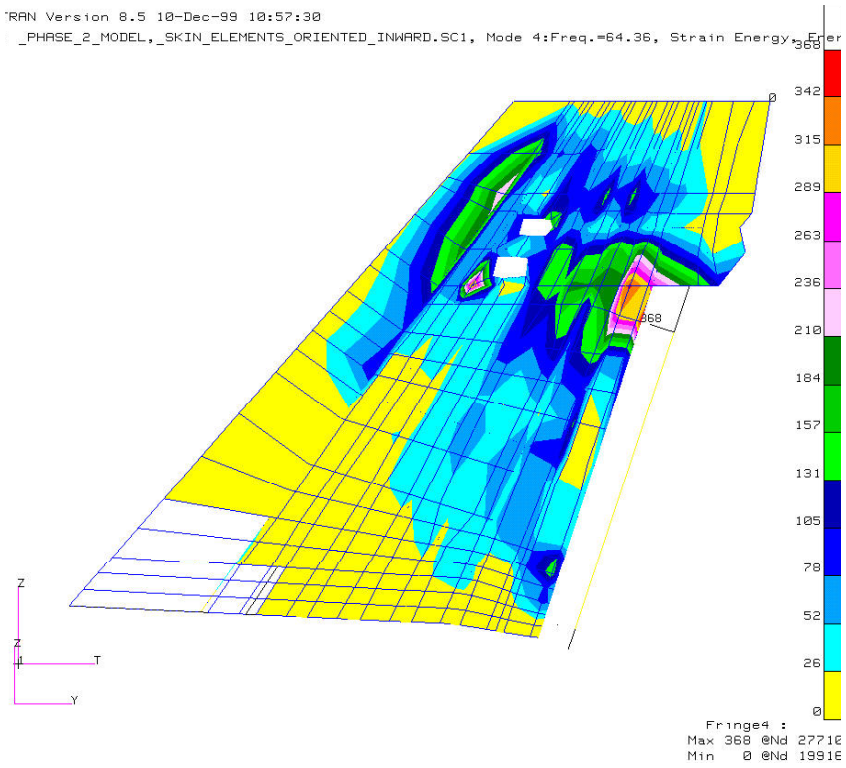

Figure 17. Baseline Modal Strain Energy Density: Mode 4, 64.4 Hz, 2nd Bending

undeflected shape is a solid line with yellow color and the deflected shape is a dashed line with blue color. Color contours of the modal strain energy densities for the external elements of the model are displayed in Figures 14 through 17. The white, yellow and blue colors represent the lowest strain energy densities, while the orange and red represent the highest strain energy densities. The component strain energy percentages for each mode are listed in Table 4. This information is useful in conjunction with the strain energy density contours in making qualitative assessments of piezoelectric actuator effectiveness. Comparisons of the mode shapes to shapes generated by the ground test were not conducted. Any differences will have an effect upon the optimal placement and orientation of the piezoelectric actuators. Before flight test, accurate mode shapes must be generated of the vertical tail and used to validate the analytical model.

Table 4. Analytical Model Modal Strain Energy Percent Distribution

	Mode 1	Mode 2	Mode 3	Mode 4
Frequency	15.3 Hz	44.7 Hz	49.6 Hz	64.4 Hz
Root Springs (Aft Fuselage)	39%	14%	1%	1%
Skin	48%	61%	23%	64%
Spars and Ribs	11%	15%	3%	13%
Rudder	1%	2%	31%	4%
Rudder Hinge Spring	0%	1%	41%	12%
Antenna and Fuel Dump	1%	7%	1%	7%

3.2 PIEZOELECTRIC ACTUATOR MODEL

The BLA system utilizes the piezoelectric actuators to actively control the vertical tail second vibration mode, mode 2 tip torsion at 45 Hz. The F/A-18 vertical tail model documented in the previous section was modified to include the piezoelectric actuator elements. The piezoelectric actuators are defined in Section 5 of this report. The piezoelectric actuators were modeled in NASTRAN as structural plate elements (CQUAD4, PSHELL, MAT1 and MAT8) and were offset

from the existing skin elements, similar to the modeling practices used in Spangler [8] and Barmac [10].

The first step in modeling the piezoelectric actuators was to determine the vertical tail skin area for attaching the actuators. The results from the normal modes analysis from the previous section were used for this evaluation along with the restrictions on where actuators can be physically attached to the vertical tail skin. The actuators can be attached to the vertical tail skin panel areas between the 22 percent and 77.5 percent spars and not within the region of the strobe light, fuel vent, ALR-67 antenna, and Fiberglas tip assembly (Figure 3.1). A color

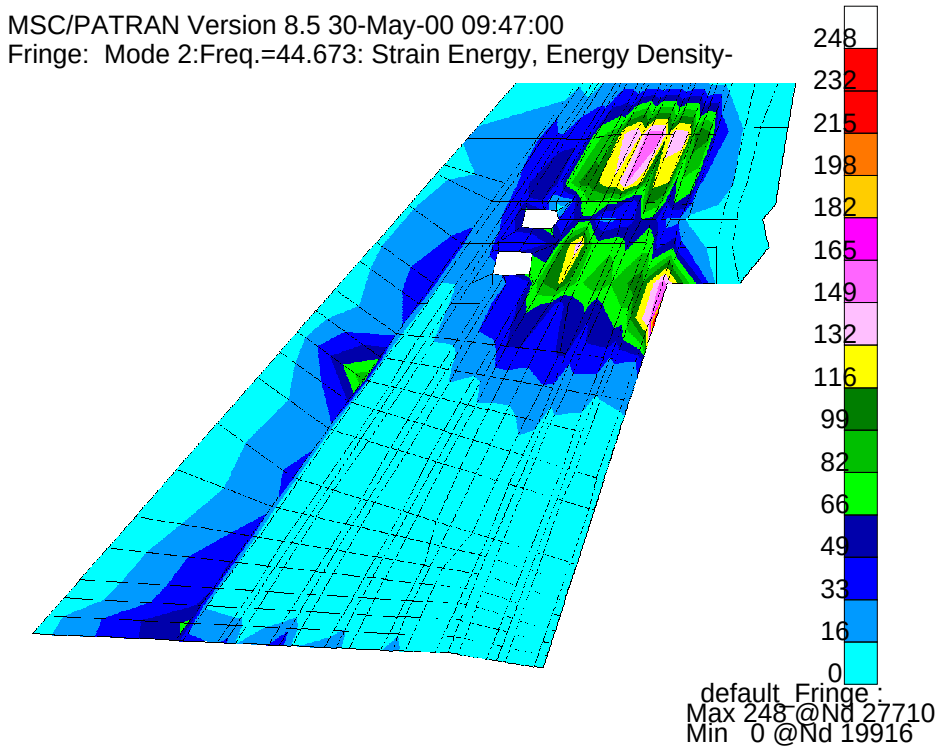

Figure 18. Mode 2 (44.7 Hz) Strain Energy Density Contour for Skin Elements

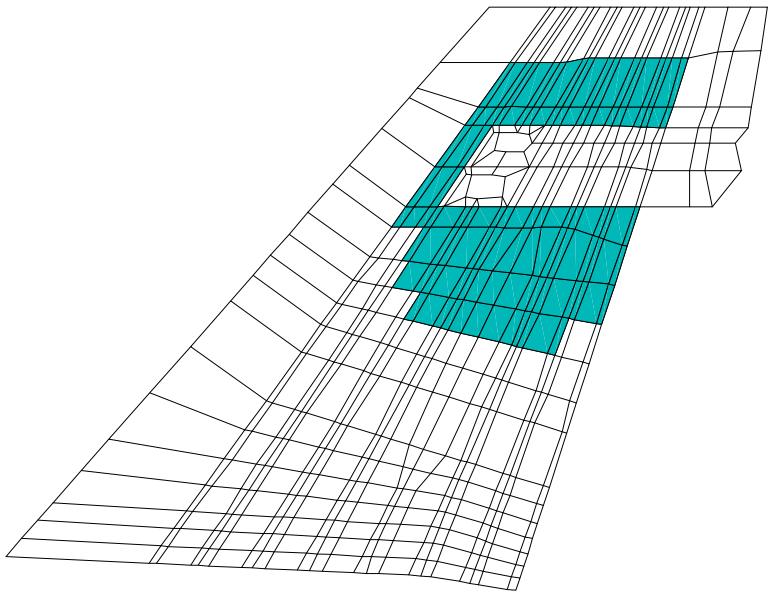

Figure 19. Analytical Model Skin Elements Selected for Piezoelectric Actuators

contour of the strain energy density for mode 2 is displayed in Figure 18 for the model skin elements. This contour reveals that the strain energy is in the upper half of the vertical tail skin and that the highest densities are in the upper third. The initial area selected for piezoelectric actuators is shown in Figure 19.

The selection of the piezoelectric actuators for the BLA system is described in Section 5, which includes a listing of the candidate actuator mechanical and electrical properties. The candidate piezoelectric actuators for the BLA system could be subdivided into two categories for FEM: 1) isotropic plates (d31 piezoelectric actuation), and 2) orthotropic plates (d33 piezoelectric actuation). The isotropic plates were used to represent the monolithic piezoceramic material with solid plate electrodes that utilize the d31 piezoelectric charge constant. The orthotropic plates were used to represent the piezoelectric actuators with interdigitated electrodes (IDE) in lieu of the solid plate electrodes. The IDE creates an electric field along the piezoceramic

material to utilize the d33 piezoelectric charge constant. A comparison of the two different piezoelectric actuation mechanisms is shown in Figure 20. The solid line depicts the undeflected shape of the piezoelectric actuator and the dashed line depicts the powered, deflected shape (not to scale) for a fixed voltage polarity. The deflected shapes would change signs for a reversal in

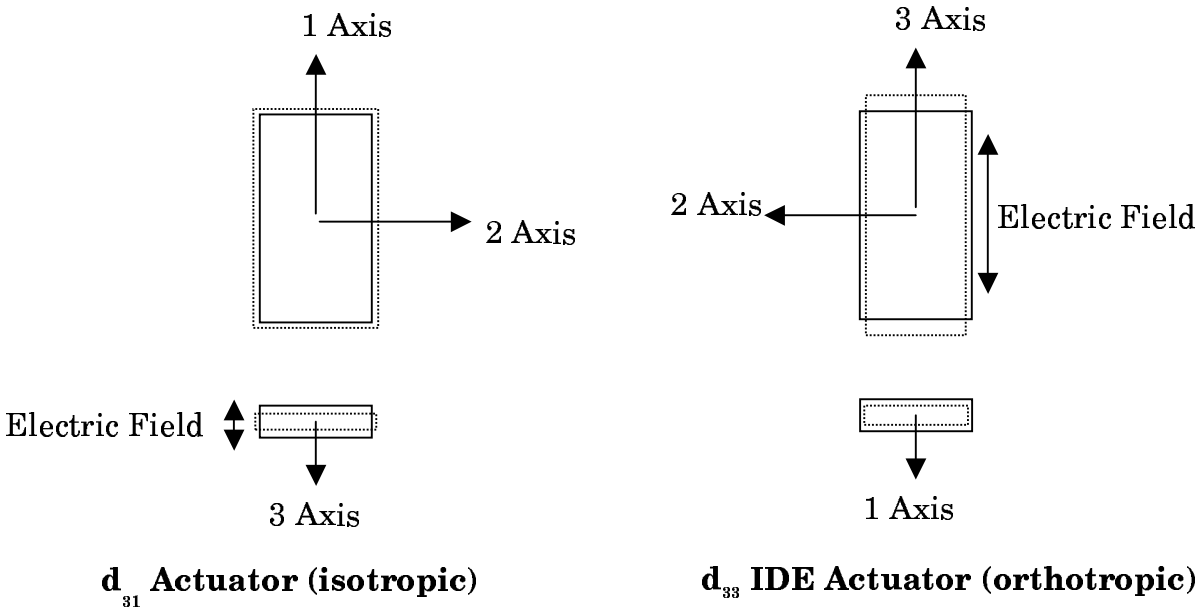

Figure 20. Comparison of Piezoelectric Actuator d31 (isotropic) and d33 (orthotropic) Mechanisms

voltage polarity. It is important to note that the longitudinal (three-axis) and transverse (two-axis) strains for the IDE actuators are out of phase with each other.

The piezoelectric actuators were added to the NASTRAN vertical tail model in a similar procedure as described in Spangler [8]. The piezoelectric actuators were modeled as NASTRAN CQUAD4/PSHELL plate elements and were attached to the grids representing the skins on both sides of the vertical tail. The midplane of the piezoelectric elements was offset half the

thickness of the existing skin elements plus the piezoelectric element thickness. For the d31, isotropic actuators, the material properties of the piezoelectric actuator were included on the NASTRAN MAT1 card and the element thickness was set to the piezoelectric material thickness of the actuator. Since the d33 IDE actuators produce directional strain, these actuators were modeled with the orthotropic material MAT8 card. The direction of the principal skin strains for the vertical tail second mode, Figure 21, were used to determine the orientation of the piezoelectric d33 IDE axis. To simplify the analysis, the principal skin strains were averaged over three regions of similar orientation, and the results are shown in Figure 22 along with the piezoelectric element area. The material axis orientation did not affect the d31, isotropic piezoelectric elements.

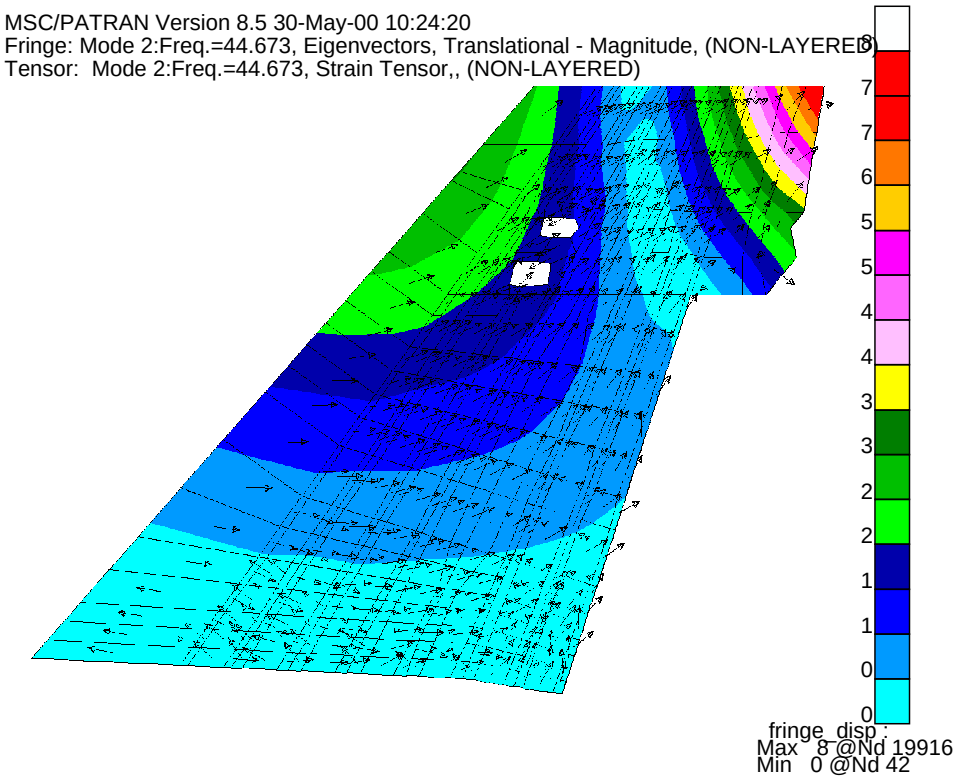

Figure 21. Mode 2 (44.7 Hz) Displacement Contour with Principal Strain Axis

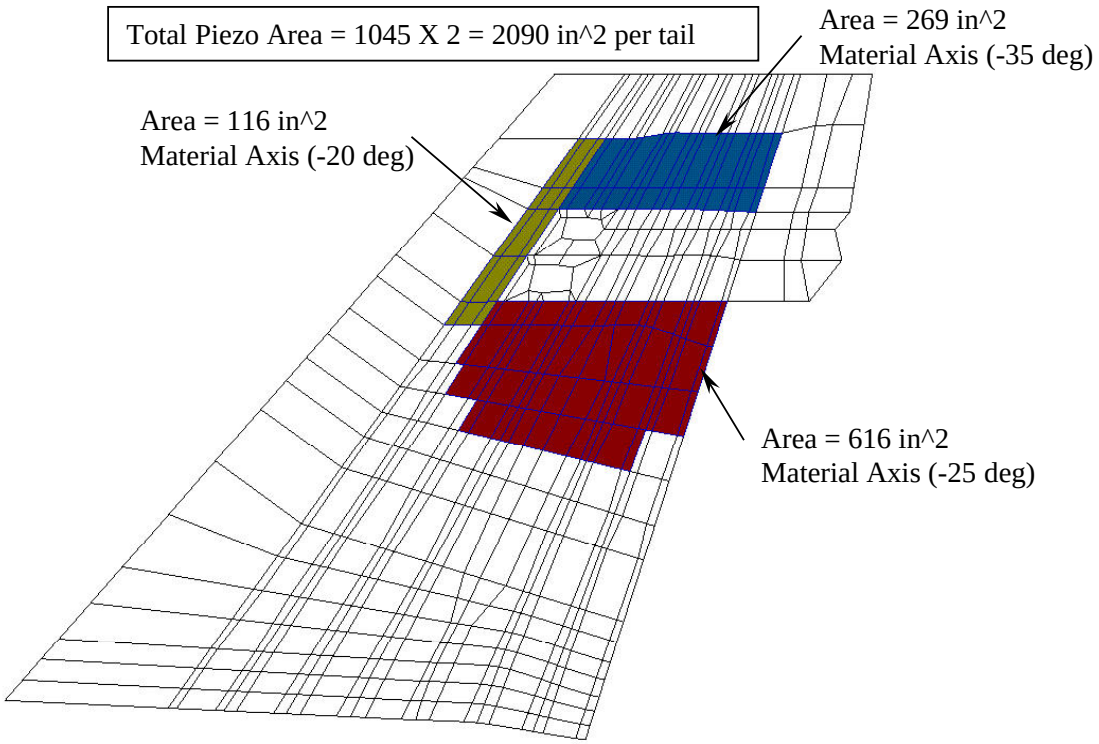

Figure 22. Piezoelectric Actuator Model Area and Material Axis Orientation

The analytical actuation of the piezoelectric elements was accomplished with the thermal analogy presented in Spangler [8]. The piezoelectric elements had a nonzero coefficient of thermal expansion (CTE), while the rest of the model had a zero CTE. The CTE was determined from the piezoelectric actuator free-strain properties at the recommended actuation limits. These recommended limits are listed in Section 5. A static solution was performed with the loading of a delta temperature, producing the limit strains in the piezoelectric elements. The results from the static analysis for a d31 isotropic piezoelectric actuator and a d33 IDE orthotropic actuator of similar thickness are shown in Figure 23 as deflected shapes (blue dash). The solid yellow line is the undeflected shape. The d31 isotropic actuators produce a bending response in the vertical tail and the d33 IDE orthotropic actuators produce a torsion response. For comparison, the vertical tail deflected shape for vibration modes 1 and 2 is shown in Figure 24. This comparison reveals that the isotropic actuators produce a response similar to the

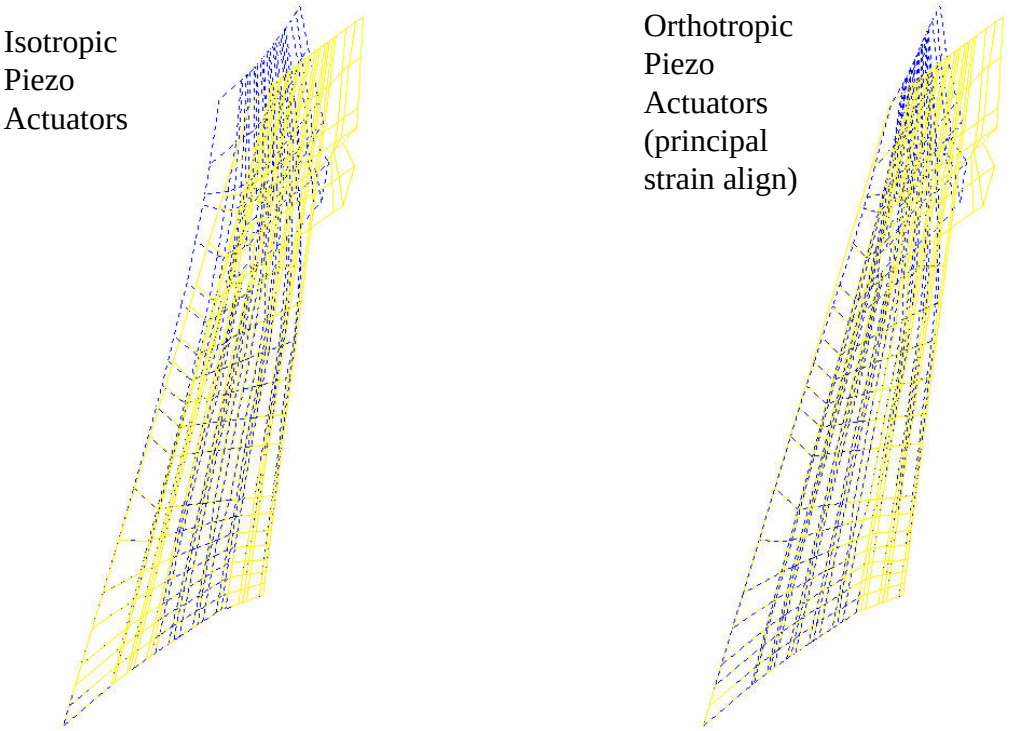

Figure 23. Static Analysis Results (deflections) for Isotropic (d31 mechanism) and Orthotropic (d33 mechanism) Piezoelectric Actuators

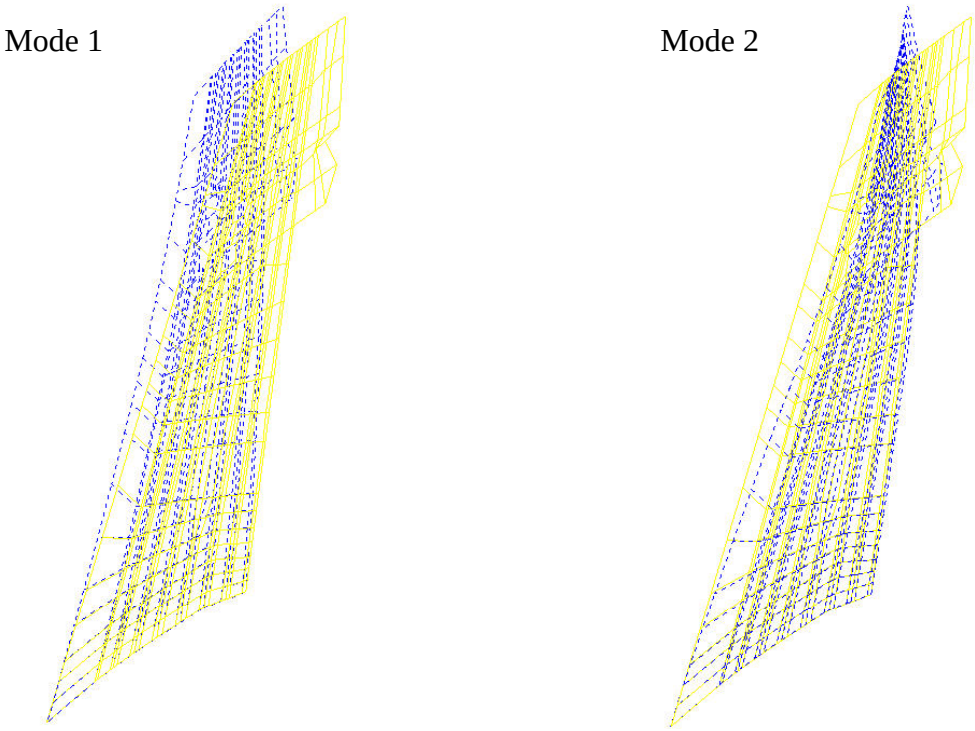

Figure 24. Baseline Analytical Model Modeshape for Mode 1 and Mode 2

vertical tail first bending mode and the orthotropic actuators produce a response similar to the second mode of vibration. The results from this comparison are significant because the piezoelectric actuators in the BLA system are required to reduce the response of mode 2 and not mode 1. This comparison explains the results found during the piezoelectric actuator selection analysis, Section 5, in which the d33 IDE actuators outperformed the d31 isotropic actuators in mode 2 response reduction. The recommended piezoelectric actuators and final configuration for the BLA system are documented in Section 5.

4.0 AERODYNAMIC MODEL

This section of the report will define the analytical aerodynamic models used in the BLA analysis. The oscillatory aerodynamic modeling is described in the first subsection, 4.1, and the buffet aerodynamic modeling is described in the next subsection, 4.2. The primary source of excitation on the vertical tails is from the buffet aerodynamic loading, as described in the background in Section 1.1. The oscillatory aerodynamic forces are generated from the vibratory motion of the vertical tail, and their primary contribution is toward system damping.

4.1 OSCILLATORY AERODYNAMICS

The dynamic motion of the vertical tail in flight generates oscillatory aerodynamic forces. These forces were included in the BLA equations of motion for the vertical tail and rudder control as defined in Section 2.3, Equations 1 and 4. The oscillatory aerodynamic forces were computed using the subsonic Doublet-lattice method and the Boeing program N5KM [11]. This is consistent with the current methods used on the Boeing F/A-18 Project Structural Dynamics team.

The Doublet-lattice aerodynamic model was completed for the vertical tail planform, as shown in Figure 25. The details of the aerodynamic model, 656 boxes, are depicted in Figure 26. The flat plate aerodynamic model consisted of four panels, two on the vertical

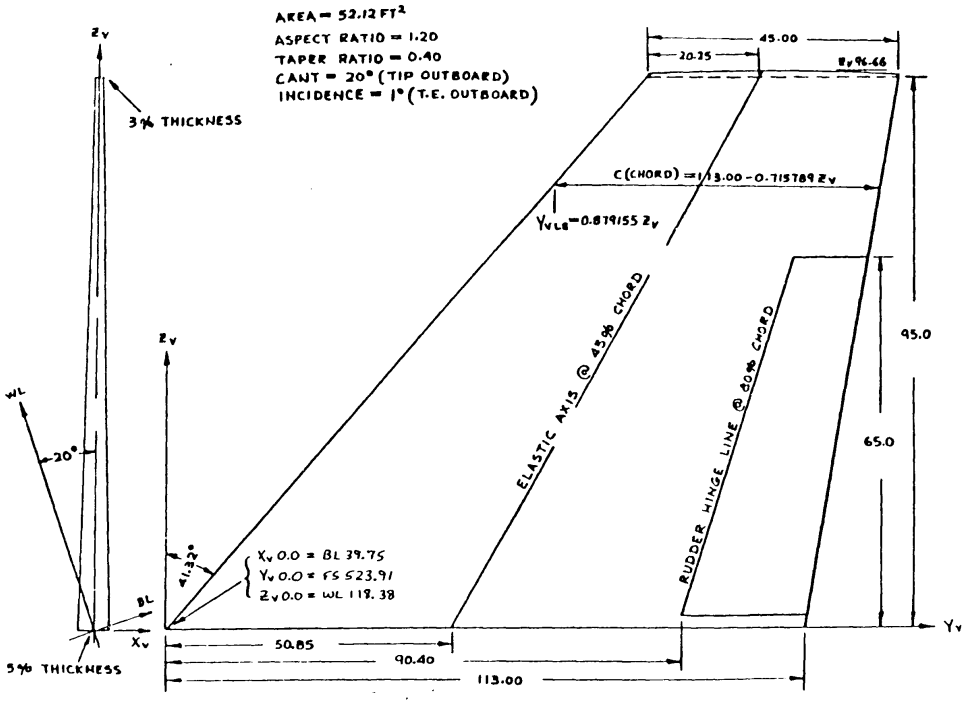

Figure 25. F/A-18 Vertical Tail Geometry

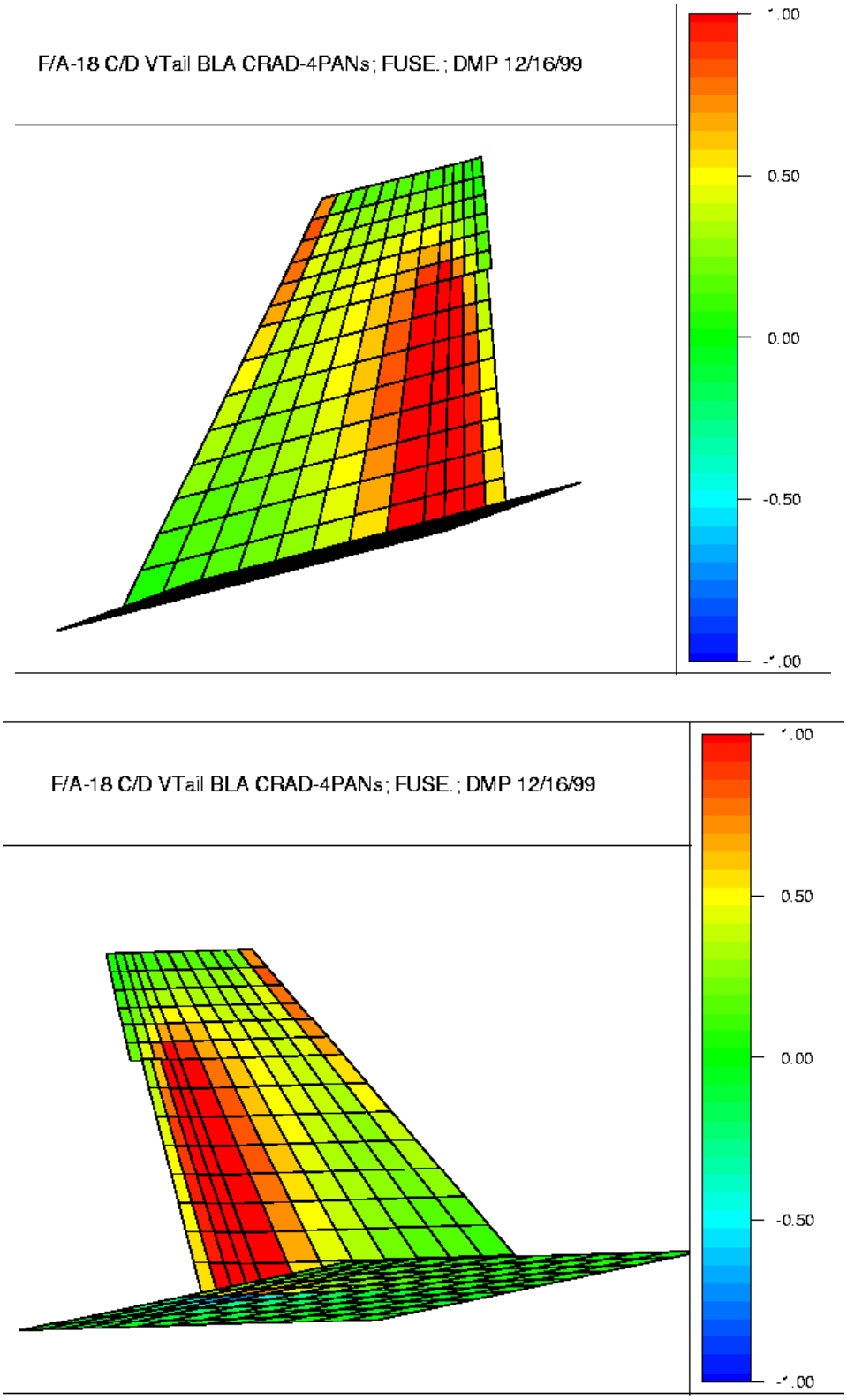

Figure 26. Aerodynamic Pressure Distribution for Unit Rudder Deflection

tail, one for the rudder, and one for the fuselage interference, as shown in Figure 26. As part of the model verification process, a steady (static) aerodynamic solution was completed at Mach 0.80 with the rudder deflected. The results from this analysis, normalized pressures, are in Figure 26. The region of maximum pressure is near the rudder hinge line, as expected for rudder deflection.

The verification of the oscillatory aerodynamic model was completed by performing a flutter solution (Equation 2 from Section 2.3) at Mach 0.80 and by comparing the results with the Boeing F/A-18 Project Structural Dynamics correlated flutter analysis. The flutter analysis results of frequency and damping versus airspeed are in Figure 27. The detailed BLA

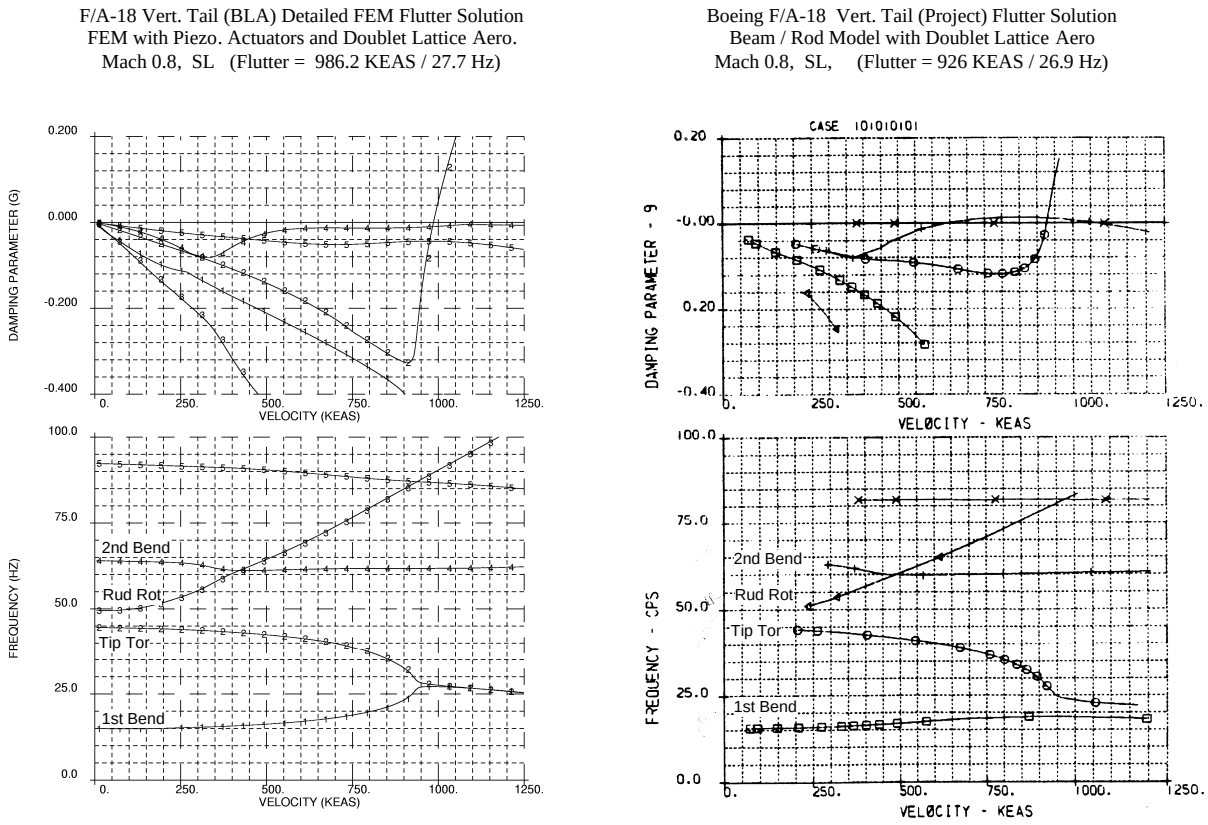

Figure 27. Flutter Analysis Results from Boeing F/A-18 Project Aeroelasticity and BLA Model Aeroelastic Analysis.

model compares well with the existing project analysis, flutter speed of 986 KEAS at 27.7 Hz compared with 926 KEAS at 26.9 Hz. The frequency tracking of the vibration modes with airspeed agrees well between the two solutions. The only major difference between the two solutions is the damping for mode 2 tip torsion. This difference can be attributed to the two structural models, detailed plate FEM for the BLA analysis versus an elastic axis beam for the project analysis. The detailed FEM produces chordwise bending for increased aerodynamic forces in the tip torsion mode, and therefore increased damping, as compared to the rigid chord representation of the beam model.

4.2 BUFFET AERODYNAMICS

This section of the report describes the analytical modeling of the buffet aerodynamic force and identifies the six flight conditions selected for the BLA analysis. The buffet aerodynamic force was modeled similar to the techniques used in Spangler [8], Gaussian white noise process with shaping filter to match the response of measured data. The measured flight test data used for selecting the analysis conditions and scaling the buffet force was obtained from the Boeing F/A-18 Project Structural Dynamics database as opposed to the Canadian and Australian government database used in Spangler [8].

As described previously in Section 1.1, the primary buffet aerodynamic force from flight originates from the wing LEX and impinges on the vertical tail as shown in Figures 1 and 2. This buffet aerodynamic excitation has been successfully simulated in the full-scale ground test facility (IFOSTP) in Melbourne, Australia, [8]. Because of this and the probability of future testing of BLA systems at the IFOSTP facility, the buffet aerodynamic force for the BLA system was analytically modeled as a point force coinciding with the IFOSTP shaker attachment

location, intersection of the vertical tail midrib and 46 percent spar (Figure 3.1). The buffet force of unit magnitude was added to the BLA system equations of motion as an input quantity varying with time, $F_{buf}(t)$, as shown in Equation 2, Section 2.3.

The Boeing F/A-18 Project Structural Dynamics database was queried to select the six flight test conditions for analysis of the BLA system. The fatigue damage of the F/A-18 vertical tail is based on the band-pass filtered response for mode 1 (10 to 20 Hz) and mode 2 (32 to 52 Hz) of the vertical tail aft-tip accelerometer KS16 as defined in Levesque [1] and Scanlon [2]. Therefore, the flight test conditions for analysis were based on the measured flight test response of this same parameter, KS16, from aircraft Bu. No. 160778 with an interim production vertical tail with LEX fence (production aircraft configuration). The selection criteria and the 6 conditions selected from the 389 available records are listed in Table 5. This table includes the condition number in column 1 and the selection criteria in column 2, followed by the flight conditions and measured acceleration response of KS16 for the three frequency ranges of interest. The first two

Table 5. Flight Conditions for BLA Analysis

Condition No.	Condition Description	Flight No.	Run No.	Mach No.	Altitude feet	AOA deg	Q psf	Nz G's	KS16 Response G's RMS 5-100 Hz	10-20 Hz	32-52 Hz
1	Mode 1 Maximum Response	766	23	0.51	11,094	35.1	252	5.5	60	36	30
2	Mode 2 Maximum Response	763	10A	0.83	28,785	31.7	323	6.8	91	13	66
3	Mode 1 Max. Fatigue Damage	766	56B	0.40	2,743	34.8	218	4.8	38	24	21
4	Mode 2 Max. Fatigue Damage	736	38	0.62	19,777	27.9	262	5.6	50	13	35
5	ACX Phase II Condition 3	741	36	0.43	1,852	23.7	258	4.9	37	9	27
6	ACX Phase II Condition 1	765	50A	0.52	10,024	15.9	271	4.2	10	2	5

Notes:
1. Flight conditions selected from Boeing F/A-18 Noise and Vibration Database
2. Flight test aircraft F/A-18 A4, Bu. No. 160778, interim production vertical tail with LEX fence.
3. Conditions selected are based on response of vertical tail aft-tip accelerometer KS16
   Mode 1 response: G's RMS from 10 - 20 Hz
   Mode 2 response: G's RMS from 32 - 52 Hz
4. Flight conditions 2, 5, and 6 are similar to the three ACX Phase II flight conditions 6, 3, and 1 (Reference 8)

conditions were selected from the maximum response for the mode 1 and mode 2 frequency ranges. Conditions 3 and 4 were selected from the Boeing F/A-18 vertical tail fatigue analysis as the conditions that cause the highest fatigue damage based on the U.S. Navy usage. Conditions 5 and 6 were selected for comparison with the results from Spangler [8]. The measured frequency response in G's root mean squared (RMS) is plotted in Figure 28 for the six flight conditions selected. The frequency range for mode 1 and mode 2 is labeled on the figure. To compare the Boeing BLA conditions selected for analysis with the conditions used by Active Control eXperts (ACX), Inc. in Spangler [8], the RMS acceleration response for similar flight conditions are listed in Table 6. The acceleration response for the first two conditions listed compare well, but the response for ACX condition 6 was ≈1.5 times larger.

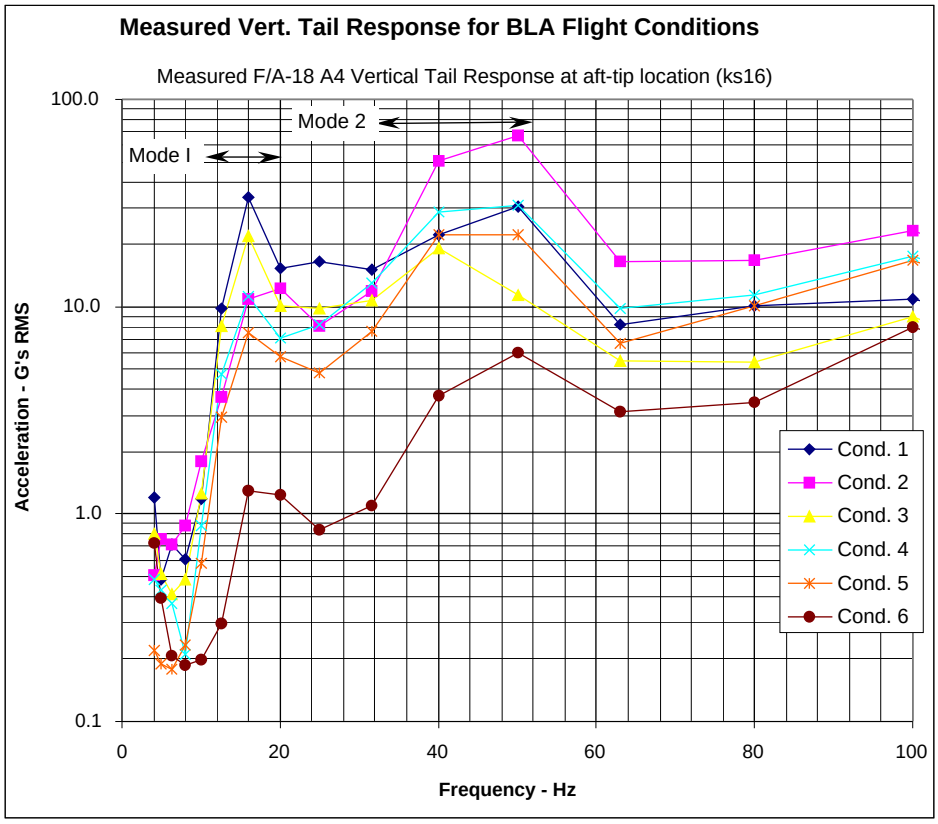

Figure 28. Measured Frequency Response for BLA Flight Conditions

Table 6. Comparison of Flight Conditions for BLA Analysis

Comparison of Flight Conditions and Response for ACX Phase II and Boeing BLA Analysis											
						RMS Acceleration (G's) for Tail aft-tip location					
Condition Number		AOA - degrees		Q - psf		0 to 300 Hz		10 to 20 Hz		32 to 52 Hz	
ACX	Boeing	ACX	Boeing	ACX	Boeing	ACX	Boeing	ACX	Boeing	ACX	Boeing
1	6	12-16	16	225-300	271	11	19	2	2	10	5
3	5	20-24	24	225-300	258	29	45	9	9	31	27
6	2	28-32	32	300-350	323	108	96	18	13	94	66

Note: ACX Phase II results were reported on pages 36 and 81 of report AFRL-VA-WP-TR-1998-3079 (Reference 8)

The final step in defining the buffet aerodynamic force was to run open-loop analytical simulations of the BLA system in SIMULINK as described in Sections 2.3 and 8.1. The buffet force analytical shaping filters were scaled to produce the G's RMS response for the six conditions and three frequency bands listed in Table 5. A final check was completed by computing the frequency response of the simulated time history response for KS16 and comparing this with the measured frequency response in Figure 28. Based on this comparison, the final adjustments were made to the buffet force shaping filters.

5.0 PIEZOELECTRIC ACTUATOR SELECTION

The selection of the piezoelectric actuator type and manufacturer was based on an analytical evaluation. A total of nine different actuators from five different manufacturers were selected for this evaluation and are listed in Table 7. The list includes standard and custom actuators, plate (d31) and IDE (d33), solid and fibrous material, and the single-crystal piezoelectric material. The manufacturer specifications and properties for the piezoelectric actuators were incorporated into the vertical tail FEM, as described in Section 3.2. It is important to note that the specifications for the piezoelectric actuators are from the free-strain performance and are obtained from measurements of free, unconstrained actuators. The free-strain specifications were selected because they are available for each

Table 7. Candidate Piezoelectric Actuators

Manufacturer	Model	Mechanism	Description
ACX	Custom	d31	Custom Quickpack actuator from Ref. 8
ACX	QP-40W	d31	Standard Quickpack actuator
ACX	QP-10Ni	d33	Quickpack with interdigitated electrodes (IDE)
NASA-LaRC	MFC-460	d33	Macro-Fiber Composite with IDE from Ref. 13
Continuum Control	AFC	d33	Active Fiber Composite with IDE 10 mil fibers
TRS	600FGHD	d31	PZT-5H with fine grain and high density
TRS	HK1HD	d31	High dielectric with high density
TRS	Single Crystal	d31	Single crystal material PZN-4.5percentPT
Mide	PowerAct	d33	Packaged actuator with IDE

actuator and are generally obtained from standardized IEEE test techniques. A dynamic response analysis was completed on the vertical tail FEM with the candidate piezoelectric actuators. The performance results from this analysis, along with the cost of the actuators, were used in the actuator selection criteria.

The dynamic response analysis, described in Section 2.3, was used to determine the Mode 2 frequency response of the vertical tail model for an applied voltage (actuation) of the candidate piezoelectric actuators. The piezoelectric actuators covered an area of 1,045 square inches per side, for a total of 2,090 in^2 per tail, as shown in Figure 29. The orientation angle used for the d33 axis of the IDE actuators is also identified in Figure 29. The dynamic response analysis was completed without aerodynamics and the structural damping was 2 percent (g=0.02). The maximum acceleration response at the tail aft-tip location was determined for the Mode 2 frequency range of 32 to 52 Hz. The ratio of this maximum response in G's acceleration divided by the applied actuator voltage was used in the evaluation of the candidate piezoelectric actuators.

5.1 PIEZOELECTRIC ACTUATOR COMPARISON

The candidate piezoelectric actuators and their free-strain mechanical and electrical properties are listed in Table 8. The column heading includes the mechanism for actuation, d31 and d33, as discussed in Section 3.2. All the candidate actuators were modeled with the same application area on the vertical tail as shown in Figure 29. The actuator area listed in Figure 29 represents the individual actuator area and was used to determine other properties, i.e., capacitance per unit area, cost per unit area etc. The active piezoelectric material thickness was not constant in the evaluation, as listed in Table 8. The ACX and TRS plate actuators were the thickest with an active layer of 20 mil (0.020 inch) and the thinnest was the Mide power actuator at 5 mil (0.005 inch). This difference in thickness was accounted for in the evaluation by determining the quantity (number of layers) of actuators required for comparable actuation. The thickness of the NASA LaRC MHD-460 actuator was increased from the standard 7 mil actuator to a custom actuator of 15 mil thickness. The voltage and strain ranges listed in Table 8 are plus or minus half of the peak limits specified by the manufacturer. The voltage range and electrode spacing is used to calculate the electric field. The actuator charge constant is calculated from the peak strain and electric field ($d=\varepsilon/E$). The last row in Table 8 lists the estimated cost per unit area of the piezoelectric actuators. The notes at the bottom of Table 8 identify the source of the actuator properties and cost estimate.

The results from the analytical evaluation of the piezoelectric actuators are listed in Table 9. The results from the dynamic response analysis are listed in the second and third rows as tail response (G's) per applied actuator voltage and the frequency associated with the peak response. The results were scaled up to a peak acceleration response of 375 G's at the tail aft-tip location

Table 8. Piezoelectric Actuator Comparison of "Free Strain" Properties

	Manufacturer	ACX	ACX	ACX	NASA LaRC	Continuum Control	TRS	TRS	TRS	Mide
	Model	Phase 2 BLA	QP-40W	QP-10Ni	MHD-460	AFC (10 mil fibers)	TRS600FGHD	TRSHK1 HD	Single Crystal	Power Actuator
	Material	PZT-5A	PZT-5A	PZT-5A	PZT-5A	PZT-5A Fibers	PZT-5H	n/a	PZN-4.5%PT	PZT-5A
	Electrodes	plate (solid)	plate (solid)	interdigitated	interdigitated	interdigitated	plate (solid)	plate (solid)	plate (solid)	interdigitated
	Mechanism	d31	d31	d33	d33	d33	d31	d31	d31	d33
	Package	1 layer pack	2 layer pack	1 layer pack	1 layer pack	1 layer pack	1 layer pack	1 layer pack	1 layer pack	1 layer pack
	Notes	1	2,4	3,4	5	6	7, 8	7, 8	7, 8	9
Parameter	Units									
Actuator Area	in^2	6.0	6.0	2.4	7.6	1.0	3.0	3.0	1.5	2.1
Thickness	in	0.020	0.020	0.015	0.015	0.011	0.020	0.020	0.020	0.005
Density	lb / in^3	0.278	0.266	0.1879	0.273	0.155	0.280	0.280	0.296	0.202
Capacitance / Area	nF / in^2	66.7	66.7	0.429	1.50	1.00	41.00	72.67	58.67	0.48
Voltage Range / 2	+/- volts	800	200	1200	2000	1500	500	500	500	1000
Electrode Spacing	in	0.020	0.010	0.060	0.042	0.045	0.020	0.020	0.020	0.059
Field Range / 2	+/- Kvolts / in	40	20	20	48	33	25	25	25	17
Young's Modulas										
longitudinal	psi	9.00E+06	9.00E+06	8.48E+06	5.30E+06	3.85E+06	9.86E+06	1.04E+07	1.74E+06	5.37E+06
transverse	psi	9.00E+06	9.00E+06	1.00E+07	1.10E+06	1.68E+06	9.86E+06	1.04E+07	1.74E+06	4.87E+06
Strain Range / 2										
longitudinal	+/- με	400	140	350	900	650	375	400	800	335
transverse	+/- με	400	140	-125	-420	-180	375	400	800	-194
d (charge constant)										
longitudinal	in / volt	-1.00E-08	-7.05E-09	1.75E-08	1.77E-08	1.95E-08	1.21E-08	1.53E-08	3.86E-08	1.98E-08
transverse	in / volt	-1.00E-08	-7.05E-09	-6.25E-09	-8.27E-09	-5.42E-09	1.21E-08	1.53E-08	3.86E-08	-1.14E-08
Cost Estimate / Area	$ / in^2	custom	$19	$40	$20	$43	$22	$20	$722	not available

Notes:
1. ACX Phase 2 BLA model actuator properties from report AFRL-VA-WP-TR-1998-3079 (Reference 8)
2. ACX QP40W Specifications from Active Control Experts, Inc., Product Information, 1999 (internet site: http::://www.acx.com/qp40w.html)
3. ACX QP10Ni Specifications from Active Control Experts, Inc., Product Information, 1999 (internet site: http::://www.acx.com)
4 ACX pricing from Active Control Experts, Inc., Product Information, 1999 (internet site: http::://www.acx.com/price_list.html)
5. NASA LaRC MHD-460 model actuator properties from Reference 13. Pricing from Dr. W. Keats Wilkie of NASA LaRC.
6. Continuum Control AFC 10 mil fiber actuator properties from Continuum Control Corporation, Dr Aaron A. Bent, President.
7. TRS actuator properties from TRS Ceramics, Inc., Mr. Wes Hackenberger.
8. TRS actuator unpackaged pricing from TRS Ceramics, Inc., Mr. Wes Hackenberger. Actuator packaging cost estimate of $9 per unit area added to unpackaged cost.
9. MIDE PowerAct properties and pricing from MIDE Technology Corporation, Dr. Marthinus van Schoor, President

Table 9. Piezoelectric Actuator Evaluation - Analysis Results and Cost Estimate

	Manufacturer	ACX	ACX	ACX	NASA LaRC	Continuum Control	TRS	TRS	TRS	Mide
	Model	Phase 2 BLA	QP-40W	QP-10Ni	MHD-460	AFC (10 mil fibers)	TRS600FGHD	TRSHK1 HD	Single Crystal	Power Actuator
	Material	PZT-5A	PZT-5A	PZT-5A	PZT-5A	PZT-5A Fibers	PZT-5H	n/a	PZN-4.5%PT	PZT-5A
	Electrodes	plate (solid)	plate (solid)	interdigitated	interdigitated	interdigitated	plate (solid)	plate (solid)	plate (solid)	interdigitated
	Mechanism	d31	d31	d33	d33	d33	d31	d31	d31	d33
	Package	1 layer pack	2 layer pack	1 layer pack	1 layer pack	1 layer pack	1 layer pack	1 layer pack	1 layer pack	1 layer pack
	Notes	1	2,4	3,4	5	6	7, 8	7, 8	7, 8	9
Parameter	Units									
Actuation Area	in^2	2090	2090	2090	2090	2090	2090	2090	2090	2090
KS16 Response / Piezo Input	G's / Volt	0.387	0.544	0.227	0.224	0.163	0.586	0.681	0.280	0.062
Peak Response Frequency	Hz	45.0	45.0	45.2	44.4	44.7	45.2	45.2	43.7	44.7
Max. Response at KS16	G's	375	375	375	375	375	375	375	375	375
Strain for Max. Response	+/- με	484	482	481	754	996	480	441	2141	2014
Voltage for Max. Response	+/- volts	969	689	1650	1677	2298	640	551	1338	6012
Piezo Limit Voltage Range	+/- volts	800	200	1200	2000	1850	600	600	800	1000
Ratio (Max./Limit Volt Range)		1.2	3.4	1.4	0.8	1.2	1.1	0.9	1.7	6.0
Capacitance * Ratio	μF	169	480	1	3	3	91	139	205	6
Capacitive Reactance	Ohms	21	7	2860	1364	1371	39	25	18	590
Current	Amps	46.2	93.6	0.6	1.2	1.7	16.6	21.8	75.3	10.2
Reactive Power	Watts	44785	64505	952	2061	3852	10601	12022	100764	61218
Weight * Ratio	lbs	14.1	38.3	8.1	7.2	4.4	12.5	10.7	20.7	12.7
Cost Estimate * Ratio	$	not available	$138,056	$114,732	$35,040	$112,510	$48,265	$38,711	$2,524,601	not available

Notes:
1. ACX Phase 2 BLA model actuator properties from report AFRL-VA-WP-TR-1998-3079 (Reference 8)
2. ACX QP40W Specifications from Active Control Experts, Inc., Product Information, 1999 (internet site: http://www.acx.com/qp40w.html)
3. ACX QP10Ni Specifications from Active Control Experts, Inc., Product Information, 1999 (internet site: http://www.acx.com)
4 ACX pricing from Active Control Experts, Inc., Product Information, 1999 (internet site: http://www.acx.com/price_list.html)
5. NASA LaRC MHD-460 model actuator properties from Reference 13. Pricing from Dr. W. Keats Wilkie of NASA LaRC.
6. Continuum Control AFC 10 mil fiber actuator properties from Continuum Control Corporation, Dr Aaron A. Bent, President.
7. TRS actuator properties from TRS Ceramics, Inc., Mr. Wes Hackenberger.
8. TRS actuator unpackaged pricing from TRS Ceramics, Inc., Mr. Wes Hackenberger. Actuator packaging cost estimate of $9 per unit area added to unpackaged cost.
9. MIDE PowerAct properties and pricing from MIDE Technology Corporation, Dr. Marthinus van Schoor, President

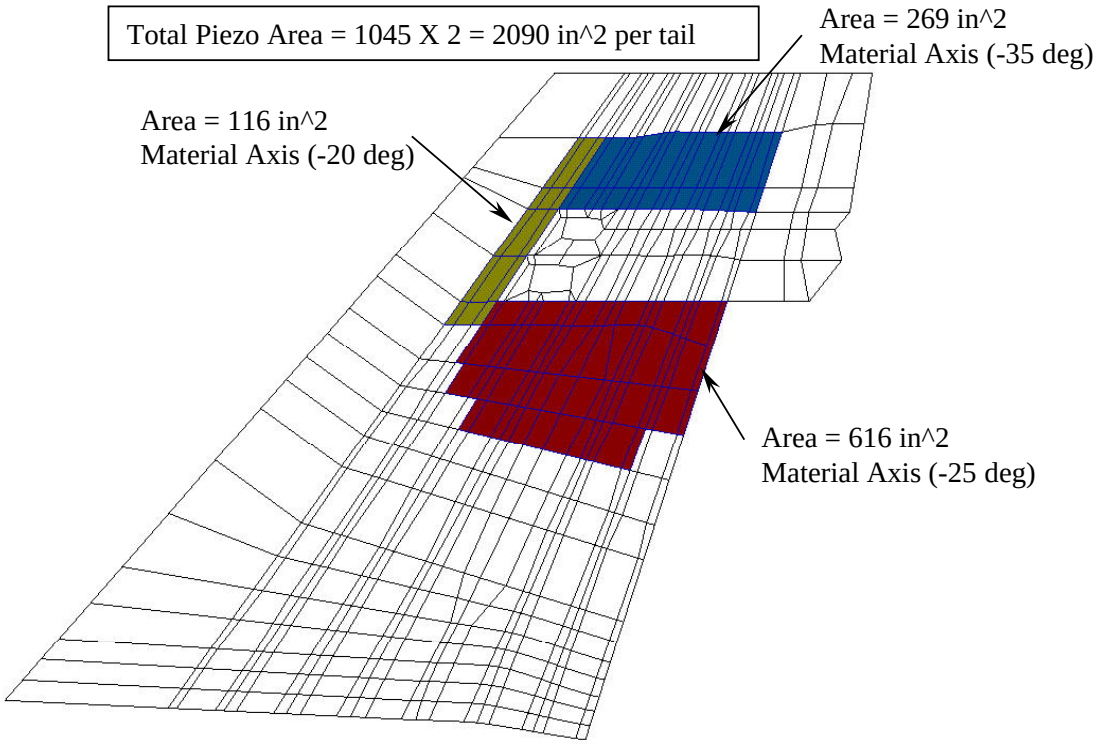

Figure 29. Piezoelectric Actuator Model Area and Material Axis Orientation

(KS16). This represents a maximum measured response from flight test with the LEX fence installed [2]. The piezoelectric actuator free strain and voltage required to produce the 375-G response is listed rows five and six of Table 9 and is followed by the manufacturer recommended voltage limit. The ratio of the required voltage divided by the limit voltage is highlighted in Table 9 because this ratio indicates the performance for one layer of the actuators for the thickness listed in Table 8. This ratio would also indicate the quantity of actuators required or number of layers to produce a peak response of 375 G's for mode 2. If the voltage ratio were the Continuum Control AFC to 0.66 and the Mide power actuator to 1.5. This indicates that the NASA LaRC MHD-460 and the Continuum Control Corporation AFC are the most effective actuators. The least effective actuator was the ACX QP-40W, with a ratio of 3.4 (this ratio is inflated by the conservative limit of ±200 volts). It is interesting to note that even though the

TRS single-crystal actuator has the largest piezoelectric charge constant, the actuator performance was reduced by the low modulas of elasticity. The d33 directional actuators with IDEs were three times more effective than the d31 isotropic actuators based on the direct comparison of the voltage ratio for the ACX QP-40W (d31) and the ACX QP-10Ni (d33). This result was expected because of the results from the static actuation discussed in Section 3.2 and presented in Figure 23. It is also consistent with the magnitude ratio of d_{33}:d_{31} of approximately 2.5.

The overall system properties for the candidate piezoelectric actuators are listed in the lower half of Table 9. The system properties for the actuation area of 2,090 in^2 on the vertical tail have been scaled by the ratio of maximum to limit voltage to produce the properties for 375 G's of acceleration at the aft-tip location of the tail. The system capacitance is two orders of magnitude lower for the d33 directional actuators with IDEs. This difference in capacitance will have to be verified in the laboratory. The lowest power requirement was less than 1,000 watts and was for the ACX QP-10Ni actuator. The cost estimate for the candidate actuators is listed in the last row of Table 9. The lowest cost estimate was for the NASA LaRC MHD-460 actuator at $35,040, and the next lowest was for the TRS HK1HD actuator at $38,711. The highest cost estimate was for the TRS single-crystal actuator at over 2 million dollars (although the single-crystal material is quite new and should come down in cost as the technology matures).

5.2 PIEZOELECTRIC ACTUATOR RECOMMENDATION

Overall, the d33 IDE actuators outperformed the d31 actuators by a factor of three for the same piezoelectric material. Therefore, it is recommended to use an actuator with the d33 mechanism

(IDE) of actuation. Based on the results from the analytical evaluation and the results discussed in the previous subsection, the NASA LaRC MHD-460 piezoelectric actuator was selected for the BLA system design. This actuator had the lowest ratio of required voltage to limit voltage and also had the lowest cost estimate. Although the standard actuator thickness is 7 mil, NASA LaRC states that the actuator thickness can be increased to 20 mil without an increase in cost because the actuator assembly labor is reduced with the thicker actuator. It is also recommended to investigate the use of the piezoelectric material from the TRS HK1HD actuator into the NASA LaRC MFC actuator. The TRS HK1HD actuator had the best performance for a d31 plate actuator and had the second lowest cost estimate.

Because of the risk associated with developing the thicker version of the NASA LaRC MHD-460 actuator and the requirement to produce a large quantity of custom actuators, it is recommended to select the Continuum Control AFC 10 mil fiber actuator as a replacement should the NASA LaRC MHD-460 actuator experience development or manufacturing problems. The Continuum Control AFC actuator had the next lowest voltage ratio (Table 9) and was the next lowest cost d33 type actuator. Continuum Control is a commercial company with experience in producing large quantities of piezoelectric actuators.

6.0 ASE MODEL

This section documents the ASE model for the BLA design study. The ASE model was developed to include the effects of the commanded rudder in the aeroelastic model. The analytical ASE model was created in FAMUSS [12], which is the software tool used by the Boeing F-18 project for aircraft ASE analysis. The equations of motion were previously developed in Section 2.3 and will be used throughout this section. The completed ASE model

was validated by comparison of the analytical results with measured results from the full-scale ground test at IFOSTP [8], measured aircraft buffet flight test response [2], and measured aircraft response from a commanded rudder frequency sweep on the NASA Dryden F-18 HARV aircraft.

6.1 ASE MODEL DEVELOPMENT

The inputs to FAMUSS for creation of the ASE model included the results from the normal modes analysis of the structural model (Section 3), the oscillatory aerodynamics generalized forces (Section 4.1) for both the motion of the vertical tail and the commanded rudder, a unit buffet input force (Section 4.2), and the modal piezoelectric actuator force (Section 3.2). These inputs can be found in the terms of Equation 4 from Section 2.3.

$$M\ddot{q}(t) + K(1+jg)q(t) - \frac{1}{2}\rho V^2 Q(k)q(t) = -M_c\ddot{U}(t) + \frac{1}{2}\rho V^2 Q_c(k)U(t) + F_{buf}U(t) + F_{piezo}U(t) \quad 4$$

The left-hand (lh) side of Equation 4 includes the structural (modal) mass, stiffness, damping, and oscillatory aerodynamic force ($1/2\rho V^2 Q(k)$) from the motion of the flexible tail. The right-hand (rh) side of Equation 4 represents the commanded inputs to the ASE model and includes the modal rudder inertia and oscillatory aerodynamic force for a unit (1 radian) of commanded rudder position, the modal buffet force for a unit (1 pound) input at the IFOSTP shaker location (mid rib and 46 percent spar, Figure 8), and the modal piezoelectric actuator force for a unit input (modal force from 2,000 volts). Details on the modal buffet force are in Section 4.2. The modal force from the piezoelectric actuators (Section 3.2) was determined from the summation of the static actuation grid point forces multiplied by the modeshape displacements for each degree of freedom, as described in Section 2.3.

The computation of the rudder inertia and oscillatory aerodynamic forces for a unit radian of commanded rudder position ($-M_c\ddot{U}(t) + \frac{1}{2}\rho V^2 Q_c(k)U(t)$) was completed outside FAMUSS with the Boeing AeroServoElastic Stability System (ASESS) program. ASESS is used as an interface program to compute generalized forces for flight control analysis software. The generalized rudder inertia mass, Mc, was calculated in ASESS by using the rudder mass matrix, rudder mode shape inertial degrees of freedom, and the mode shape defining the rudder control surface motion. The generalized oscillatory aerodynamic forces from the control surface motion were calculated from the AIC, mode shapes for the AIC degree of freedoms, and the mode shape of the control surface rotation for the AIC degrees of freedom. It is important to note that the analytical rudder actuator model, that represents the commanded input and output of the rudder actuator, was not included in the ASE model in FAMUSS. This model was obtained from the Boeing F-18 project flight controls group and was included in the closed-loop simulations in SIMULINK, Section 8.0.

The outputs from FAMUSS included the transfer function response and an equivalent state space model for the three inputs: 1) commanded rudder position, 2) buffet force, and 3) piezoelectric actuator force. The transfer function response was computed from Equation 7 (Laplace variable, $s=j\omega$) as described in Section 2.3 for the frequency range of interest, 0.5 to 100 Hz. The structural damping used for the analysis was 2 percent, g=0.02. A separate transfer function was calculated for each input-output pair. FAMUSS creates an equivalent state space model from the transfer function response and Equation 10 using a nonlinear optimization technique as described in Pitt [12]. The six flight conditions for analysis were described previously in Section 4.2:

$$H_q(s) = \left[Ms^2 + K(1 + jg) - \frac{1}{2}\rho V^2 Q(k) \right]^{-1} \bullet \left[-M_C s^2 + \frac{1}{2}\rho V^2 Q_C(k) + F_{buf} + F_{piezo} \right] \qquad 7$$

$$\hat{H}(s) = C\left[sI - A\right]^{-1} B + D. \qquad 10$$

The transfer function response of magnitude and phase from FAMUSS for BLA flight condition 4 (Mach 0.62, 20K feet) is in Figure 30. The response is in G's acceleration at location KS16 (tail aft-tip) for each of the three commanded inputs. The difference in response magnitude, over 40 dB, between each of the different inputs is due to the different unit input magnitudes: 1) 1 radian of rudder, 2) 2,000 volts of piezoelectric actuation, and 3) 1 pound of buffet excitation. To assess the addition of the oscillatory aerodynamics on the BLA system, the transfer function response with and without aerodynamics is in Figure 31. The oscillatory aerodynamic forces reduce the magnitude of the response by effectively increasing the system damping for all the peaks. The one response that increased with the addition of the aerodynamics was the vertical tail first bending mode (15 Hz) with a rudder input. This response increased because of the additional force from the aerodynamics on the rh side of Equation 7. The rh side aerodynamic force was not as significant for the higher frequency modes because the oscillatory aerodynamic force is a function of displacement, which is inversely proportional to the frequency squared.

Additional analyses were completed to verify the setup in FAMUSS and quantify the individual terms of Equation 4. The terms of Equation 4 were removed individually and collectively to verify the inputs to FAMUSS. With only the commanded rudder inertia force on the rh side of Equation 4 ($M_c\ddot{U}(t)$), the vertical tail displacement response from the lh side of Equation [4] ($\phi q(t)$) is 180° out of phase with the commanded rudder displacement and the rudder displacement response ($\phi q(t)$) is 0° in phase with the commanded rudder displacement. This means that for only a rudder inertia load, the tail responds opposite of the rudder and the rudder response is in the same direction as the commanded rudder. With only the commanded rudder

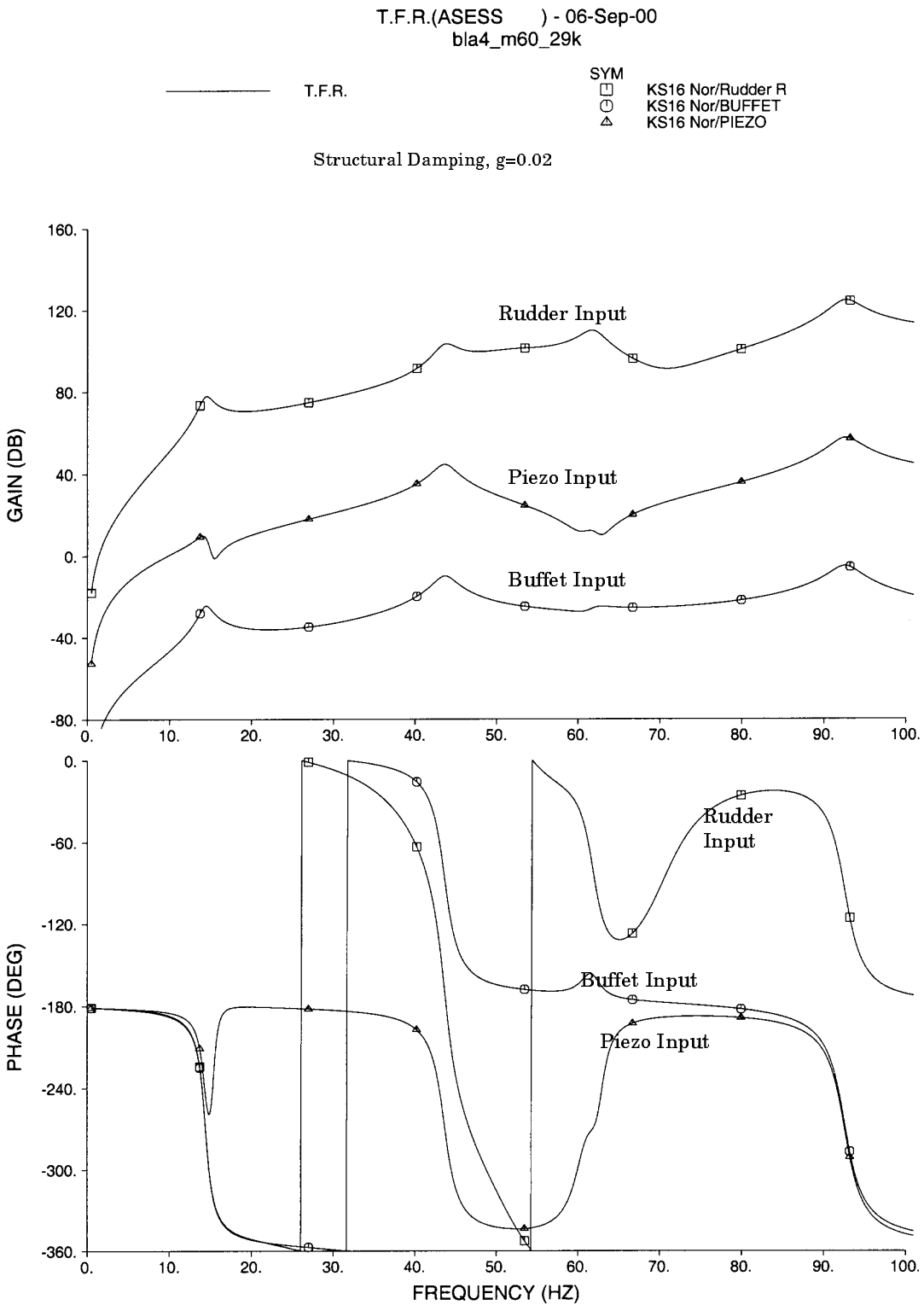

Figure 30. Transfer Function Response at KS16 (G's) for BLA Condition 4

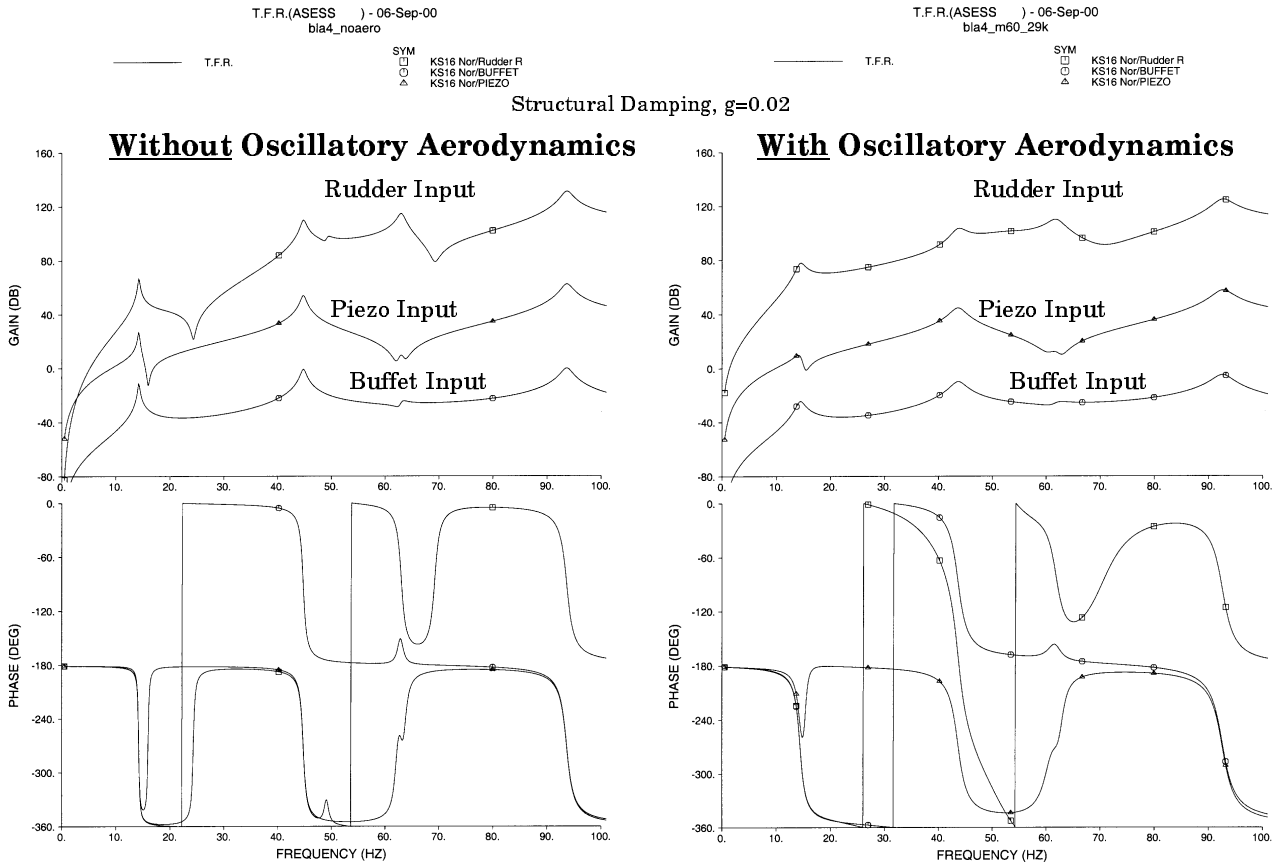

Figure 31. Transfer Function Comparison for Oscillatory Aerodynamics

aerodynamic force on the rh side of Equation 4 ($\frac{1}{2}\rho V^2 Q_c(k)U(t)$), both the vertical tail and rudder displacement response are 180° out of phase with the commanded rudder displacement.

A plot of the vertical tail transfer function acceleration response is in Figure 32 for three different combinations of the rh side commanded rudder forces. The green curve is the response per degree of commanded rudder for both of the rudder rh side forces (inertia plus aero). The red curve is the response to the commanded rudder inertia force only and the purple curve is the response from the rudder aerodynamic force. The acceleration response of the tail for pseudo

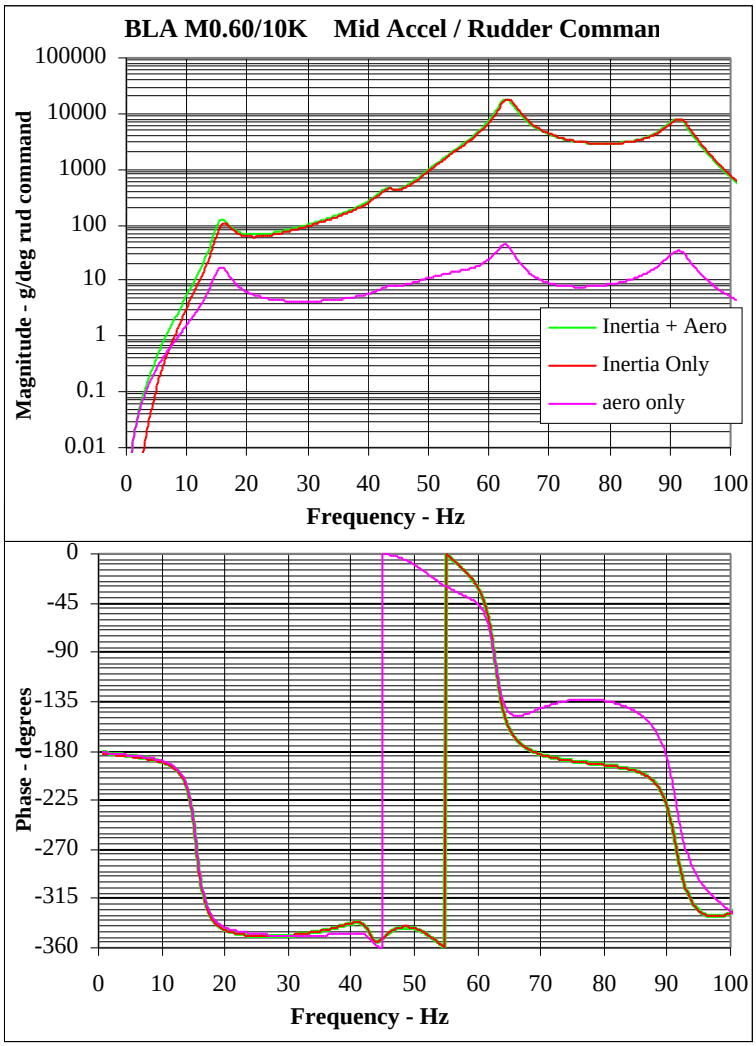

Note: The frequency response is for rudder position and does not include the rudder actuator model (actuator command to actuator position).

Figure 32. Tail Acceleration Response for Commanded Rudder Input

static conditions (less than 3 Hz) is 180° with the commanded rudder rotation because the sign convention for a positive rudder rotation (θ about z axis) produces a negative (x axis) displacement of the rudder, and since the vertical tail responds opposite of the rudder, a positive x-axis displacement of the vertical tail acceleration is 180° out of phase. The response from the oscillatory aerodynamic force of the commanded rudder is large at low frequencies, less than 10 Hz, and the response from the commanded rudder inertia force is much larger at frequencies

above 10 Hz, as shown in Figure 32. The crossover frequency is 7 Hz in which the response from each force is equal. For the frequency of the tail first bending mode that the rudder is controlling, 15 Hz, the response from the rudder inertia force is about seven times larger than the response from the aerodynamic force. This was a significant finding because it supported the decision to not reduce the rudder aerodynamic effectiveness as has been done in previous research [5]. It also provides support for including the active rudder in a ground test that does not have flight aerodynamics.

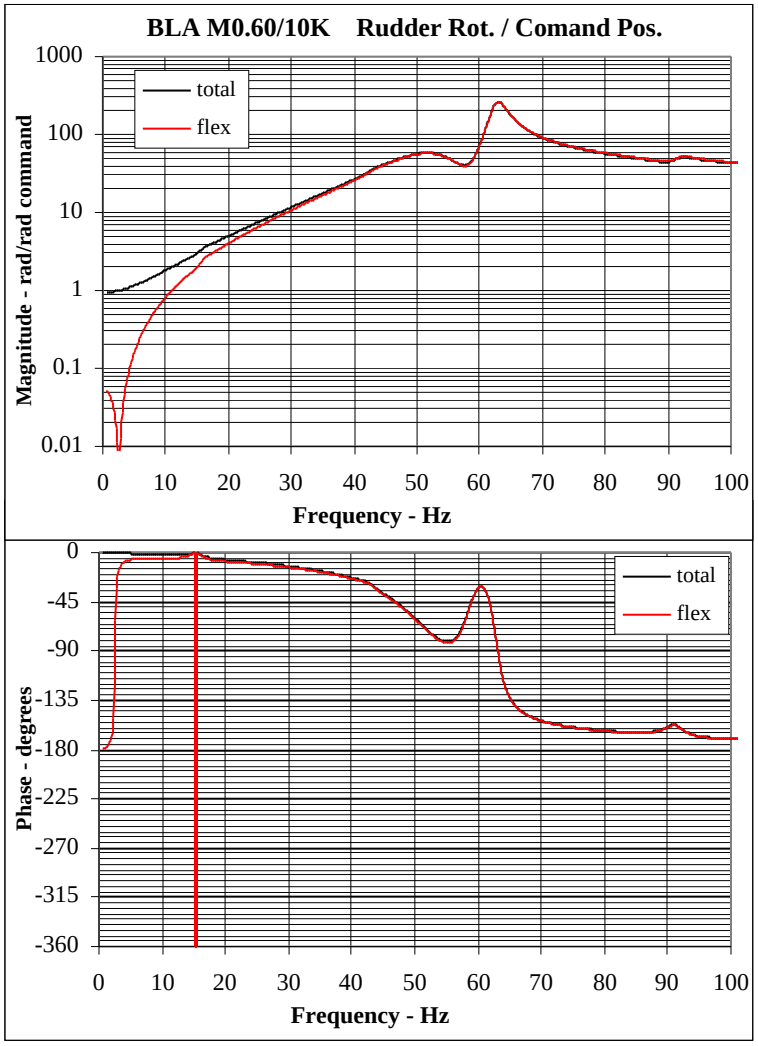

Note: The frequency response is for rudder position and does not include the rudder actuator model (actuator command to actuator position).

Figure 33. Rudder Rotation Response for Commanded Rudder Input

The transfer function response for rudder rotation in radians is in Figure 33 for a unit (1 radian) input of commanded rudder rotation. The flex rudder rotation response is the response from the

lh side of Equation 4 ($\phi q(t)$) and the total rudder rotation response is the flex response plus the commanded input of 1 radian. The plot of phase identifies the transition frequency from a rudder aerodynamic force to a rudder inertia force occurs at 5 Hz. The low frequency response from the aerodynamic force drives the rudder opposite of the commanded input (180°) and the rudder inertia force drives the rudder in phase (0°) with the commanded input.

6.2 ASE MODEL VALIDATION

The vertical tail ASE model was validated by comparison of the analytical results with measured results from the full-scale ground test at IFOSTP [8], with measured aircraft buffet flight test response [2], and with measured aircraft response from a commanded rudder frequency sweep on the NASA Dryden F-18 HARV aircraft.

To validate the buffet force model, the analytical state space model without oscillatory aerodynamics was forced in SIMULINK with the measured shaker load cell time history from the full-scale IFOSTP ground test [8]. Power spectral densities of the analytical (dashed line) and measured (solid line) response at the tail aft-tip location are in Figure 34. The analytical results are presented for two different structural damping values. The analytical model with a structural damping of 8 percent compared the best with the measured vertical tail response at IFOSTP, as shown in Figure 34.

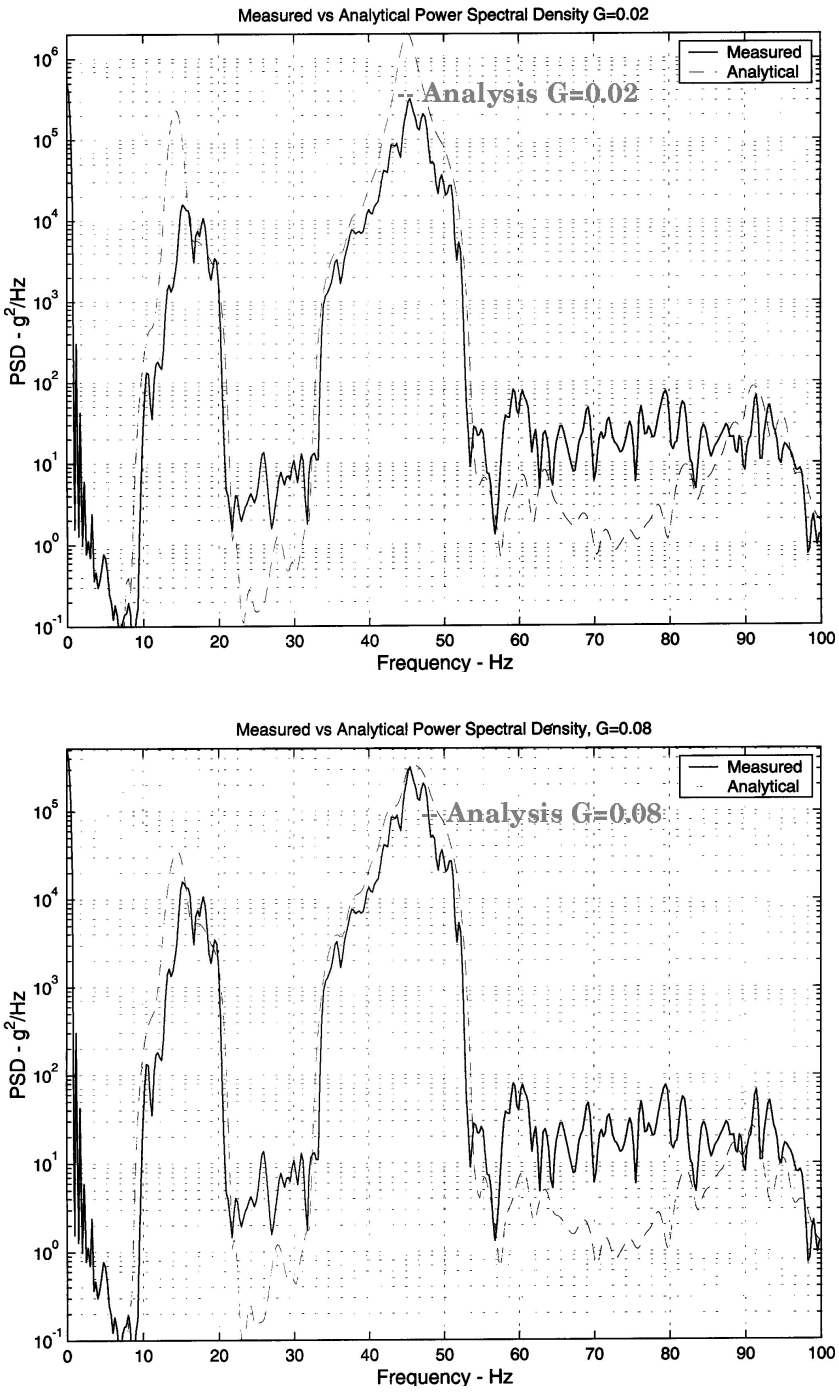

Figure 34. Measured and Analytical Response to Buffet Shaker Force

The oscillatory aerodynamic force was validated by comparison with measured buffet flight test response of the F-18 vertical tail [2]. The analytical state space model poles of frequency and

damping were compared with the measured frequency and damping from flight for several buffet flight conditions. The measured frequency and damping was obtained from applying the half-power method to the measured response PSD. The analytical and measured results agreed well for mode 2, tip torsion at 45 Hz. The measured frequency ranged from 44 to 45 Hz versus 44 Hz analytical and the measured structural damping ranged from 5 percent to 7 percent, which was the same for the analytical model. The results for mode 1 indicated that the analytical oscillatory aerodynamic force was low and could be increased. The measured frequency ranged from 15 to 16 Hz versus the analytical range of 14 to 15 Hz, and the measured damping ranged from 15 percent to 20 percent versus the analytical results of 10 percent to 11 percent. One possible reason for this damping difference could be the increase in spanwise flow across the vertical tail as AOA is increased. This could account for the larger measured damping in the

first bending mode compared to the analytical aerodynamic model, which did not include the rigid aircraft pitch from AOA. The decision was made to not change the analytical model at this time until further research can be completed in this field. Also, based on these results, the decision was made to not reduce the oscillatory aerodynamics as was done in previous research [5]. These reductions were as large as 50 percent above 30 degrees AOA and were based on the aircraft steady aerodynamic coefficient of yaw due to rudder deflection. This would only increase the differences between measured and analytical results.

The rudder control surface ASE model was validated by comparison with the measured response from an in-flight rudder sweep on the F/A-18 HARV aircraft. To get good agreement with the measured results, the analytical rudder response in SIMULINK was changed to include the commanded position along with the addition of the flexible rudder rotation response (lh side of Equation 4, $\phi q(t)$). Response transfer functions computed from this total rudder position in the

denominator agreed well with the measured transfer function, as shown in Figure 35. The measured results were from an in-flight rudder sweep on the NASA Dryden F/A-18 HARV aircraft. The flight conditions for this comparison were straight and level at Mach 0.60 at 10K feet. The transfer function processing of the measured data produced a range of response as shown by the filled area in Figure 35.

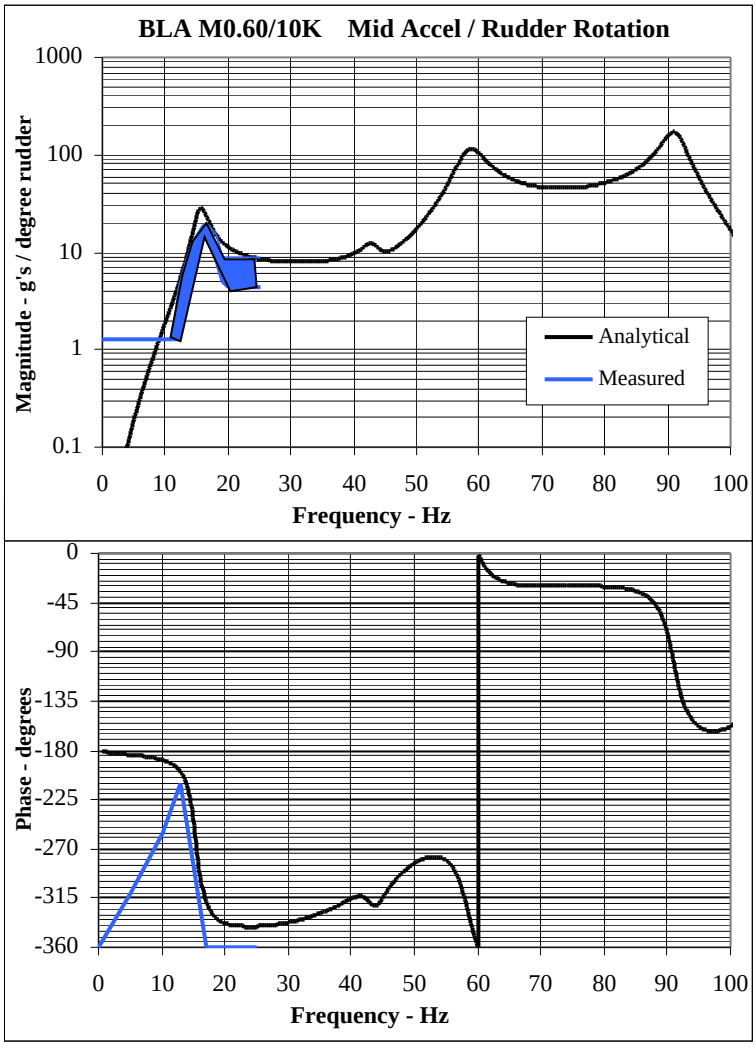

Figure 35. Measured and Analytical Tail Response for Rudder Input

7.0 CONTROLLER DESIGN

The classical control laws for the BLA system were developed independently as single-input, SISO controllers for the rudder to control mode 1 at 15 Hz and the piezoelectric actuators to control mode 2 at 45 Hz. Because of his experience with previous BLA controller design [7, 9], Dr. Robert Moses of NASA-Langley led the development of the control law design. The feedback sensor for each control law was selected as the vertical tail aft tip accelerometer (KS16 in Figure 7). This location was selected because it is currently used to assess fatigue damage of the F/A-18 vertical tail, and therefore, a reduction in response of KS16 is the logical choice for the controller objective. The final control laws for the BLA system were selected based on performance and stability. The final (best) control law for the rudder was based on the simple feedback of vertical tail displacement, which is similar but out of phase with the results found in Ashely [5] that recommended the direct feedback of fin tip acceleration (KS01 in Figure 7). The final control law for the piezoelectric actuators was the feedback of velocity from location KS16 in conjunction with a notch filter. These control laws were effective for the six flight conditions analyzed and required only a change to the gain to go from one condition to the next. This would be beneficial for integration onto the airplane, since it would only require the controller to have gain scheduling with flight parameters.

The analytical control law development and system simulations were completed in MATLAB® using the SIMULINK toolbox. A simplified block diagram of the SIMULINK model with the rudder and piezoelectric feedback control is shown in Figure 36 and the detailed SIMULINK model is shown in Figure 37. At the center of the system is the state space representation of the ASE model with the three inputs and two outputs as described in Section 6.1. The three inputs are rudder position, buffet force excitation, and piezoelectric actuator voltage. The two outputs

from the state space model were the vertical tail acceleration response at KS16 and the flexible rudder rotation response. The net rudder position is the sum of the flexible rudder response plus the commanded rudder position, as shown in Figure 36 and described in Section 6.1. Figure 36 also includes expanded views of the rudder and piezoelectric actuator feedback

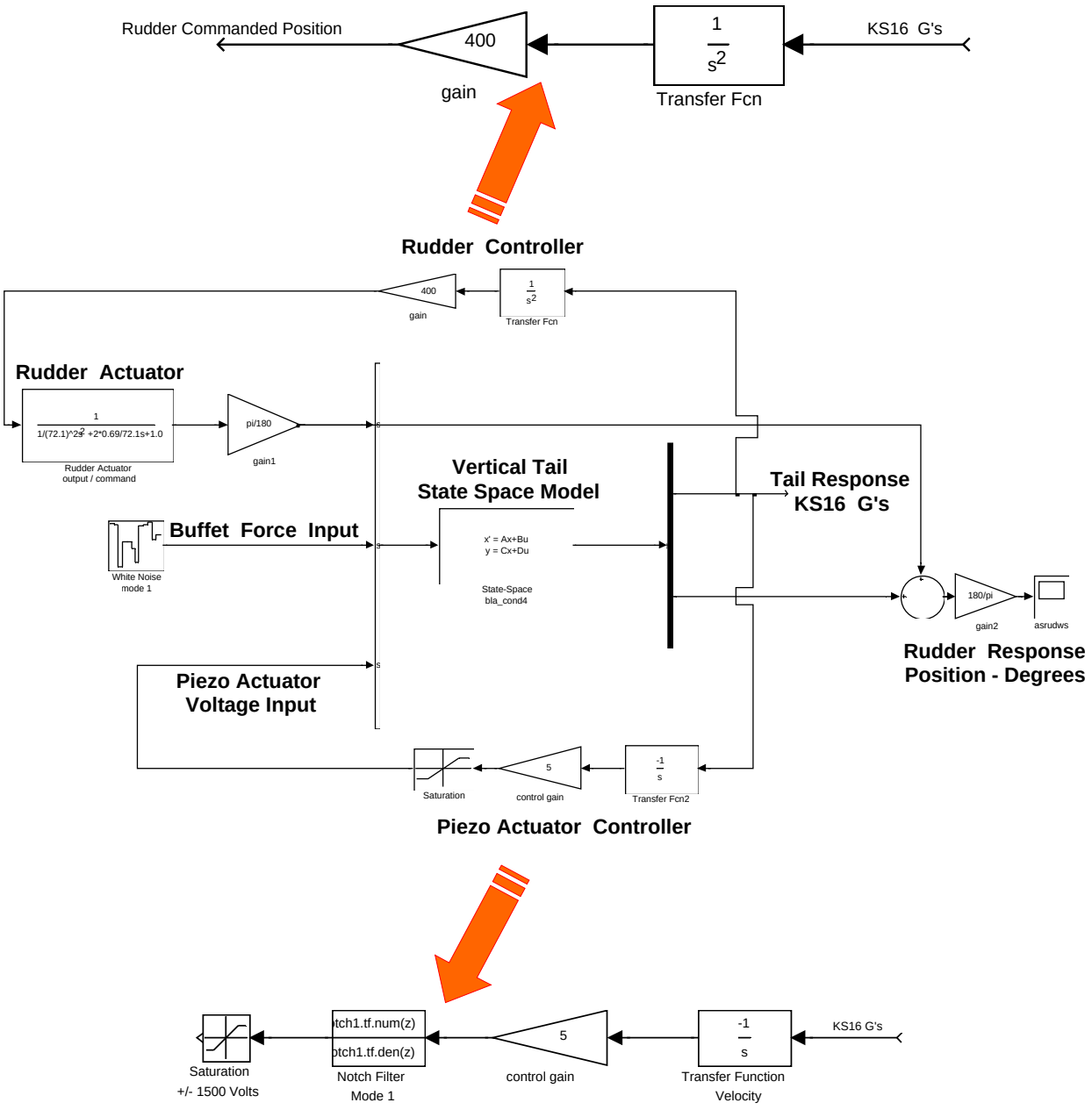

Figure 36. Overview of BLA Feedback Control Model

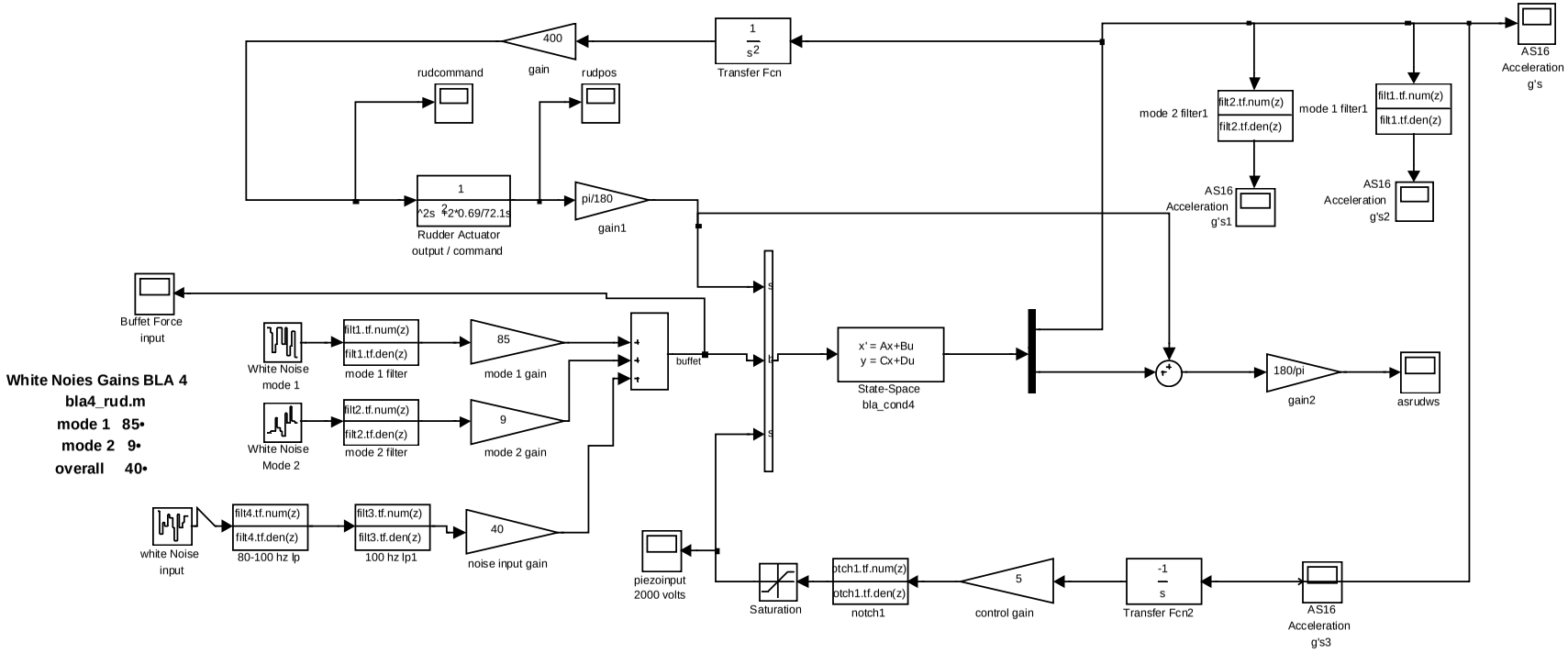

Figure 37. BLA SIMULINK Model with Rudder and Piezo Feedback Control

controllers. The piezoelectric actuator controller includes a notch filter at 15 Hz to reduce the feedback of the mode 1 response.

The rudder actuator model shown in Figure 36 was obtained from the Boeing F/A-18 Flight Controls Team. This second order model of the rudder actuator has an input of commanded rudder position and outputs the rudder position. A transfer function plot of this model is in Figure 38. The roll off in gain is 20 dB down at 45 Hz, and this is why the rudder has been

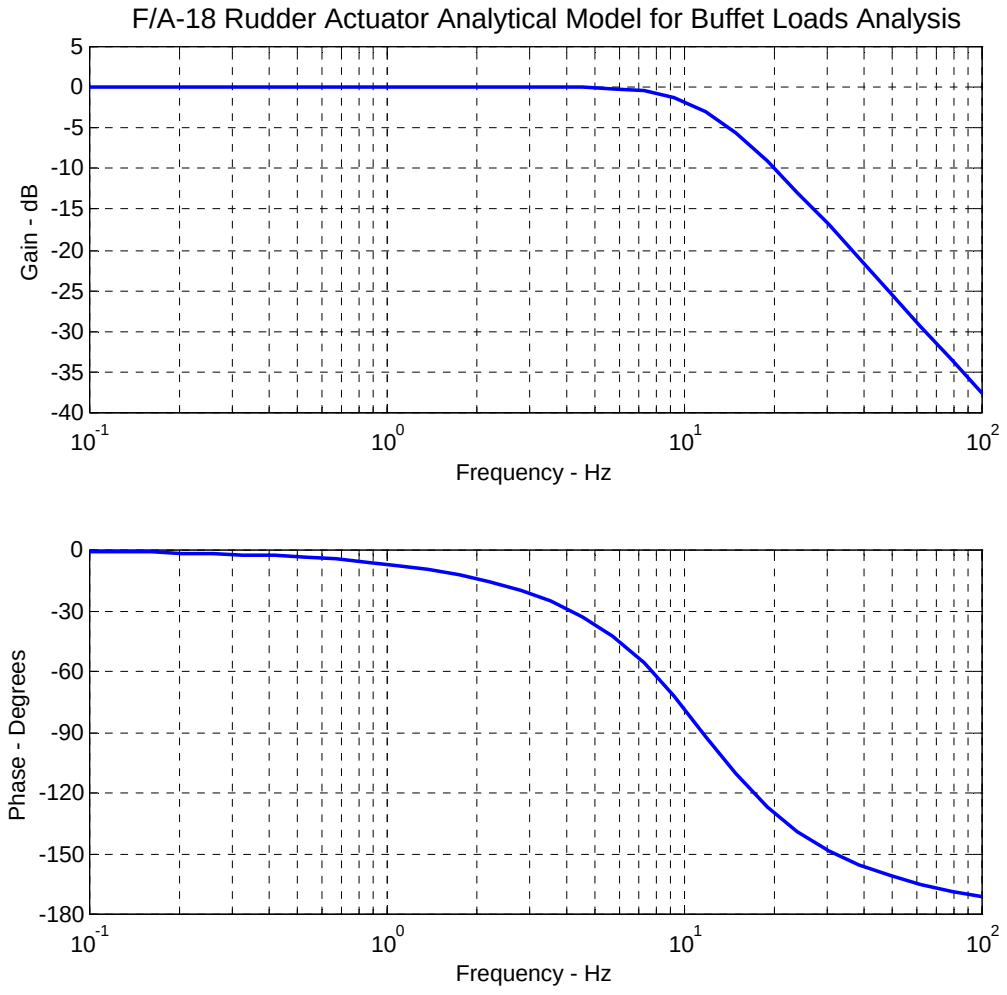

Figure 38. F/A-18 Rudder Actuator Analytical Model Transfer Function

limited in previous research to controlling the tail first mode at 15 Hz and not the second mode at 45 Hz. This rudder actuator model does not include the rudder structural stiffness or inertia because both of these quantities are in the vertical tail state space model.

phase with the acceleration response.

8.0 BLA SYSTEM PERFORMANCE

The complete analytical model of the BLA system was incorporated into the MATLAB® SIMULINK toolbox where both open- and closed-loop time history simulations were completed to determine the system performance. The results from the closed-loop analyses were used to determine the piezoelectric actuator requirements (location, area, thickness, voltage range). The six buffet flight conditions analyzed are listed in Table 10. The results from the active control for each system individually and combined are in Subsections 8.1, 8.2 and 8.3. The final Subsection, 8.4, includes the results from the fatigue analysis.

Table 10. Flight Conditions for BLA Analysis

Condition No.	Condition Description	Flight No.	Run No.	Mach No.	Altitude feet	AOA deg	Q psf	Nz G's	KS16 Response G's RMS 5-100 Hz	10-20 Hz	32-52 Hz
1	Mode 1 Maximum Response	766	23	0.51	11,094	35.1	252	5.5	60	36	30
2	Mode 2 Maximum Response	763	10A	0.83	28,785	31.7	323	6.8	91	13	66
3	Mode 1 Max. Fatigue Damage	766	56B	0.40	2,743	34.8	218	4.8	38	24	21
4	Mode 2 Max. Fatigue Damage	736	38	0.62	19,777	27.9	262	5.6	50	13	35
5	ACX Phase II Condition 3	741	36	0.43	1,852	23.7	258	4.9	37	9	27
6	ACX Phase II Condition 1	765	50A	0.52	10,024	15.9	271	4.2	10	2	5

Notes:
1. Flight conditions selected from Boeing F/A-18 Noise and Vibration Database
2. Flight test aircraft F/A-18 A4, Bu. No. 160778, interim production vertical tail with LEX fence.
3. Conditions selected are based on response of vertical tail aft-tip accelerometer KS16
   Mode 1 response: G's RMS from 10 - 20 Hz
   Mode 2 response: G's RMS from 32 - 52 Hz
4. Flight conditions 2, 5, and 6 are similar to the three ACX Phase II flight conditions 6, 3, and 1 (Reference 8)

8.1 PIEZOELECTRIC ACTUATOR PERFORMANCE

Open- and closed-loop analyses for the piezoelectric actuator control of mode 2 was completed in SIMULINK with the model depicted in Figures 37 and 38. A voltage limit of±1,500 volts was used for the analysis. This voltage limit was well within the limits of the manufacturer limit of ±2,000 volts for the NASA LaRC MFC actuator.

The performance objective was for a 50 percent reduction in mode 2 response for the critical mode 2 fatigue condition, BLA condition 4 from Table 10. The final configuration of piezoelectric actuators that met the performance objective is shown in Figure 39. The NASA LaRC MFC actuators (d33 IDE [13]) covered the vertical tail skin area above the fuel vent and below the fin

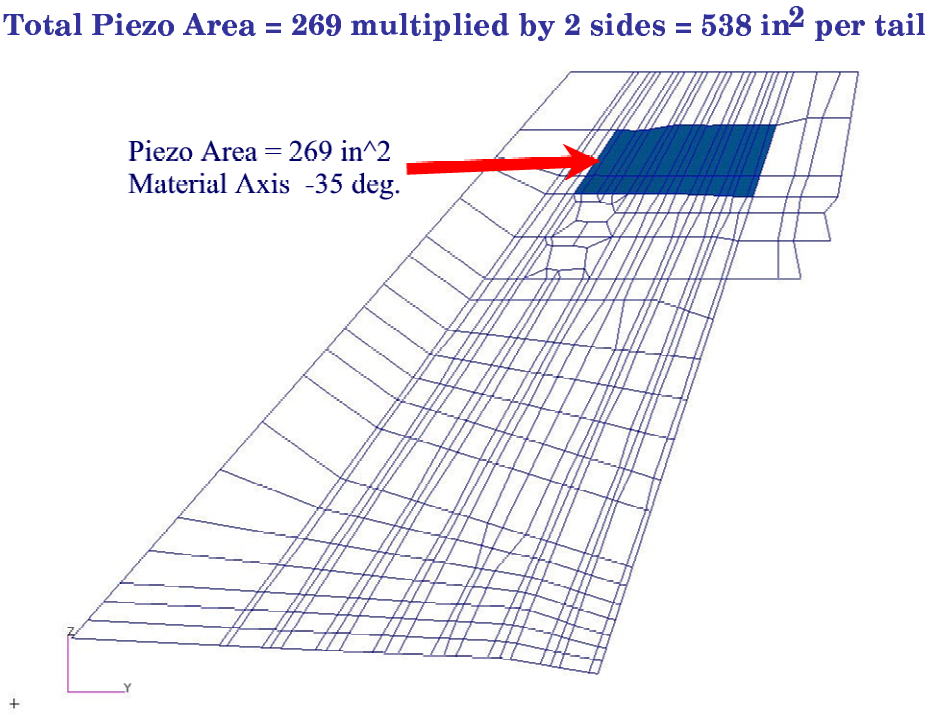

Figure 39. Final Piezoelectric Actuator Configuration for BLA System

cap, for a total area of 538 in^2 (269 in^2 times 2 sides). Using a density of 0.273 lb/in^3, this equates to about 9 pounds of piezoelectric actuators per tail. The actuators were aligned with the direction of principal strain for mode 2, as described in Section 3.2. The active piezoelectric material thickness for the actuators was 60 mil. One possibility for implementation would be to bond three layers of 20 mil actuators, as was done previously with the ACX Quickpack (custom) actuators in the full-scale test at IFOSTP [8]. Similar results could be obtained by halving the actuator thickness to 30 mil and by doubling the application area to include 600 in^2 (2 times 300 in^2 per side) that would include area below the fuel vent (Figure 22).

The results from the analysis for the open- and closed-loop response are in Figure 40. For each of the six conditions analyzed, Figure 40 includes a table with a summary of the results for different control gains, a PSD plot of the open- and closed-loop response at the optimally set gains for accelerometer KS16 (Figure 7), and a PSD plot of the commanded piezoelectric voltage at the optimally set gains. The summary tables in Figure 40 list the control gain, the RMS response for three different frequency bands representing an overall response (5 to 100 Hz), mode 1 response (10 to 20 Hz), and mode 2 response (32 to 52 Hz), the RMS of the piezoelectric actuator voltage, and the last column lists the percent reduction in mode 2 response from 32 to 52 Hz. The open-loop response shown as the blue dashed line in Figure 40 corresponds to a control gain of zero. The best performance from the closed-loop analysis is highlighted in the summary table with a border and is shown as the closed loop response red curve in Figure 40.

Overall, the piezoelectric actuator control reduced the mode 2 response from 30 percent to 67 percent with a 50 percent reduction for the performance objective, BLA condition 4. An additional result from the piezoelectric control was the reduction in response of the tail second

BLA Condition 1

BLA Condition 1 Controller Evaluation
Controller Filename: simulation_5_bla2_pzt_plant_direct
Plant name: bla1_pzt_plant
Simulation Model: bla1_pzt_controller

	Control Gain	KS16 G's RMS Response 5-100 Hz	10-20 Hz	32-52 Hz	Piezo Control RMS	Piezo Volts RMS	Reduction 32-52 Hz %
baseline	0.00	56	36	30	0.00	0	
	2.00	47	36	21	0.26	520	-30.0
	3.00	45	36	19	0.36	724	-36.7
	4.00	45	36	18	0.43	860	-40.0
	5.00	45	36	17	0.48	960	-43.3

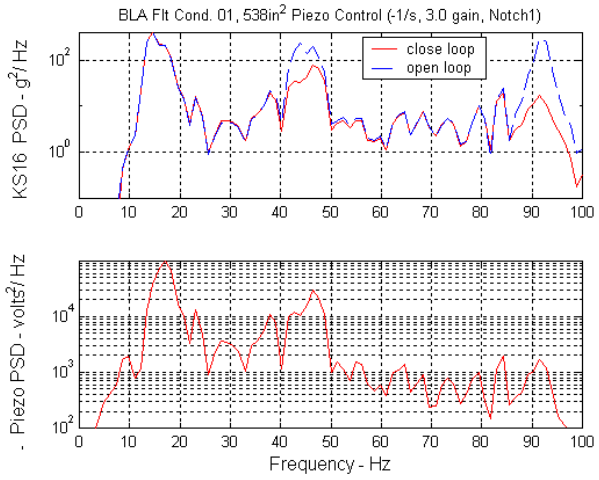

BLA Condition 2

BLA Condition 2 Controller Evaluation
Controller Filename: simulation_5_bla2_pzt_plant_direct
Plant name: bla2_pzt_plant
Simulation Model: bla2_pzt_controller

	Control Gain	KS16 G's RMS Response 5-100 Hz	10-20 Hz	32-52 Hz	Piezo Control RMS	Piezo Volts RMS	Reduction 32-52 Hz %
baseline	0.00	91	13	66	0.00	0	
	1.00	70	13	54	0.21	420	-18.2
	1.50	65	13	50	0.29	580	-24.2
	2.00	61	13	46	0.37	740	-30.3
	3.00	57	13	42	0.45	900	-36.4

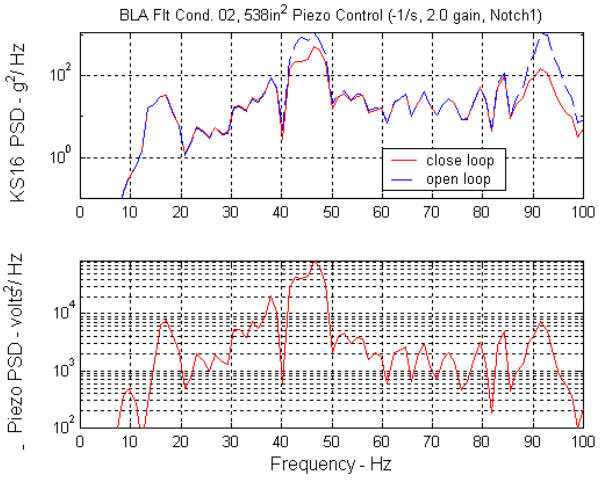

BLA Condition 3

BLA Condition 3 Controller Evaluation
Controller Filename: simulation_5_bla2_pzt_plant_direct
Plant name: bla3_pzt_plant
Simulation Model: bla3_pzt_controller

	Control Gain	KS16 G's RMS Response 5-100 Hz	10-20 Hz	32-52 Hz	Piezo Control RMS	Piezo Volts RMS	Reduction 32-52 Hz %
baseline	0.00	39	24	21	0.00	0	
	2.00	32	24	14	0.17	340	-33.3
	3.00	30	24	13	0.25	500	-38.1
	4.00	30	24	11	0.32	640	-45.7
	5.00	30	24	11	0.38	752	-49.5
	6.00	29	24	10	0.42	840	-52.4
	10.00	29	24	10	0.53	1060	-54.3

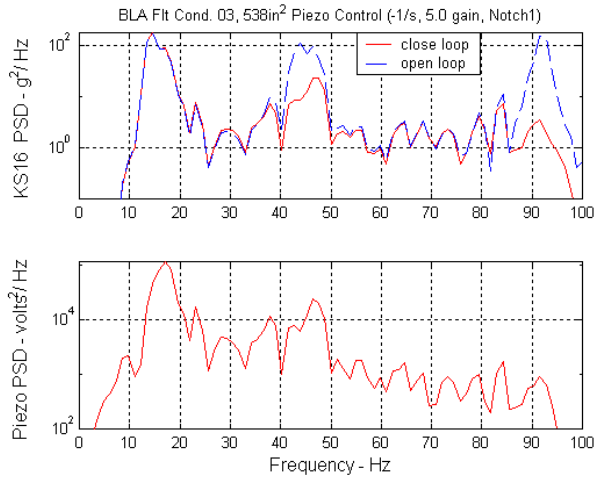

BLA Condition 4

BLA Condition 4 Controller Evaluation
Controller Filename: simulation_5_bla2_pzt_plant_direct
Plant name: bla4_pzt_plant
Simulation Model: bla4_pzt_controller

	Control Gain	KS16 G's RMS Response 5-100 Hz	10-20 Hz	32-52 Hz	Piezo Control RMS	Piezo Volts RMS	Reduction 32-52 Hz %
baseline	0.00	49	13	36	0.00	0	
	2.00	34	13	25	0.21	412	-30.6
	3.00	30	13	22	0.28	560	-38.9
	4.00	28	13	20	0.34	680	-44.4
	5.00	27	13	18	0.39	780	-50.0
	6.00	26	13	17	0.43	860	-52.8
	7.00	26	13	16	0.45	900	-55.6
Note 1	7.00	24	13	15	0.52	1040	-58.3

Note 1. The piezo control limit of +/-0.75 (1500 volts) was removed for this run

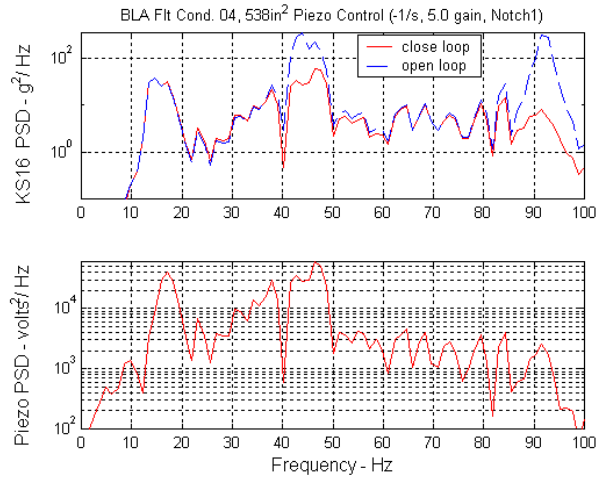

Figure 40. Open/Closed-Loop Response with Piezoelectric Actuator Control

BLA Condition 5

BLA Condition 5 Controller Evaluation
Controller Filename: simulation_5_bla2_pzt_plant_direct
Plant name: bla5_pzt_plant
Simulation Model: bla5_pzt_controller

	Control Gain	KS16 G's RMS Response 5-100 Hz	10-20 Hz	32-52 Hz	Piezo Control RMS	Piezo Volts RMS	Reduction 32-52 Hz %
baseline	0.00	36	9	27	0.00	0	
	2.00	24	9	18	0.15	300	-33.3
	3.00	22	9	16	0.20	400	-40.7
	4.00	20	9	14	0.25	500	-48.1
	5.00	19	9	13	0.29	580	-51.9
	6.00	18	9	12	0.33	650	-56.7
	10.00	16	9	9	0.43	854	-65.2

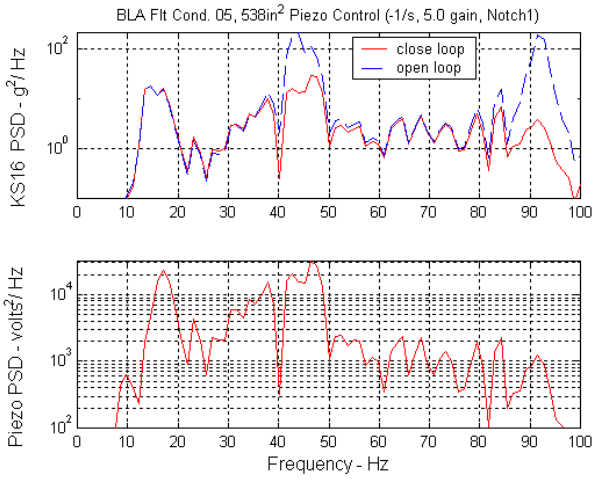

BLA Condition 6

BLA Condition 6 Controller Evaluation
Controller Filename: simulation_5_bla2_pzt_plant_direct
Plant name: bla6_pzt_plant
Simulation Model: bla6_pzt_controller

	Control Gain	KS16 G's RMS Response 5-100 Hz	10-20 Hz	32-52 Hz	Piezo Control RMS	Piezo Volts RMS	Reduction 32-52 Hz %
baseline	0.00	7	2	5	0.00	0	
	3.00	4	2	3	0.04	81	-40.0
	5.00	4	2	3	0.06	120	-50.0
	7.00	4	2	2	0.08	152	-58.0
	10.00	3	2	2	0.10	200	-67.0

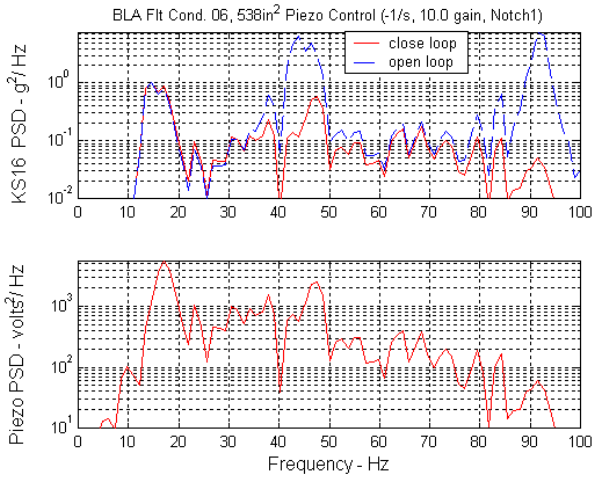

Figure 40. (Continued)
Open/Closed-Loop Response with Piezoelectric Actuator Control

torsion mode around 93 Hz, as shown throughout Figure 40. Even though a notch filter was used to reduce the mode 1 (10 to 20 Hz) voltage command, a significant amount of commanded voltage was in this frequency band, as shown in Figure 40. This certainly is an area that could be improved with some more development of the notch filter. Overall, the results were good with the performance objective met with less than 10 pounds of piezoelectric actuators added to the tail and the actuators were limited to 75 percent of their recommended maximum voltage range.

8.2 RUDDER ACTUATOR PERFORMANCE

Similarly, open- and closed-loop analyses for the rudder actuator control of mode 1 was completed next in SIMULINK with the model depicted in Figures 37 and 38. The analysis was similar to that described for the piezoelectric actuator control, except that the rudder feedback circuit was closed and the piezoelectric feedback circuit was open. The performance objective of 50 percent reduction in the mode 1 response at the critical fatigue condition, BLA condition 3, was close to being met, with the best performance being 46 percent response reduction. Overall, the mode 1 response was reduced from 35 percent to 55 percent for the six conditions analyzed, and the maximum commanded rudder input was ±2 degrees peak and the maximum rudder response was ±3.6 degrees peak.

The results from the open- and closed-loop analyses are in Figure 41. This figure is similar to Figure 40 except that the table includes the commanded rudder response (degrees RMS) and the actual rudder response (degrees RMS), with the final column being the percent reduction in mode 1 response (10 to 20 Hz). Again, the best performance from the closed-loop analysis is highlighted in the summary table with a border and is shown as the closed-loop response red curve in Figure 41. The best performance from the active rudder was the 53 percent mode 1 response reduction for the maximum mode 1 response, BLA condition 1. It was difficult for the feedback control to be effective for BLA condition 2, which is the condition of maximum mode 2 response, and the result was limited to a 35 percent response reduction in mode 1. In addition to reducing the response of mode 1, the rudder was effective in reducing the response of mode 2 by 20 percent for BLA condition 4. This was unexpected because of the rudder actuator rolloff in

BLA Condition 1

BLA Condition 1 Controller Evaluation
Controller Filename: feedback 1/s^2 times KS16 acceleration
Plant name: bla1_rud_plant
Simulation Model: bla1_rud_control

	Control Gain	KS16 G's RMS Response 5-100 Hz	10-20 Hz	32-52 Hz	Rudder Command deg RMS	Rudder Response deg RMS	Reduction 10-20 Hz %
baseline	0	56	36	30	0.00	0.09	
	100	49	26	28	0.30	0.50	-27.8
	200	46	22	27	0.48	0.80	-38.9
	300	45	19	25	0.61	1.02	-47.2
	400	43	17	25	0.71	1.20	-52.8
	500	43	16	25	0.79	1.35	-56.9
	800	44	12	25	0.96	1.70	-68.1
see Note	1,000	216	10	41	1.80	5.40	-72.2

Note: For Gain=1000, forced response between 55-65 Hz

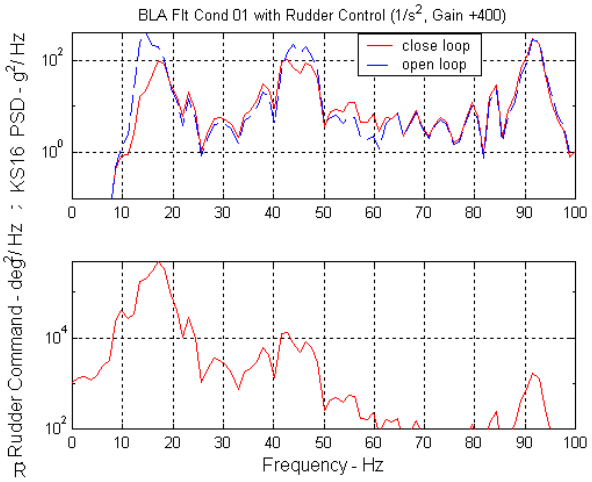

BLA Condition 2

BLA Condition 2 Controller Evaluation
Controller Filename: feedback 1/s^2 times KS16 acceleration
Plant name: bla2_rud_plant
Simulation Model: bla2_rud_control

	Control Gain	KS16 G's RMS Response 5-100 Hz	10-20 Hz	32-52 Hz	Rudder Command deg RMS	Rudder Response deg RMS	Reduction 10-20 Hz %
baseline	0	89	13	66	0.00		
	100	88	11	64	0.15	0.30	-15.4
	200	89	10	63	0.28	0.54	-23.1
	300	90	9	63	0.40	0.80	-30.8
	400	92	9	63	0.52	1.07	-34.6
	500	95	8	65	0.65	1.40	-40.0

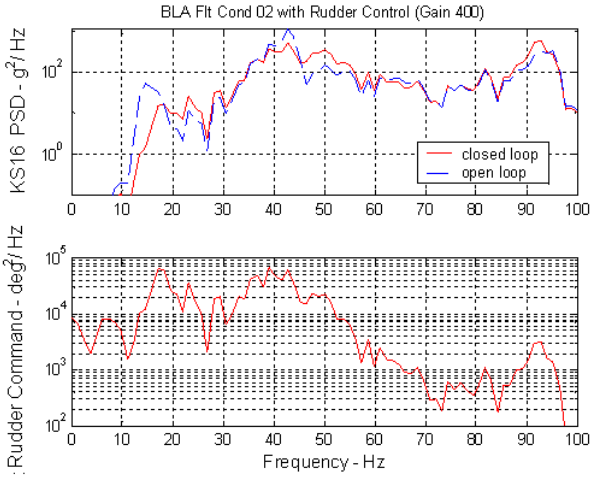

BLA Condition 3

BLA Condition 3 Controller Evaluation
Controller Filename: feedback 1/s^2 times KS16 acceleration
Plant name: bla3_rud_plant
Simulation Model: bla3_rud_control

	Control Gain	KS16 G's RMS Response 5-100 Hz	10-20 Hz	32-52 Hz	Rudder Command deg RMS	Rudder Response deg RMS	Reduction 10-20 Hz %
baseline	0	39	24	21	0.00	0.07	
	100	35	18	21	0.35	0.21	-25.0
	200	34	16	21	0.34	0.57	-33.3
	300	34	14	20	0.44	0.74	-41.7
	400	34	13	20	0.52	0.87	-45.8
	500	34	12	20	0.59	0.98	-50.0
	800	34	9	20	0.72	1.21	-62.5
see Note	1,000	36	8	19	0.79	1.34	-66.7

Note: For Gain=1000, forced response between 55-65 Hz

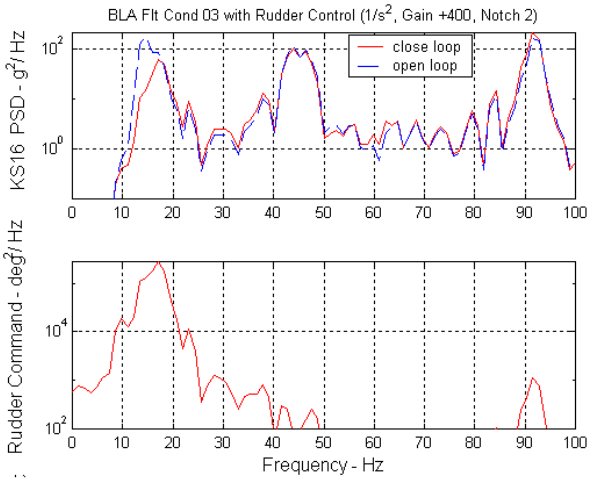

BLA Condition 4

BLA Condition 4 Controller Evaluation
Controller Filename: feedback 1/s^2 times KS16 acceleration
Plant name: bla4_rud_plant
Simulation Model: bla4_rud_control

	Control Gain	KS16 G's RMS Response 5-100 Hz	10-20 Hz	32-52 Hz	Rudder Command deg RMS	Rudder Response deg RMS	Reduction 10-20 Hz %
baseline	0	48	13	35	0.00	0.08	
	100	46	10	33	0.11	0.21	-26.9
	200	45	8	31	0.19	0.35	-38.5
	300	44	7	29	0.25	0.48	-46.2
	400	43	6	28	0.30	0.59	-53.8
	500	43	6	27	0.34	0.69	-57.7
	800	46	4	25	0.47	1.03	-69.2
see Note	1,000	354	4	64	2.60	7.00	-69.2

Note: For Gain=1000, forced response between 55-65 Hz

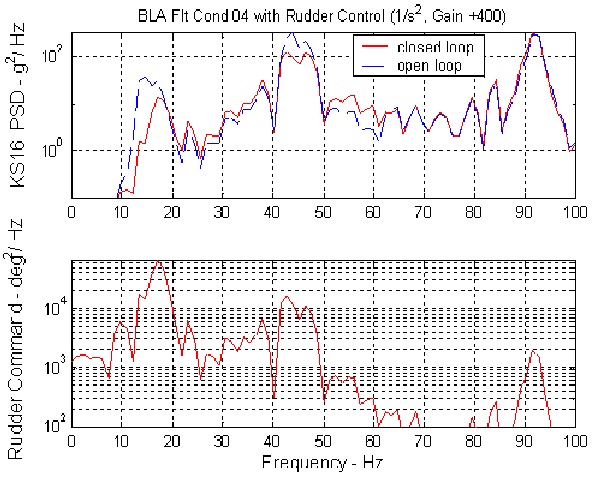

Figure 41. Open/Closed-Loop Response with Rudder Actuator Control

BLA Condition 5

BLA Condition 4 Controller Evaluation
Controller Filename: feedback 1/s^2 times KS16 acceleration
Plant name: bla5_rud_plant
Simulation Model: bla5_rud_control

	Control Gain	KS16 G's RMS Response 5-100 Hz	10-20 Hz	32-52 Hz	Rudder Command deg RMS	Rudder Response deg RMS	Reduction 10-20 Hz %
baseline	0	37	9	27	0.00	0.09	
	100	34	7	26	0.08	0.15	-22.2
	200	34	6	26	0.14	0.27	-33.3
	300	34	5	25	0.19	0.38	-44.4
	400	34	4	26	0.23	0.49	-51.1
	500	34	4	26	0.28	0.61	-55.6
	800	37	3	27	0.41	0.98	-66.7
see Note	1,000	50	3	30	0.58	1.50	-71.1

Note: For Gain=1000, forced response between 55-65 Hz

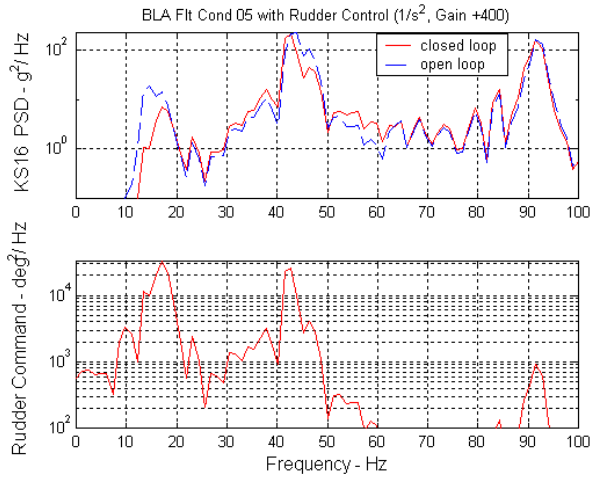

BLA Condition 6

BLA Condition 6 Controller Evaluation
Controller Filename: feedback 1/s^2 times KS16 acceleration
Plant name: bla6_rud_plant
Simulation Model: bla6_rud_control

	Control Gain	KS16 G's RMS Response 5-100 Hz	10-20 Hz	32-52 Hz	Rudder Command deg RMS	Rudder Response deg RMS	Reduction 10-20 Hz %
baseline	0	8.0	2.0	6.0	0.00	0.01	
	100	7.8	1.5	5.4	0.02	0.03	-25.0
	200	7.6	1.2	5.0	0.03	0.06	-40.0
	300	7.5	1.0	5.0	0.04	0.08	-50.0
	400	7.5	1.0	5.0	0.05	0.10	-52.5
	500	7.5	0.8	4.8	0.06	0.12	-58.0
	800	8.0	0.6	4.9	0.08	0.18	-68.5
see Note	1,000	43	1	8	0.32	1.07	-70.0

Note: For Gain=1000, forced response between 55-65 Hz

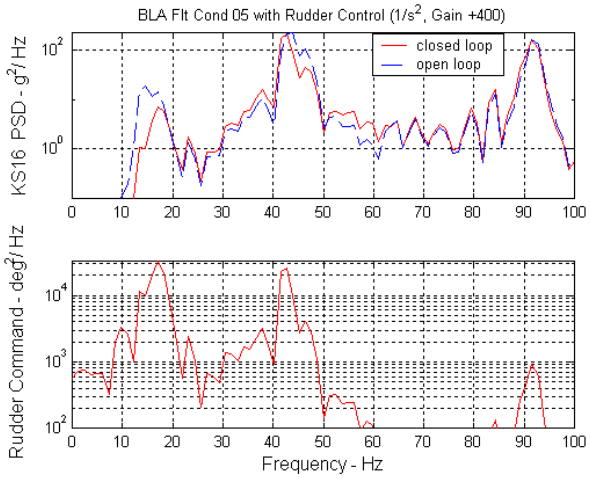

Figure 41. (Continued)
Open/Closed-Loop Response with Rudder Actuator Control

gain above 20 Hz, as shown in Figure 38. But Figure 38 does not include the effect of the rudder mass inertia on the response, and when the large rudder inertia forces are included near 45 Hz, the rudder is effective. This increased effectiveness of the rudder has also been observed from flight tests of the F/A-18 for flight controls. The use of the rudder to control the second mode at 45 Hz was not pursued under this analysis but could be the subject of additional research.

8.3 COMBINED PIEZOELECTRIC - RUDDER PERFORMANCE

The final analyses in SIMULINK were completed with both the piezoelectric and rudder actuator control systems active, as described in Sections 8.1 and 8.2. The performance from the combined control was similar to the performance from the individual control. The mode 1 response was reduced from 39 percent to 51 percent for the combined system, and the mode 2 response was reduced from 33 percent to 70 percent. The mode 2 response was reduced further in the combined system because the rudder is contributing toward the response reduction at 45 Hz, as described in the previous section. Again, the performance objective of a 50 percent response reduction for mode 2 at BLA condition 4 was exceeded by the combined system and the mode 1 performance objective of 50 percent reduction for BLA condition 3 was nearly met by the 43 percent response reduction for the combined system.

A summary of the results from the open- and closed-loop analyses of the combined system are listed in Table 11 for the six conditions analyzed (Table 10). The open-loop response levels are listed in the row with a gain of zero, and the closed-loop response is included on the nonzero rows. The final two columns list the mode 1 and mode 2 percent response reduction that was based on the RMS for the frequency band listed. Plots of the open- and closed-loop response along with the commanded signals are in Figure 42 for each of the conditions analyzed. These results are similar to the results discussed previously for the individual systems, Sections 8.1 and 8.2.

The overall performance of the combined feedback control system produced 70 percent to 30 percent vertical tail buffet response reductions for flight conditions ranging from moderate to

Table 11. Results from Combined Control of Piezoelectric and Rudder

BLA Condition	Rudder Control Gain	Piezo Control Gain	KS16 G's RMS Response 5-100 Hz	10-20 Hz	32-52 Hz	Rudder Command deg RMS	Piezo Command Volts RMS	Reduction 10-20 Hz %	Reduction 32-52 Hz %
1	0	0	56	36	30	0.00	0		
1	400	4	30	18	16	0.72	811	-50.8	-47.0
2	0	0	74	13	66	0.00	0		
2	300	3	49	8	44	0.29	854	-38.5	-33.3
3	0	0	39	24	21	0.00	0		
3	400	5	21	14	10	0.54	740	-42.9	-50.5
4	0	0	48	13	35	0.00	0		
4	400	5	24	6	16	0.28	744	-50.8	-54.3
5	0	0	36	9	27	0.00	0		
5	400	5	17	5	12	0.20	558	-50.0	-55.6
6	0	0	8	2	6	0.00	0		
6	400	10	3	1	2	0.04	216	-50.0	-70.0

Notes:
1. Piezo Control: rudder feedback -1/s times KS16 acceleration (with mode 1 notch filter)
2. Rudder Control: rudder feedback 1/s^2 times KS16 acceleration
BLA Condition 3 rudder controller has additional notch filter for Mode 2

severe buffet. This was accomplished with a maximum commanded rudder position of±2 degrees (15 Hz) and about 10 pounds of piezoelectric actuators operating at a maximum voltage range of ±1,500 volts and a peak power level of 2,000 watts.

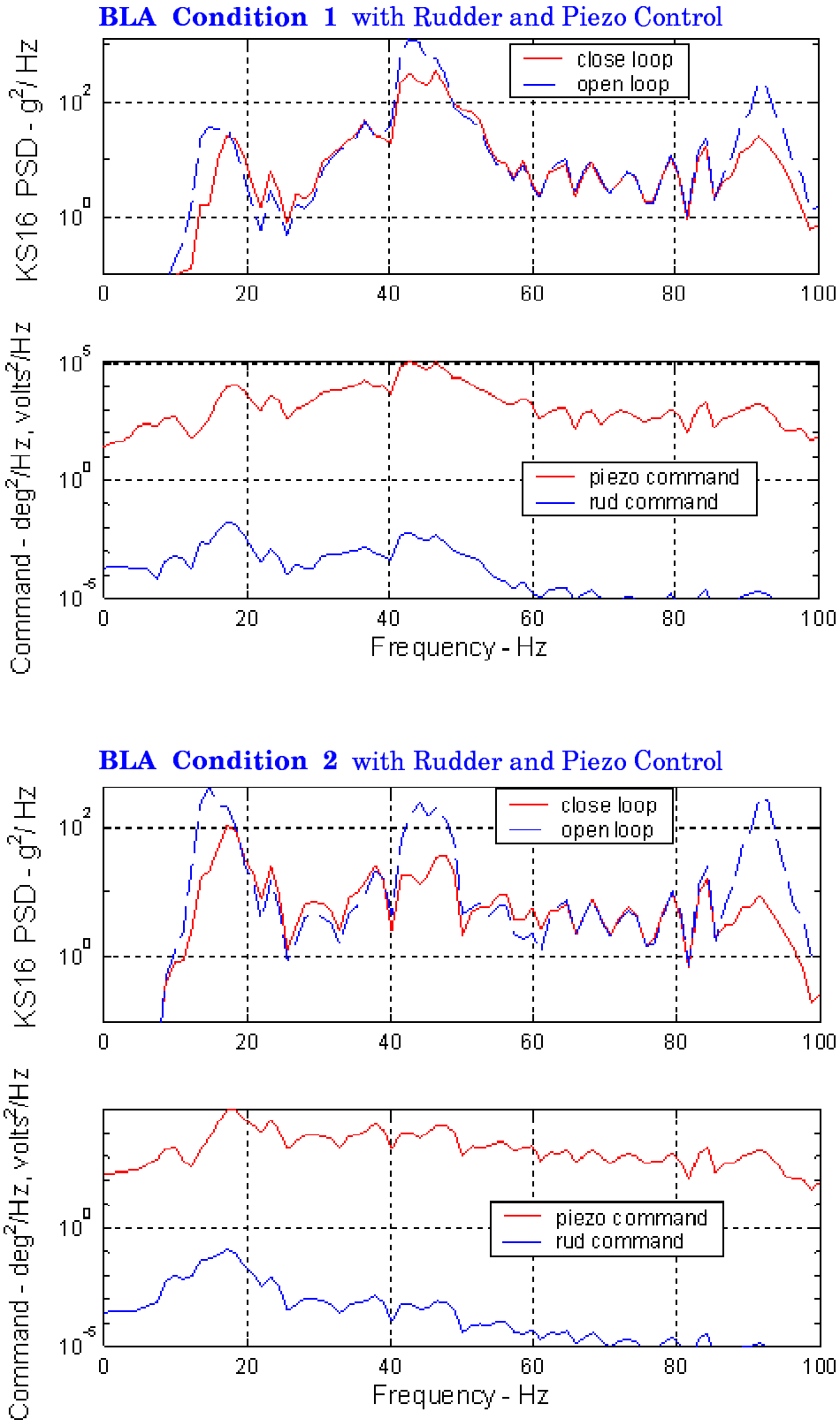

Figure 42. Open/Closed-Loop Response with Combined Piezoelectric and Rudder Actuator Control

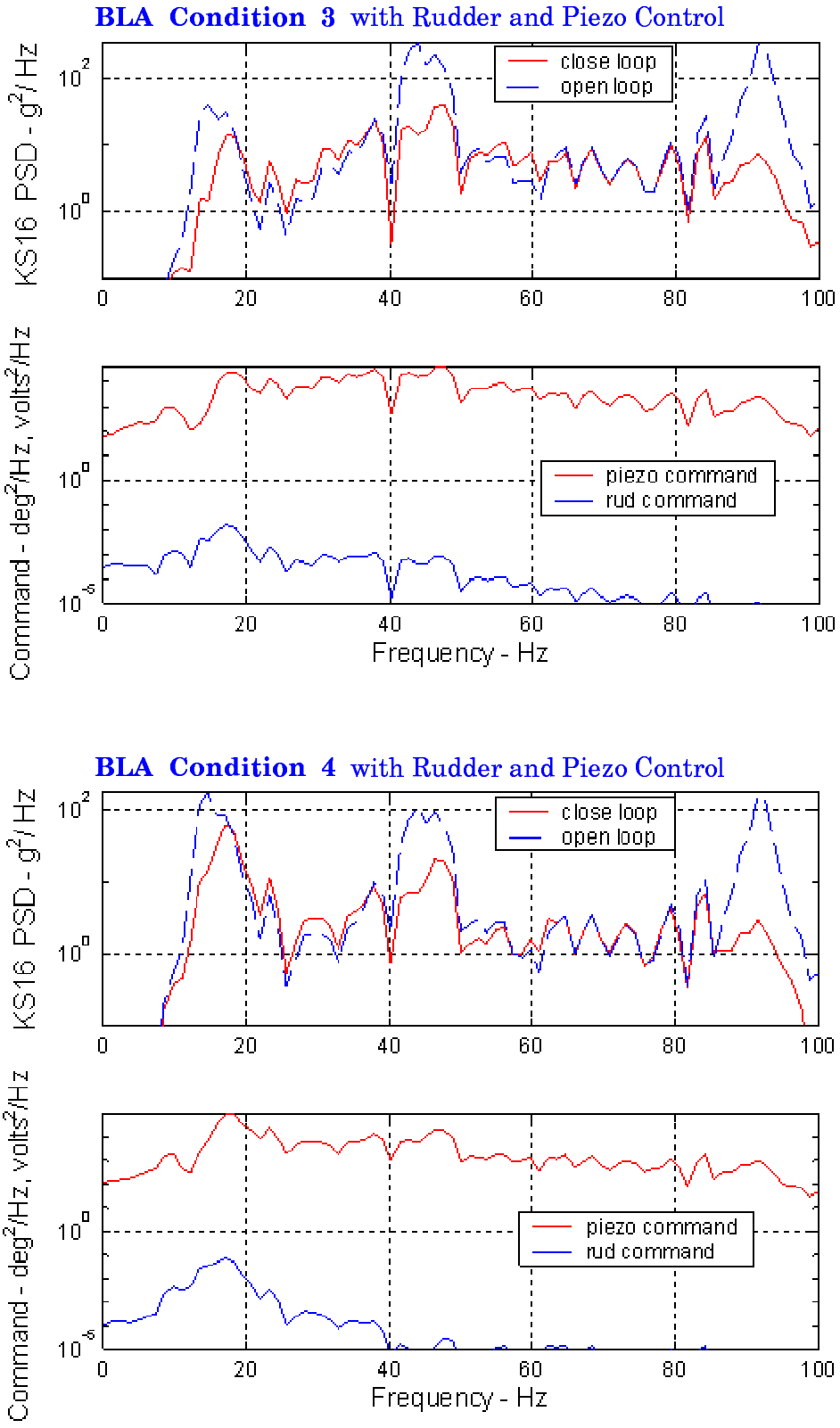

Figure 42. (Continued) Open/Closed-Loop Response with Combined Piezoelectric and Rudder Actuator Control

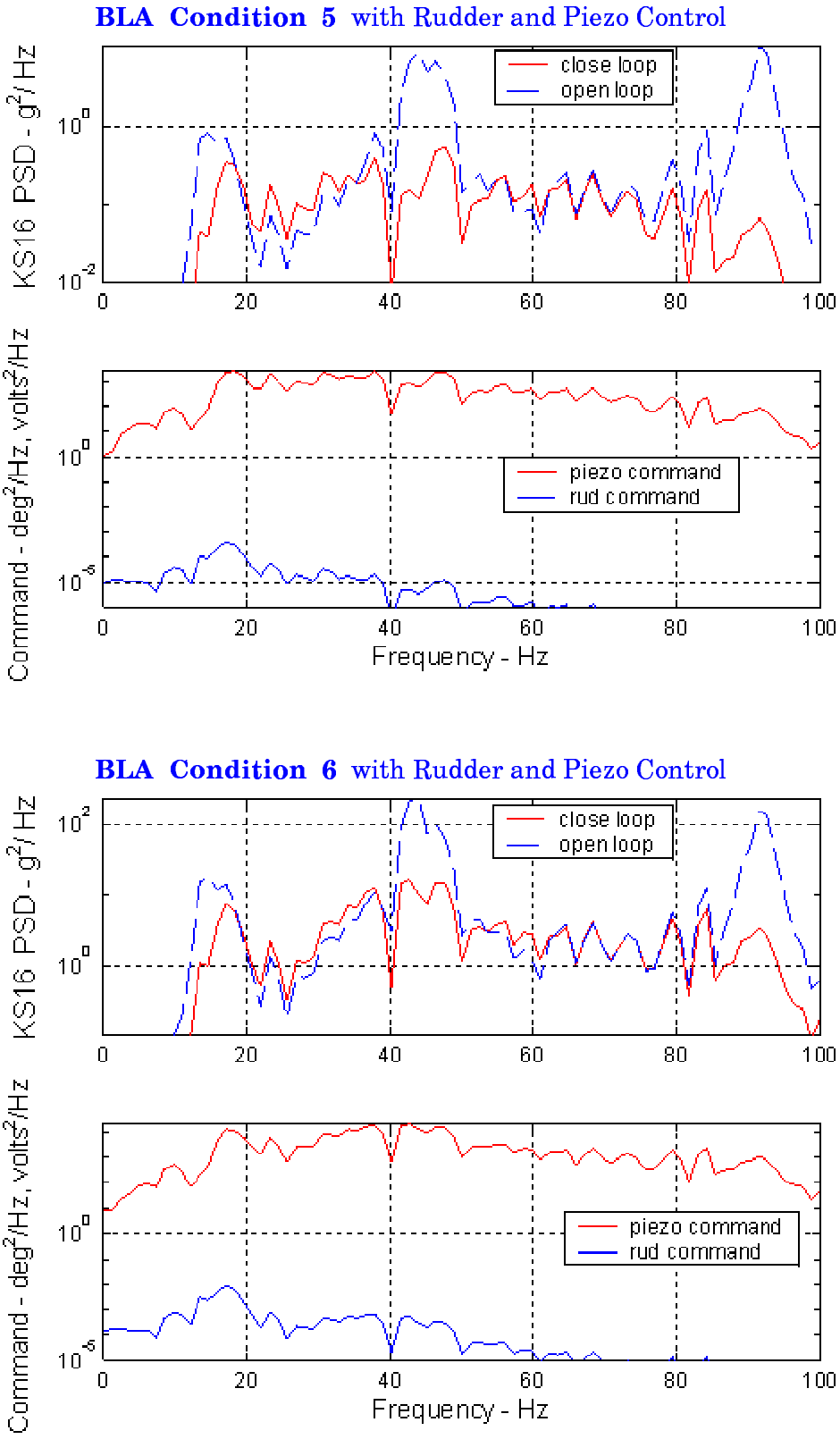

Figure 42. (Continued) Open/Closed-Loop Response with Combined Piezoelectric and Rudder Actuator Control

8.4 FATIGUE LIFE

The fatigue life improvement for the vertical tail with the BLA system was determined using a similar procedure as described in Section 8 [8]. The results from the open- and closed-loop performance were used in a fatigue LIF calculation. The analysis was completed for the F/A-18 vertical tail critical fatigue location of the root spar. The existing U.S. Navy F/A-18 vertical tails exceed the 6,000-hour aircraft lifetime with a 7,500-hour fatigue life. With the fatigue life improvement from the closed-loop BLA system, the vertical tail fatigue life increased to over 17,000 hours. This fatigue life improvement exceeded the BLA system objective for a 12,000-hour vertical tail, as described in Section 2.2.

The fatigue life of the F/A-18 vertical tail is a function of the aircraft usage, dynamic loads, and steady maneuver loads. The fatigue damage from the steady maneuver loads was assumed to remain unchanged by the addition of the BLA system. The fatigue LIF calculation was completed using the BLA system performance results for the dynamic loads of mode 1 and mode 2. The existing fatigue damage tables were used that provide the fatigue damage for each mode as a function of dynamic response, 10 to 20 Hz for mode 1 and 32 to 52 Hz for mode 2, and aircraft usage, dynamic pressure (q) and AOA. The BLA system performance results (Table 11) for the six flight conditions were fit using a linear regression technique to establish a performance trend over the buffet flight envelope. The results from the linear fit for mode 1 are in Figure 43 and for mode 2 are in Figure 44. Each figure includes the performance ratio of closed-loop to open-loop (CL/OL in Figure 44) for the six analysis points and the resulting linear fit equation and curve. The BLA system performance for mode 1 produced a relatively flat trend of closed-loop response near 53 percent of the open-loop response because the rudder authority

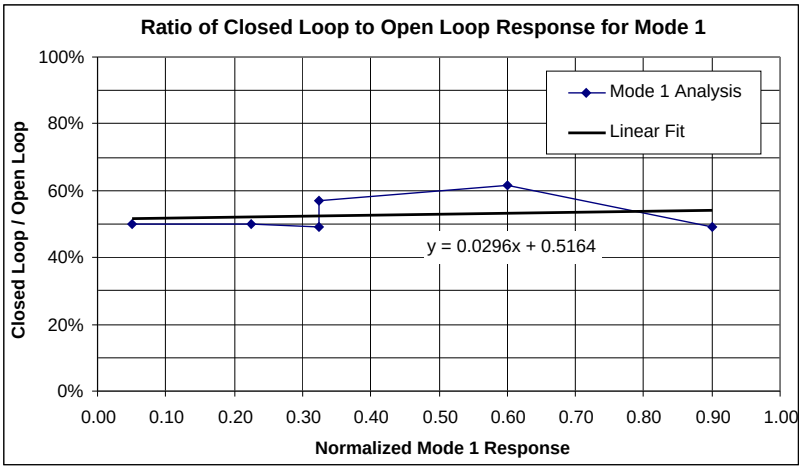

BLA cond.	Q psf	AOA deg	Mode 1 G's RMS	Mode 1 % of Max	Reduction %	Ratio CL/OL
1	252	35.1	36	0.90	51%	49%
3	218	34.8	24	0.60	38%	62%
2	323	31.7	13	0.33	43%	57%
4	262	27.9	13	0.33	51%	49%
5	258	23.7	9	0.23	50%	50%
6	271	15.9	2	0.05	50%	50%

Note
1. % of Max for Mode 1 calculated using 40 g's RMS

Figure 43. Ratio of Closed-Loop to Open-Loop Response for mode 1

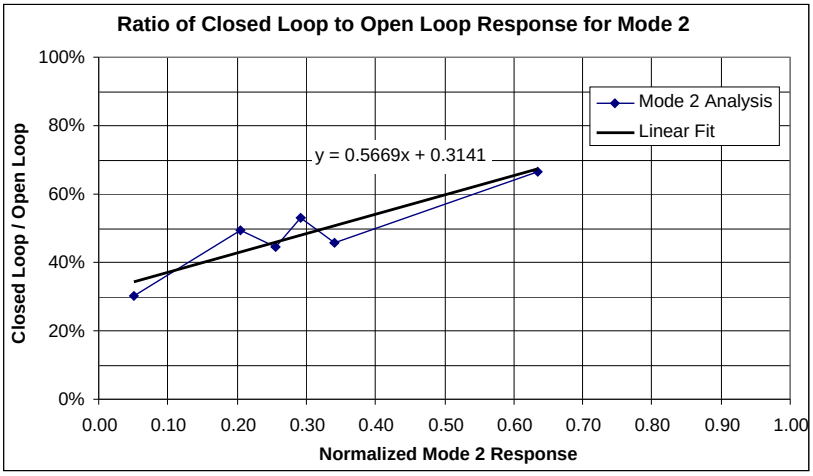

BLA cond.	Q psf	AOA deg	Mode 2 G's RMS	Mode 2 % of Max	Reduction %	Ratio CL/OL
2	323	31.7	66	0.64	33%	67%
4	262	27.9	35	0.34	54%	46%
1	252	35.1	30	0.29	47%	53%
5	258	23.7	27	0.26	56%	44%
3	218	34.8	21	0.20	50%	50%
6	271	15.9	5	0.05	70%	30%

Note
1. % of Max for Mode 2 calculated using 93 G's RMS

Figure 44. Ratio of Closed-Loop to Open-Loop Response for mode 2

did not reach a limit. In contrast, the piezoelectric actuators were limited to a voltage range of ±1,500 Volts and this resulted in a mode 2 performance trend that was inversely proportional to the mode 2 tail response, as shown in Figure 44. Also in Figure 44, the maximum open-loop response for mode 2 was from BLA condition 2 and was 66 G's RMS as compared to the maximum mode 2 response of 93 G's RMS used for the fatigue LIF calculation. One possible reason for this discrepancy was that the BLA analysis conditions were selected from PSDs in the noise and vibration database as described in Section 4.2, and the fatigue damage table data is from peak-valley time history data.

The results from the fatigue LIF calculation for the BLA system are in Table 12. The first two columns list the open-loop fatigue damage and associated lifetime hours for mode 1, mode 2, and

Table 12. Open-Loop and Closed-Loop Fatigue Life Comparison

	Open Loop Damage	Open Loop Lifetime Hours	Closed Loop Lifetime Improvement Factor	Closed Loop Damage	Closed Loop Lifetime Hours
Mode 1	0.26	1950	57.6	0.01	186
Mode 2	0.33	2475	28.3	0.03	482
Maneuver	0.41	3075	1.0	0.96	16929
Total	1.00	7500		1.00	17598

Note: Fatigue life for critical location, zone 1, vertical tail root.

the steady maneuver loads. For the fatigue critical location, 26 percent of the damage is from mode 1, 33 percent from mode 2, and 41percent of the damage is from steady maneuver loads. The open-loop fatigue life is approximately 7,500 flight hours. The results from the closed-loop BLA system performance are included in the last three columns of Table 12. The results from the fatigue LIF calculation are included that provide a fatigue life improvement factor for the addition of the BLA system. The BLA system reduces the fatigue damage from dynamic loads to

4 percent and this results in a vertical tail fatigue life of over 17,000 flight hours. This exceeded the BLA system objective of 12,000 flight hours as stated in Section 2.2.

9.0 CONCLUSIONS AND RECOMMENDATIONS

9.1 CONCLUSIONS

The preliminary development of an advanced BLA system for use on the F-18 vertical tail has been completed. The BLA system uses the most effective features of two systems, the rudder actuator and control surface are used to control the response of the tail first bending mode near 15 Hz, and piezoelectric actuators are used to control the response of the second tail mode, tip torsion, near 45 Hz. The analytical ASE model was validated by good agreement with measured results from a full-scale ground test, measured aircraft buffet flight test response, and an in-flight commanded rudder frequency sweep.

The overall performance of the BLA system produced 70 percent to 30 percent vertical tail buffet response reductions for flight conditions ranging from moderate to severe buffet. This was accomplished with a maximum commanded rudder position of ±2 degrees (15 Hz) and about 10 pounds of NASA LaRC MFC piezoelectric actuators attached to the vertical tail skin and operating at a peak power level of 2,000 watts. The actuators were limited to an operating voltage that was 75 percent of their recommended maximum voltage range. The control laws only required a change to the gain to go from one condition to the next and this simplifies the aircraft system integration. The BLA system reduces the vertical tail fatigue damage from dynamic loads and more than doubled the vertical tail fatigue life, exceeding the BLA system objective of 12,000 flight hours, two aircraft lifetimes. This system is also adaptable to other aircraft surfaces and vehicle platforms.

9.2 RECOMMENDATIONS

The first recommendation would be to validate the analytical model of the piezoelectric actuators with measured test results. This will require some research and development into the piezoelectric actuator type, configuration, and layout for optimum performance. Included in this research should be an investigation to verify the capacitance difference from IDE to plate electrodes for the piezoelectric actuators as reported in Section 5.1. It is also recommended to investigate the use of the piezoelectric material from the TRS HK1HD actuator into the NASA LaRC MFC actuator. The TRS HK1HD actuator had the best performance for a d31 plate actuator and had the second lowest cost estimate.

Because of the risk associated with developing the thicker version of the NASA LaRC MHD-460 actuator and the requirement to produce a large quantity of custom actuators, it is recommended to select the Continuum Control AFC 10-mil fiber actuator as a replacement should the NASA LaRC MHD-460 actuator experience development or manufacturing problems.

Even though the feedback control laws were effective, research into alternative controllers should be pursued to improve the system performance.

Finally, it is recommended to include the active rudder control surface in the follow-on ground test because the primary control force is from the rudder inertia force and not the aerodynamic force. The use of the rudder to control the second mode at 45 Hz was not pursued under this analysis but could be the subject of future research.

10.0 REFERENCES

1. Levesque, G. S., "F/A-18 Vertical Tail/LEX Fence Dynamic Response Flight Test Program," Boeing Co. Report MDC B1430, 1 March 1989.
2. Scanlon, R.W., "F/A-18 Vertical Tail/LEX Fence Dynamic Response Wind Tunnel Test Program," Boeing Co. Report MDC B1393, 31 January 1989.
3. Liguore, S., Ferman, M., and Yurkovich, R., "Integral damping treatment for primary aircraft structures," Damping '91 Conference, San Diego, CA, 13-15 February 1991.
4. Ferman, M. A., et al., "Composite `Exoskin' Doubler Extends F-15 Vertical Tail Fatigue Life," AIAA Paper 93-1341.
5. Ashley, H., Rock, H., Digumarthi, R., Chaney, K., and Eggers, A., "Active control for fin buffet alleviation," United States Air Force Research Laboratory Report WL-TR-93-3099, January 1994.
6. Pado, L. E., Lichtenwalner, "Neural Predictive Control for Active Buffet Alleviation," AIAA-99-1319, 40th AIAA Structures, Structural Dynamics, and Materials Conference, St. Louis, MO, April 1999.
7. Moses, R. W., "Vertical Tail Buffeting Alleviation Using Piezoelectric Actuators – Some Results of the Actively Controlled Response of Buffet-Affected Tails (ACROBAT) Program," SPIE's 4th Annual Symposium on Smart Structures and Materials, Industrial and Commercial Applications of Smart Structures Technologies Conference, San Diego, CA, 4-6 Mar 97.
8. Spangler, R. L., "An Active Smart Material System for BLA," United States Air Force Research Laboratory Report AFRL-VA-WP-TR-1998-3079, November 1998.
9. Moses, R. W., "Contributions to Active Buffeting Alleviation Programs by the NASA Langley Research Center," 40th AIAA Structures, Structural Dynamics, and Materials Conference, St. Louis, MO, 12-15 April 1999.

10. Barmac, T.K., and Campbell, J.F., "Non-Linear Finite Element Modeling of THUNDER Piezoelectric Actuators," SPIE Conference on Smart Structures and Integrated Systems, Newport Beach, CA, Mar 99.
11. Kalman, T.P. and Giesing, J.P., Subsonic Steady and Oscillatory Aerodynamics for Multiple Interfering Wings and Bodies, Boeing Report MDC-J7295, Volume I, Oct. 1976.
12. Pitt, D.M. and Goodman, C.E., FAMUSS: A New Aeroservoelastic Modeling Tool, AIAA Paper 92-2395.
13. Wilkie, W.K., et al., "Low-Cost Piezocomposite Actuator for Structural Control Applications," SPIE 7th International Symposium on Smart Structures and Materials, Newport Beach, CA, March 5-9, 2000.

LIST OF ABBREVIATIONS

Acronym	Description
a/c, ac	aircraft
ACX	Active Controls eXperts, Inc.
AFC	Active-Fiber-Composite actuator
AFRL	Air Force Research Laboratory
AIC	Aerodynamic influence coefficient
AOA	Angle of attack
ASE	Aero servo elasticity
ASESS	Aero-Servo-Elastic Stability System
BLA	Buffet Load Alleviation
CG, cg	Center of gravity
CTE	Coefficient of thermal expansion
deg	degree
F/A-18	Fighter/Attack Aircraft, F/A-18
FAMUSS	Flexible Aircraft Modeling Using State Space
FCC	Flight Control Computer
FEM	Finite element model
GVT	Ground vibration test
Hz	Hertz (cycles/second)
IDE	Inter-Digitated Electrode
IFOSTP	International Follow-On Structural Test Program
KEAS	Knots Equivalent Air-Speed
LaRC	Langley Research Center

LEX ..... Leading Edge extension

lh .....Left hand

LIF ..... Life improvement factor

MFC..... Macro-Fiber-Composite actuator

MIMO .....Multi-Input, Multi-Output controller

NASA .....National Aeronautics and Space Administration

NASTRAN..... NASA Structural Analysis Program

PSD .....Power spectral density

rh .....Right hand

RMS .....Root mean squared

RVDT ..... Rotary variable displacement transducer

SIDEKIC ..... Scaling Influences Derived from Experimentally Known Impact of Controls

SISO..... Single-Input, Single-Output controller

STAP ..... Structural Technology and Analysis Program

TRS .....TRS Ceramics (Manufacturer of Piezoelectric Actuators)

TTCP .....The Technical Cooperation Program

LIST OF SYMBOLS

Symbol	Description
A	Aerodynamic inertia
A,B,C,D	State space model matrices
B	Aerodynamic damping
B	Semi-chord
c	control surface, rudder
C/C_c	Critical damping ratio, non-dimensional
d_{31}	Strain in direction 1 per unit electric field in direction 3
d_{33}	Strain per unit electric field in direction 3
F_{buf}	Buffet forcing function
F_{piezo}	Piezoelectric Actuator forcing function
G	Acceleration (1G = 386.4 inch/second^2)
g	Structural damping
H	Transfer function
I	Identity matrix
J	Imaginary value, $\sqrt{-1}$
k	Reduced frequency
K	Generalized stiffness of mode
M	Generalized mass of mode
Q	Generalized aerodynamic force
$q, \ddot{q}$	Generalized displacement, acceleration of mode

s ..... Laplace variable

t ..... Time

U,u..... System input

V ..... True airspeed

y..... System output

ρ..... Air density

ω ..... Frequency

φ..... .Normalized mode shape